Adipose Tissue Engineering:
Obesity Disease Model and Soft Tissue Regeneration

A dissertation submitted by

Evangelia Bellas

In partial fulfillment of the requirements for the degree of

Doctor of Philosophy

In

Biomedical Engineering

TUFTS UNIVERSITY

Advisor: David L. Kaplan, Ph.D.

Tufts University

Medford, MA. USA.

April 10th, 2012

1:30 PM

Research Committee:

Prof. David L. Kaplan, Dept. of Biomedical Engineering, Tufts University

Prof. Lauren Black, Dept. of Biomedical Engineering, Tufts University

Prof. Jonathan Garlick, Division of Cancer Biology and Tissue Engineering, Tufts University

Prof. Kacey Marra, University of Pittsburgh

ABSTRACT OF DISSERTATION

The need for physiologically relevant sustainable adipose tissue models is crucial for understanding tissue development and disease progression, *in vitro* drug and product development as well as for *in vivo* soft tissue regeneration.

Adipose tissue is a complex organ whose many roles are becoming better understood. Once thought of a static organ for energy storage, adipose tissue has now been discovered to have more dynamic roles, namely those in metabolism and endocrine signaling. Our understanding of its biology is crucial on many levels. Excess adipose tissue is linked to obesity, type II diabetes, increased cardiovascular risk and any associated co-morbidities. On the other hand, a lack of adipose tissue also carries its own metabolic consequences. Currently, adipose tissue biology is mainly studied in the context of monolayer *in vitro* cultures, or small animal *in vivo* studies. Both methods offer insight to the system, yet neither approximate the complex nature of human adipose tissue.

Adipose tissue also functions as a protective layer for our organs and maintains body contours. Soft tissue defects, most often are the result of trauma, congenital defects, or tumor removal. These defects have emotional and social consequences associated with the deformity and fear of not being accepted. One treatment for filling these defects is fat grafting. However, fat grafting, as with other fillers, does not retain volume over time, with 20-90% lost over the first few months. Therefore, there is a large unmet clinical need for a soft tissue filler that maintains its volume.

The goal of this research is to create a physiologically relevant adipose tissue construct to be used as an *in vitro* platform for studying tissue and disease development, as well as a platform for testing potential therapeutics. This adipose tissue construct can serve as a template for *in vivo* soft tissue regeneration.

In this dissertation the work centers on exploiting our knowledge of adipose tissue engineering and silk biomaterials. Silk biomaterials can be processed to have a range of physical, mechanical and degradation profiles. Our long-term vascular adipose tissue construct served as a foundation for further long term studies in obesity modeling as well as for soft tissue regeneration. The long-term vascular adipose tissue maintained adipose-like outcomes over a 6 month period, and was

improved by dynamic culture. From this, we developed a model of diet-induced obesity by challenging this system with free fatty acids and monocytes to generate inflammation. This model is in line with clinical readouts and can be generated from a patient's own cells. We showed we use therapeutics to try and reverse the inflammatory cascade of obesity. Finally, our *in vivo* 18 month study was the first to show that we can maintain volume while actually regenerating tissue when silk sponges are soaked with lipoaspirate. This model now is being translated into injectable formats to be minimally invasive. Ongoing pre-clinical studies are underway in a horse model for soft tissue regeneration.

ACKNOWLEDGEMENTS

I wish to thank my committee for their wonderful support, insight and motivation throughout my time at Tufts, Lauren Black III, Jonathan Garlick, Kacey Marra and David Kaplan. I'd like to thank the Department of Biomedical Engineering as a whole for support and allowing me to achieve this PhD degree. I'd like to thank the Armed Forces Institute of Regenerative Medicine (AFIRM) and NIH Tissue Engineering Resource Center (TERC) for financial support. Many faculty have contributed to my growth here and I am very happy to have had the opportunity to work with them. From Tufts BME, I'd like to especially thank Irene Georgakoudi and Fiorenzo Omenetto for their support and always constructive feedback. From Columbia, I'd like to thank Gordana Vunjak-Novakovic for her research feedback during our TERC meetings, and for being a career and life-after-PhD mentor. Her advice has been invaluable. I also thank her lab members who have always contributed thoughtfully at TERC meetings.

This work was possible with a long list of collaborators. From the University of Pittsburgh, Kacey Marra and J. Peter Rubin and their lab members have made a great soft tissue team along with James Yoo and San Jin Lee at Wake Forest. They have been wonderful mentors and hosts every time I visited Pittsburgh, however, I do not support their choice in football teams☺. From Tufts, I'd like to thank Jonathan Garlick and his lab for being great full thickness skin tissue engineering teammates and for their help with getting me on my feet with histology. From J&J, Miri Seiberg and her team are the other part to the skin tissue engineering team. Also, from Tufts, I'd like to thank Irene Georgakoudi's group for our non-invasive image collaboration, especially Kyle Quinn who is a research superstar, smart, hard-working, patient, thorough and a great team player. I'd like to thank the Tufts Vet School crew under Carl Kirker-Head, especially Marianne Stark, Kimberly Flink for help with the small animal studies and Mandy Rollins for the large animal studies. Gary Leisk and Tim Lo have been a fun pair to work with for the foam work, where we had great synergy. Tim always has a most pleasant demeanor and I found it hard not to be smiling when we've worked together, I still owe him iced coffees thanks to bets I've lost.

There are many amazing people I've met through the work done with AFIRM, in no particular order: Tony Atala, Tony Mikos, Ben Harrison, Rocky Tuan, Kurt Kasper, George Christ, David Baer, Tom Walters, Joan Schanck, Patrick Spicer, and all the members of the AFIRM fellows

council, Katie Megley, Brent Uhrig, Kelly Chen, Catherine Ward, Chad Market, Tracy Criswell, Won Hyuk Suh.

I'm indebted to the students (Tina Jumani, Sorabh Kothari, Michael Schecht, Tanzeel Ahmed, Aleksandar Mijailovic, Andrew Ward, Elliot Graziano) who have worked with me, who have given me the chance to teach and mentor them. I appreciated every moment. They've reinforced my passion for teaching and research and challenged me constantly. I hope they have taken some of that passion with them in their next career move. Aleksandar Mijailovic especially has been a pleasure because his interest and curiosity has helped motivate me along the way, and because he was with me the longest, I have been proud of his progress from sophomore year up through his senior thesis.

I've been lucky to have awesome labmates in the Kaplan lab and throughout the department. Jen (Kang) Choi took me under her wing and showed me the ways of adipose tissue engineering and I owe a lot of my knowledge base to her. Dean Glettig and Kelly Burke have been my closest partners in crime along the way and more recently Jodie Moreau has been an amazing co-pilot. I'm happy to have had such smart and hard-working lab mates. There are a handful of people who have been very helpful along the way: Michaela Reagan, Balaji Subramanian, Michael House, Jelena Rnjak, Rebecca Scholl Hayden, Lindsay Wray, Tessa DesRoaches, Amanda Baryshyan, Amy Hopkins, Philipp Seib, Lin Sun, Sarah Sundelacruz, Marie Tupaj, Michael Lovett, Eun Seok Gil, Amy Thurber, Andrew Reeves, Lee Tien, Ethan Golden, Tuna Yucel, Danielle Rockwood, Nan Zhao, Xiaoqin Wang, Amanda Murphy, Monica Serban, Aneta M Mieszawska, Reynald Lescarbeau, Jon Kluge, Jabier Gallego Llamas, Jeff Brown, Joe Marturano, Zak Schiller, Charles Banos, Joanna Xylas, Joshua Resnikoff. My time here would not have been half as happy if it hadn't been for my 141 officemates- Lindsay Wray, Rebecca Scholl Hayden, Amy Thurber, Kyle Alberti, Dan Hines, Balaji Subramanian, Wei-Che Ko, Kate Blanton. I had some my best laughing fits here with them. I have to give a shout-out to my fellow SeriLuxe co-founders- Lindsay Wray and Amanda Baryshyan, it's been such a great experience learning about what it takes to start a hair and skin care product line. None of the work would be possible without Carmen Preda, Milva Ricci, Martin Hunter and Keleigh Sanford, whose hard work behind the scenes to keep everything running is always greatly appreciated.

From my previous life at MIT, I have made amazing friends who I have looked up to and who have been such great support and cheerleaders for me through my PhD time- Jason Burdick, Chris Bettinger, Jason Fuller, Joost Bruggeman, Grace Kim, Kerry Mahon, Chris Highley and Dan Anderson. I'm incredibly proud of everything they've accomplished. I'd like to thank Robert Langer for all his support, hilarious stories and the inspiration he's given me to know that hard work always pays off.

Outside of lab, I thank all of friends who have balanced my life with fun and support especially, Kate Donlan, Kara Cohen, Michelle and Chris Beans, Emma Tzioumis, Colin Pederson, Rich and Mirella Young, Jeremy and Meghann Warnick, Chris Benker, Megan Ruebsamen, Erin Frane, Matt Eliadi, Lauren Grasso, Kristen Pilkiewicz, Mia Becze, Anna McLean, Andrea Taylor, Vanessa Pelligrino, Manny Simons, Kate Morrison, Laura Lipscei, Jill Lizotte.

I thank my family, my dad, Chris, my mom, Mary-ann, my little brother, Peter, my aunt, Aristea, and my adorable cousin, Katerina, for all of their love always. I dedicate this work to my grandparents, Peter and Ekaterina Tikellis, who passed away the summer I started at Tufts. They inspired me to go into biomedical engineering and sparked my interest in natural biomaterials because I was intrigued by their stories about their hip replacements and bypass graft surgeries. They have inspired me throughout my time here, even though they were no longer around; I knew they have been looking out for me. I love them and miss them every day.

Most of all, I'd like to thank my advisor, David Kaplan. I appreciate all his support and mentorship and his trust in me. I'm always proud to represent his lab whenever I go to meetings/conferences because as soon as someone finds out whose lab I come from, they always say the same things: "Oh! He's a great guy, you're so lucky". I have to agree. I've been so lucky to have such a great advisor who really cares about his students and staff as if they're part of his family. I'm looking forward to the next part of my career, because I've had a great training experience here with David, and I look forward to continuing a working relationship with him in a new context.

Table of Contents

List of Figures and Tables

CHAPTER 1. INTRODUCTION

1.1 ABSTRACT

Adipose tissue was once considered a static organ whose role was only to store energy until needed by other tissues. Our view of adipose tissue has changed to that of a dynamic organ responsible not only for energy storage but for endocrine signaling and metabolic function. Excess adipose tissue is responsible for obesity, type II diabetes and other associated co-morbidities, while little adipose tissue leads to other metabolic consequences and undesirable esthetic. This review will serve to break down adipose tissue function and highlight current biomedical research in the area of adipose tissue engineering and soft tissue regeneration.

1.2 INTRODUCTION

The need for physiologically relevant sustainable adipose tissue models is crucial for understanding tissue development and disease progression, *in vitro* drug and product development as well as for *in vivo* soft tissue regeneration.

Adipose tissue is a complex organ whose many roles are becoming better understood. Once thought of a static organ for energy storage, adipose tissue has now been discovered to have more dynamic roles, namely those in metabolism and endocrine signaling. Our understanding of its biology is crucial on many levels. Excess adipose tissue is linked to obesity, type II diabetes, increased cardiovascular risk and any associated co-morbidities. The rates of obesity are soaring across the world, with more than one in ten adults being obese (WHO | Obesity, 2012). On the other hand, a lack of adipose tissue also carries its own metabolic consequences. Currently, adipose tissue biology is mainly studied in the context of monolayer *in vitro* cultures, or small animal *in vivo* studies. Both methods offer insight to the system, yet neither approximate the complex nature of human adipose tissue.

Adipose tissue also functions as a protective layer for our organs and maintains body contours. Soft tissue defects, most often are the result of trauma, congenital defects, or tumor removal. These defects have emotional and social consequences associated with the deformity and fear of not being accepted. A treatment for filling these defects is fat grafting. However, fat grafting, as

with other fillers, does not retain volume over time, with 20-90% lost over the first few months. Therefore, there is a large unmet clinical need for a soft tissue filler that maintains its volume.

The goal of this research is to create a physiologically relevant adipose tissue construct to be used as an *in vitro* platform for studying tissue and disease development, as well as a platform for testing potential therapeutics. This adipose tissue construct can serve as a template for *in vivo* soft tissue regeneration.

1.3 ADIPOSE TISSUE

Adipose tissue is a complex organ comprised of several cell types and extracellular matrix (ECM) proteins. The cellular portion is comprised of mainly of adipocytes, adipose derived stem cells (ASCs), fibroblasts, blood vessels (endothelial cells, pericytes), and various inflammatory cells. The ECM is comprised of collagen type IV, fibronectin, proteoglycans and laminin. The cells secrete a variety of growth factors, cytokines/adipokines, and hormones and these will discussed as they become introduced.

Types of Adipose Tissue (Table 1.1)

Adipose tissue is found both subcutaneously and viscerally in mammals. Each depot has different roles. Most often, we associate fat with white adipose tissue (WAT), however, brown adipose tissue (BAT), a thermogenic adipose tissue, has become researched more heavily since it was found that adult humans have small BAT depots[1,2]. BAT adipocytes are multilocular, or have many lipid droplets, and get their brown color from their many mitochondria. The multilocular phenotype allows for "easy access" to the stored triglycerol (TG) that is used by the mitochondria for FFA oxidative phosphorylation to release heat[3]. In humans, BAT is found interscapularly at birth, and cervical, supraclavicular and paravertrebral regions, albeit scarcely, in adults[1]. The research discussed in this work will focus mainly on WAT.

By contrast, the defining factor for WAT adipocytes is the large central lipid droplet, thus WAT mature adipocytes are unilocular. This central lipid droplet is the site of TG storage for energy usage.

The Adipocyte

The adipocyte is the principal feature of adipose tissue. The adipocyte is a terminally differentiated cell made up of a centrally located lipid droplet (LD), in white adipocytes, or several, smaller lipid droplets in immature or brown adipocytes. The droplet(s) are responsible for maintaining the reservoir of triglycerol (TG) that can be released as fatty acids (FAs) and glycerol for energy use by other organs[3–6]. TG is a large molecule comprised of a glycerol head with three fatty acid tails. The adipocyte performs a balancing act to regulate metabolism: 1) uptake of FA from plasma, 2) intracellular lipogenesis or FA esterification to generate TG for *energy storage* and, 3) intracellular lipolysis or TG hydrolysis to generate FA for *energy use* by other tissues.

Uptake of FA from Plasma

Lipoprotein lipase (LPL) is synthesized by mature adipocytes and translocated to endothelial cell lumens via proteoglycans to take up TGs bound to lipoproteins, such as very low density lipoprotein (VLDL), as they are too large to pass through the endothelium on their own[4]. LPL hydrolyzes VLDL-TG into FA and can then be taken up by the adjacent cells (Fig1.1)[7]. In some cases, FA can be "flipped" into the cell through the phospholipid bilayer, however this mechanism of uptake is rare. The more common routes involve protein mediated uptake by CD36, Fatty Acid Transport Proteins (FATPs) or caveolins, but exact mechanisms are still under debate[4].

Intracellular Lipid Metabolism

Within the adipocyte, the FA is converted to acyl-coA via ACS (acyl-coA synthase) at the endoplasmic reticulum (ER). Acyl-CoA is then used as a substrate for TG synthesis in one of

two pathways. The first pathway involves acylation of monoglycerol (MG) to diaglycerol (DG), while the other pathway involves glycerol-3-phosphate (from glucose metabolism) acylated sequentially to form DG. DG, from either pathway, is acylated to TG. TG droplets are released from the ER coated with perilipin or adipose differentiation related protein (ADRP). The mechanisms determining which and how much of the protein coated the TG droplet are still not understood. However, large lipid droplets are found coated with only perilipin. Perilipin is emerging as a gatekeeper to accessing the lipid droplet[8–10]. The understanding of lipogenesis, as described briefly here, is continuously evolving as more of the key players and interactions are being identified.

Lipolysis, by contrast, is the process of breaking down TGs (Fig 1.1), but its understanding is also still under progress. When the adipocyte is hormonally activated, either by glucocorticoids or insulin binding at the cell surface, this leads to cyclic adenosine monophosphate (cAMP) mediated activation of protein kinase A (PKA), which phosphorylates perilipin and hormone sensitive lipase (HSL) at the surface of the lipid droplet. Perilipin upon phosphorylation dissociates from CGI58, a co-activator of adipose triglyceride lipase (ATGL). ATGL translocates from the cytosol to the surface of the lipid droplet and enzymatically breaks down TGs to DGs. HSL then hydrolyzes DGs into MGs, and MGs are hydrolyzed by monoglyceride lipase (MGL) to glycerol and FA (Fig1.2)[4]. FAs and glycerol are effluxed from the cell, either by CD36 or aquaporins, respectively, however these mechanisms are still under investigation. The balance of lipogenesis and lipolysis is regulated by the nutritional state (fed versus fasted) and stimulation state (basal versus stimulated/ hormonal) of the body.

Development

In human neonates, WAT is a mix of multilocular and unilocular cells, undergoing both hypertrophy (increased cell size) and hyperplasia (increased proliferation). At the same time, the BAT has decreasing mitochondrial activity and begins to transdifferentiate into WAT. The metabolic nature of adipose tissue requires that blood vessels are nearby[11]. Angiogenesis, the formation of blood vessels, and adipogenesis, the formation of adipocytes, are seen to be

intimately involved throughout development, with the capillary density being greater than even that of skeletal muscle[11].

Adipogenesis, the differentiation of adipocyte precursors into mature adipocytes, is a well-studied *in vitro* process[12–14]. Adipogenesis can be looked at as a staged process, starting with the proliferation stage, then the growth arrest stage, the commitment stage and finally the mature adipocyte stage[12,15]. Whether starting with a cell line, such as 3T3-L1, or a stem cell, such as adipose derived stem cells, ASCs, the precursor cells are expanded until confluence. Confluence begins the growth arrest state by contact inhibition. At this time, the cells are exposed to adipogenic induction media containing dexamethasone (DEX), insulin, isobutyl methyl xanthine (IBMX), thiazolidinediones (TZDs), pantothenate, and biotin[16]. DEX and IMBX are necessary for cAMP activation for lipolysis. Insulin is needed for the uptake of glucose into the cell and to activate the IGF axis. Pantothenate and biotin are required for FA synthesis. TZD is a specific perixosome proliferation activator receptor gamma (PPARγ) agonist. PPARγ is the master adipogenic transcriptional regulation factor (Figure 1.3). No factor has been found to rescue adipogenesis without PPARγ[17]. It is also the target of an antidiabetic class of drugs, TZDs. PPARγ is activated downstream of C/EBPβ/δ. C/EBPβ/δ is activated by DEX, insulin, IBMX[17].

1.4 OBESITY

The World Health Organization (WHO) broadly defines those individuals who have a body mass index of greater than 30 to be obese (WHO | Obesity, 2012). Obesity is a risk factor for other noncommunicable diseases, such as diabetes, cancer, and cardiovascular disease. Obesity affects people of all ages, races, and socio-economic statuses. The WHO estimates about 200 million men and 300 million women were obese in 2008, or about $1/10^{th}$ of the world adult population being obese. As of 2010, about 43 million children under the age of 5 were classified as being overweight (BMI: 25-30), where 35 million lived in developing countries and 8 million in developed countries. The epidemic attributes more deaths to being overweight rather than underweight. In the simplest form, one can define the cause of obesity to be in the balance of energy in versus energy out, where the balance is shifted towards taking more energy in. Calorie

rich foods and an increasingly sedentary lifestyle are thought to be the biggest contributions to this worldwide epidemic.

Chronic Inflammation of Adipose Tissue

Obesity is characterized as a chronic inflammation of the adipose tissue. In the presence of increased dietary stimuli in the form of FAs, the adipocyte attempts to store the FA as TG in the lipid droplet by lipogenesis. However, as the lipid droplet expands the cell experiences cytoskeletal stresses. This causes the release of macrophage chemokines, which cause macrophage infiltration and a local inflammatory response and MMPs, that breakdown the surrounding matrix to allow for continued growth. It is not well understood what role exactly the ECM breakdown and remodeling plays, whether it is more of a cause or effect for obesity[18,19]. Infiltration of macrophages leads to the release of inflammatory cytokines, such as TNFα and Il-6. TNFα, among other factors, can directly influence lipolysis rates by cAMP phosphorylation of hormone sensitive lipase (HSL)[20–22]. TNFα also acts to impair PPARγ transcription, which can suppress lipogenesis in mature adipocytes and suppress adipogenesis in resident pre-adipocytes. This elevates levels of circulating TG, ultimately leading to ectopic lipid droplets in muscle and liver[20]. TNFα, along with the increase in FAs from enhanced lipolysis and diet, contribute to further aggravation of the inflammatory cycle via the classic innate immune pathway, Toll-Like Receptor 4 (TLR4). Animal models of TLR4 knockdown leads to decreased levels of inflammatory markers and maintenance of insulin sensitivity, while in wild-type animals the downstream activation of FA-TLR4 leads to release of TNFα, Il-6 and insulin resistance[23]. TLR4 is found on both macrophages and adipocytes. The inflammation continues to cycle if left untreated (or without changes in diet) to eventually lead to insulin resistance, type II diabetes, ectopic lipid droplets, and cardiovascular disease.

1.5 SOFT TISSUE REGENERATION

Soft tissue regeneration can be viewed as having two different purposes, as a method to fill a defect or to augment already existing normal tissue. Soft tissue defects can be the result of trauma, congenital disorders, or tumor removal and constitute about 4.8 million reconstructive

surgery cases per year in the U.S. alone[24]. Autografts and lipotransfer have been the a treatment for soft tissue reconstruction, however, the success is unpredictable, with 20-90% graft resorption within months[25–27]. This leaves significant problems for the patient and thus the regeneration of large soft tissue defects remains an unmet clinical need. Other strategies for soft tissue filling include the use of natural and synthetic biomaterials. As with autologous fat grafting, their success is also unpredictable.

1.6 ADIPOSE TISSUE ENGINEERING

1.6.1 History

In vitro 3D adipose tissue engineering is a relatively new field, the first cited study is by Patrick et al., 1999, on pre-adipocytes seeded on poly-lactic-glycolic acid (PLGA) scaffolds[28]. The study included harvesting rat pre-adipocytes, culturing until pre-confluence in basic growth media (not much was known about differentiation at this time), and then seeding onto a 12mm x 2.5mm porous PLGA disk for 14 days. These seeded disks were also implanted *in vivo* for 2 and 5 weeks. The pre-adipocytes, upon contact with one another, differentiated into large, multilocular adipocytes with eccentric nuclei. Since this first study, research in adipose tissue engineering is steadily growing (Fig. 2). Our lab and others have demonstrated the feasibility of adipose tissue engineering with a variety of biomaterials (Table 1.2) and cell sources (Table 1.3)[29–31].

1.6.2 Biomaterials

Biomaterials for adipose tissue engineering vary from synthetic to natural. Poly-lactic-co-glycolic acid (PLGA) and poly-ethylene glycol (PEG) are most common synthetic materials used for adipogenesis. PLGA is a FDA approved polymer and has been commonly used for drug delivery. Many of the studies conducted with PLGA in adipose tissue engineering involved attaching cells to PLGA spheres for in vivo delivery[32–34]. Two studies used PLGA as porous scaffolds for adipogenesis[35,36]. In all PLGA studies, adipogenesis was well supported both *in vivo* and *in vitro*, however, only for short-term time frames. An *in vivo* study demonstrated a loss

in adipogenic outcomes by 3 months of implantation although the study was intended to extend to 12 months[36]. The loss of adipogenic outcomes coincided with the degradation of the PLGA scaffold. One way to alter the degradation rate of PLGA is by the ratio of the co-polymers. As glycolic acid increases so does the rate of degradation (i.e. faster degradation)[37]. In the study, if the ratio of lactic acid to glycolic acid was greater, the degradation rate may have allowed for better sustained adipose tissue.

PEG, also supports adipogenesis, however, inherently does not contain any cell-binding motifs and must be modified to enhance attachment[38]. Adipocytes and their precursors are anchorage dependent cells and would need modified forms of PEG. The bio-inert feature of PEG biomaterials renders the material non-biodegradable[38]. In a 2007 study performed by Stosich and Mao, comparing collagen and PEG biomaterials with adipocytes for sustained soft tissue regeneration *in vivo*, demonstrated volume stable PEG constructs, and a loss of volume in collagen over a 4 week period[25]. The lack of cell-binding motifs and therefore inability of cells to remodel their environment in PEG biomaterials, do not make these an appropriate choice for adipose tissue models of disease or especially for soft tissue regeneration where host infiltration is important for angiogenesis and remodeling.

Natural biomaterials contain cell binding motifs and are able to be remodeled by the body. Collagen, alginate, gelatin, hyaluronic acid (HA), extracellular matrix proteins (ECM) and silk have all been explored for adipose tissue engineering and support adipogenesis[39–53]. Collagen and HA have been studied for adipose tissue engineering and are currently in use as dermal fillers- Evolence™, Cosmoderm™, Restylane™, Juvederm™. Itoi et al., compared collagen and HA scaffolds seeded with ASCs, in a 4 and 8 week *in vivo* study, and found collagen was a better environment for ASCs to form into mature adipocytes[54]. A pilot study, performed in humans using HA scaffolds ± autologous preadipocytes, found that volume was maintained up to 8 weeks when pre-seeded, however no mature adipocytes were found within either group[55]. The authors reported HA supported adipogenesis and pre-adipocytes in a rodent model yet did not reference the work being referred to. Gelatin has been shown to support bone marrow mesenchymal stem cell (MSC) adipogenesis *in vitro* for up to 6 weeks[53]. Alginate also has been shown to support adipogenesis when pre-seeded with preadipocytes, *in vitro and in vivo*, but

only maintained 2/3 of its volume over an 8 week period when pre-seeded[48]. ECM is an attractive matrix because it contains the many of the proteins naturally found in tissue. Adipose tissue can be readily decellularized, and when exposed to physiological temperature will form a gel[50]. In a 2D study, decellularized adipose tissue ECM supported ASC growth, similarly to collagen coated or uncoated wells[50]. Decellularized placenta ECM was found to support adipogenesis in a 2D, 7 day study[43]. In a subsequent study, decellularized placenta ECM was blended with HA[56]. The ECM allowed for better handlability, while HA allowed the cells to become encapsulated. This combination supported adipogenesis *in vitro* for 14 days[56]. Silk biomaterials have also been shown to support adipogenesis of both ASCs and MSCs in 14 and 21 day *in vitro* cultures, respectively[16,45]. Additionally, adipogenic outcomes on silk scaffolds were maintained for 1 month *in vivo*[45].

1.6.3 Cell Sources

Many different cell sources have been explored for adipose tissue engineering (Table 1.3). All sources, when exposed to adipogenic media, differentiate and are able to accumulate intracellular lipid droplets, the hallmark sign of differentiating adipocytes. Therefore, cell source becomes dependent on the model being developed. For soft tissue regeneration applications, it would be more appropriate to use adipose derived stem cells which are readily harvested from the patient themselves, so there is no risk of immune rejection. Adipose derived stem cells can be aseptically isolated from lipoaspirate within 1 hour in the operating room using TGI™ system (Tissue Genesis, Inc, Honolulu, HI). In patients with little subcutaneous adipose tissue, bone marrow derived stem cells would still offer the same benefits of patient matched cells, although the process is more invasive, and the isolation process is lengthier. In animal models for soft tissue regeneration, it is appropriate to use human derived stem cells to show proof-of-concept in an immune-compromised animal; however, the healing process may be affected by the compromised immune system. To this end, it is reasonable to use autologous stem cells to fully understand how the grafted material integrates, remodels and heals within an animal model. When developing an *in vitro* disease model, one could argue using an established cell line, such as the 3T3-L1 preadipocyte mouse cell line, is best so that results can be consistently compared across many studies. In fact, many published 2D studies on obesity are performed on 3T3-L1

differentiated cells. However, cell lines and primary cells respond to cues differently[57]. Therefore, while cell lines may be useful for preliminary experiments and source homogeneity, primary cells are likely better suited for modeling complex cell-cell, cell-matrix interactions of a disease model. Furthermore, using primary cells allows for the development of patient specific drug testing platforms.

1.6.4 Ideal Characteristics

The ideal characteristics for an adipose tissue engineered construct material would be a slowly degrading, natural biomaterial, to allow for cell binding, remodeling, that can be easily manipulated and handled. For soft tissue regeneration, it is important that the material is robust enough to be handled in a surgical setting, and slowly degrading, such that the rate of material degradation and tissue regeneration are matched. For development of a disease model, it is also important that the material sustains the structure over a long period to truly mimic a chronic disease state. The ideal characteristics for an adipose tissue engineered construct cell choice would be human source (patient match when needed), primary stem cells, capable of being isolated rapidly and can undergo adipogenesis *ex vivo*.

1.7 ACKNOWLEDGEMENTS

I would like to thank Kacey Marra, J. Peter Rubin for discussions on soft tissue regeneration, Jeff Gimble for discussions on adipose derived stem cells. We would like to thank the NIH P41 Tissue Engineering Resource Center and AFIRM for support.

1.8 FIGURES

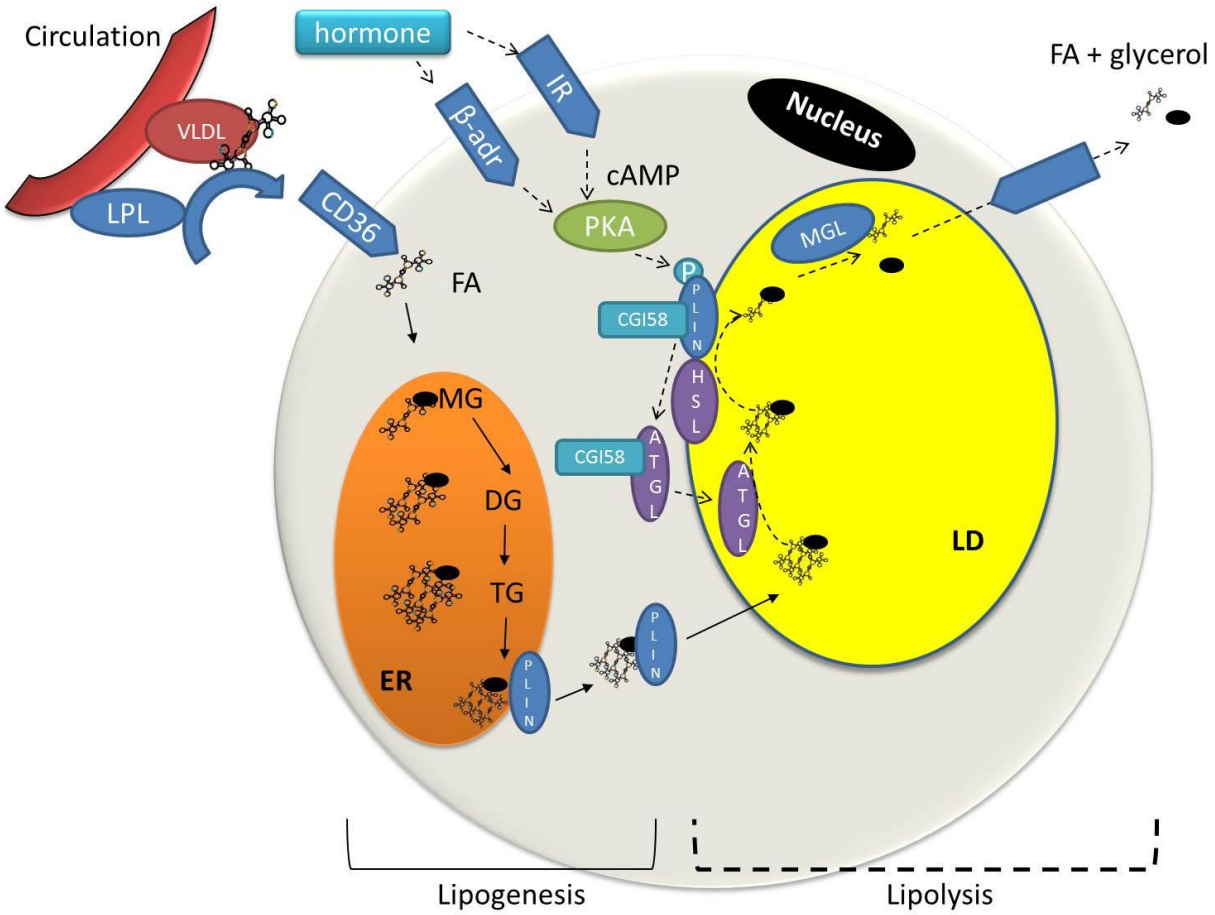

Figure 1.1- Overview of the process of lipid metabolism within the adipocyte. To store energy, fatty acids (FA) and/or triglycerides bound to very low density lipoproteins (VLDL) are taken up from the bloodstream (upper left corner) and broken down by lipoprotein lipases (LPL) into fatty acids. The fatty acids are transported into the cell by CD36 (a fatty acid transporter) and to the endoplasmic reticulum (ER). The fatty acid is sequentially acylated to monoglyceride (MG), diaglycerol (DG), then triglycerol (TG). The TG leaves the ER coated with perilipin (PLIN) and trafficked to the lipid droplet (LD) for storage. Solid arrows denote part of the lipogenesis pathway. In order to produce energy, the TG within the LD is hydrolyzed by adipose triglycerol lipase (ATGL), then hormone sensitive lipase (HSL) then monoglycerol lipase (MGL) to fatty acids and glycerol. The FA and glycerol are shuttled out of the cell, likely by CD36 or aquaporins. Dashed arrows denote the process of lipolysis. The process is regulated hormonally. See figure 1.2 for more details. Abbreviations: FA- fatty acid, VLDL- very low density lipoproteins, LPL- lipoprotein lipases, ER- endoplasmic reticulum, MG-monoglycerol, DG-diaglycerol, TG-triglycerol, PLIN- perilipin, LD- lipid droplet, ATGL- adipose triglycerol lipase, HSL- hormone sensitive lipase, MGL- monoglycerol lipase. β-adr- β-adrenegic receptor, IR-insulin receptor, cAMP- cyclic adenosine monophosphate, PKA- protein kinase A, P-phosphorylation, CGI58- a co-activator of ATGL.

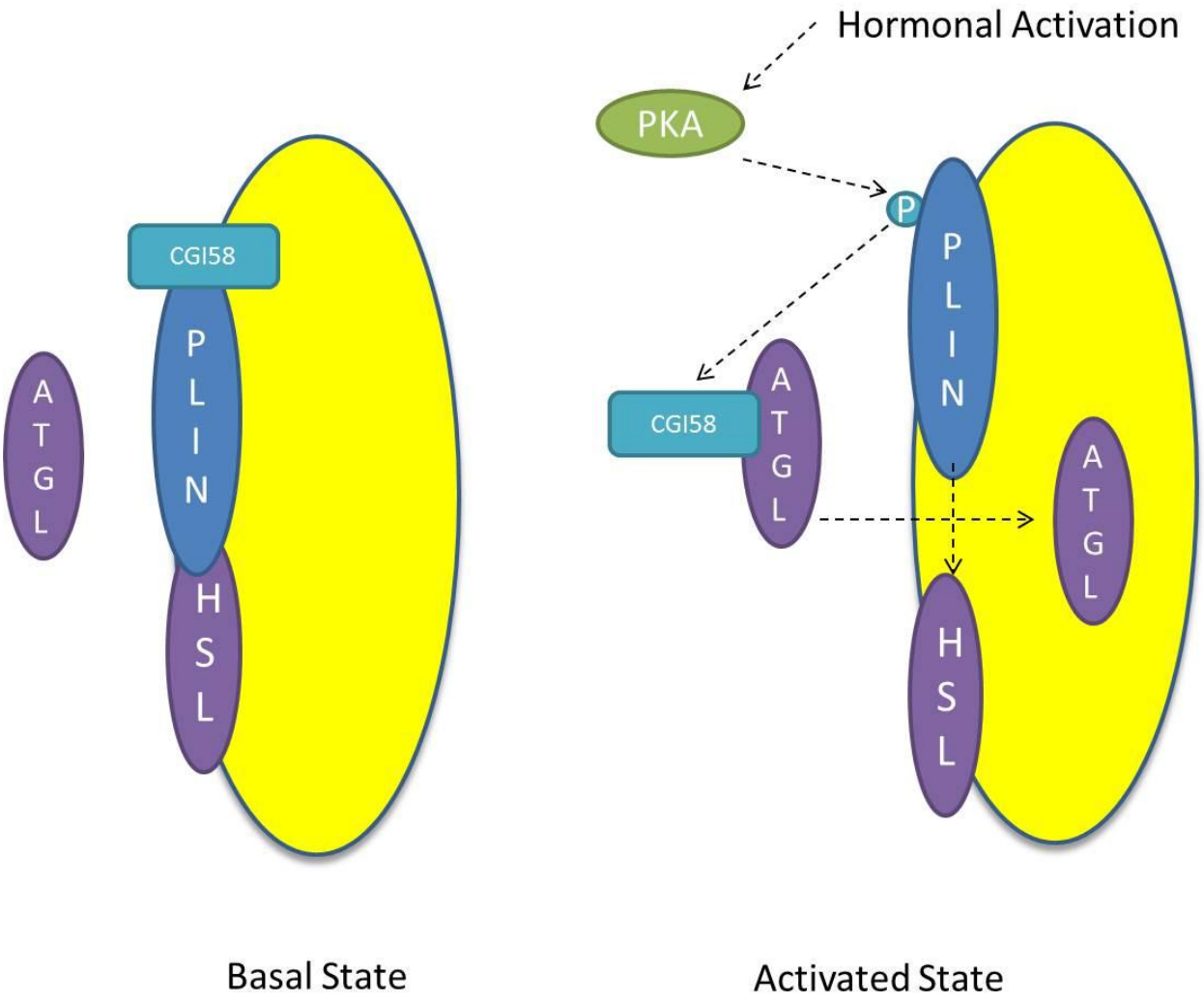

Figure 1.2- Regulation of lipid droplet associated proteins under basal (left) versus activated (right) conditions. In the basal state, ATGL resides in the adipocyte cytosol, while CGI58, PLIN, and HSL form a complex on the surface of the lipid droplet. Upon hormonal activation, PKA activated phosphorylation of PLIN, causes CGI58 and HSL to dissociate. CGI58 binds to and activates ATGL. ATGL translocates to the lipid droplet. Abbreviations: PLIN- perilipin, ATGL- adipose triglycerol lipase, HSL- hormone sensitive lipase, PKA- protein kinase A, P- phosphorylation, CGI58- a co-activator of ATGL.

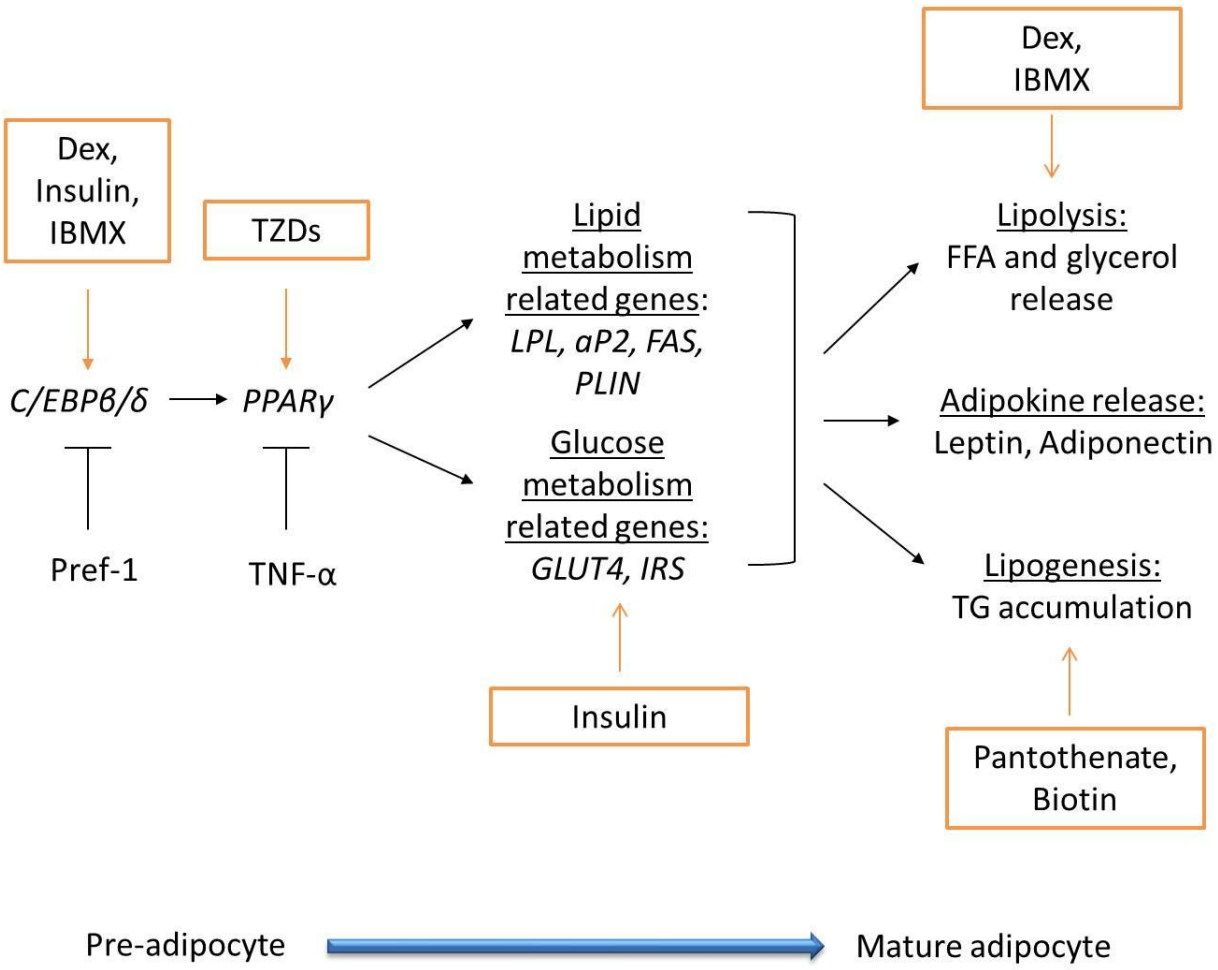

Figure 1.3- Adipogenesis regulation. The process of adipogenesis begins from a stem cell, or pre-adipocyte. C/EBPβ/δ activates Peroxisome Proliferator-Activated Receptor gamma (PPARγ), the master transcriptional regulator of adipogenesis. PPARγ activates many pro-adipogenic genes related to lipid and glucose metabolism. Upon expression of pro-adipogenic genes, the cell can undergo lipolysis, lipogenesis and adipokine release as a mature adipocyte. *In vitro* adipogenic differentiation is controlled by a chemically defined media. Its components and where they act during the process are outlined in orange boxes. Preadipocyte factor -1 (Pref-1) is found only on pre-adipocytes and acts to inhibit adipogenesis. Tumor necrosis factor alpha (TNFα) also negatively impacts adipogenesis. Abbreviations used: C/EBPβ/δ- CCAAT-enhancer-binding proteins beta/delta , PPARγ- Peroxisome Proliferator-Activated Receptor gamma, Pref-1- preadipocyte factor 1, TNFα – tumor necrosis factor alpha, LPL- lipoprotein lipase, aP2- adipogenic protein 2, FAS- fatty acid synthase, PLIN- perilipin, GLUT4- glucose transporter 4, IRS- insulin receptor substrate, Dex- dexamethasone, IBMX- isobutyl methyl xanthine, TZDs- thiazolidinediones.

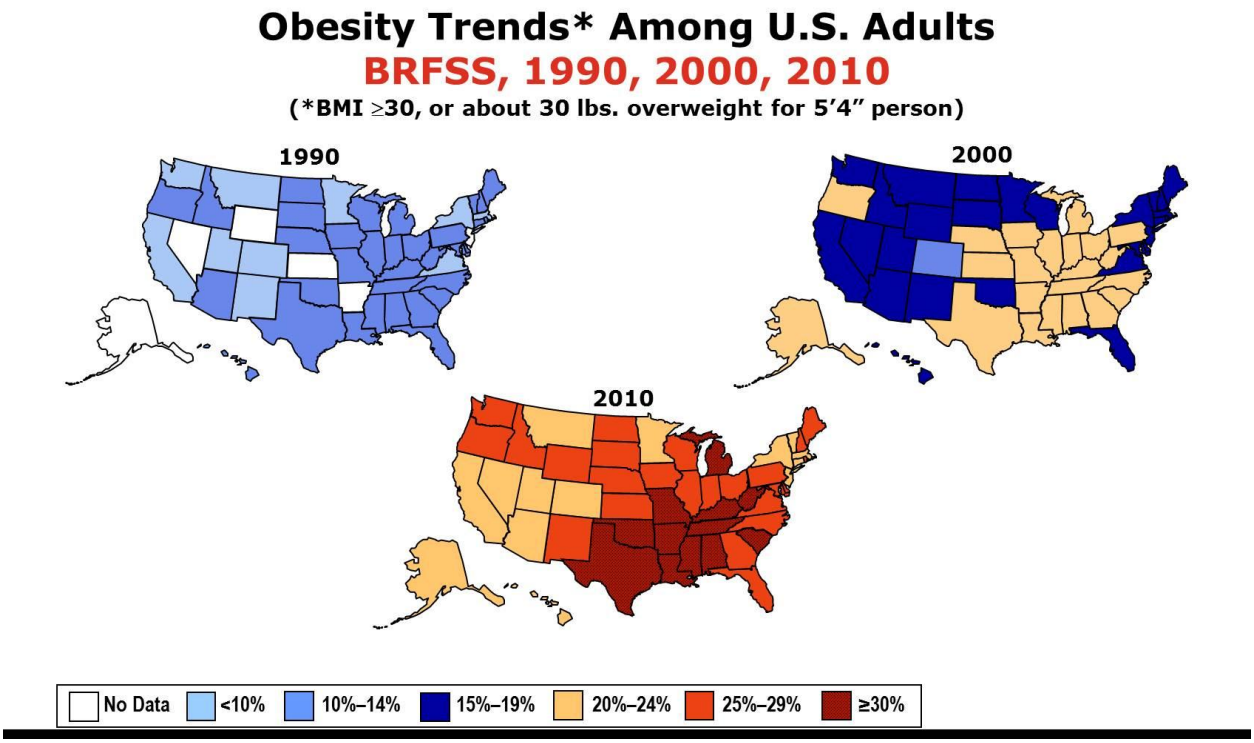

Figure 1.4- Obesity Trends in U.S. Source: CDC.gov Accessed March 19, 2012

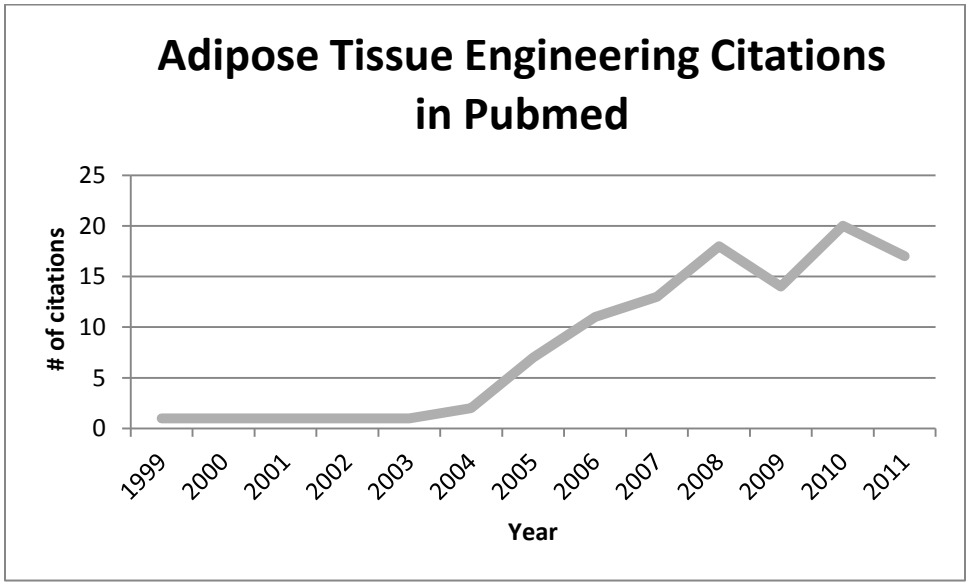

Figure 1.5- Trends in adipose tissue engineering research (Pubmed, 1999-2011)

1.5 TABLES

Table 1.1- Types of adipose tissue in humans

Type	Defining Feature	Role	Locations
White	White adipocytes: unilocular lipid droplet	Energy storage, release energy, metabolic homeostasis	Subcutaneous depots (abdominal, gluteal, facial, cranial), visceral depots (omental, retroperitoneal), retro-orbital, periarticular, bone marrow, intramuscular, pericardial
Brown	Brown adipocytes: multilocular, many mitochrondria	Thermogenesis, fatty acid oxidation	Cervical, supraclavicular, paravertebral, intrascapular (at birth)

Table 1.2- Biomaterials shown to support adipogenesis.

	Biomaterial	References
Synthetic	PLGA	Patrick 1999
		Choi 2005
		Neubauer 2005
		Choi 2006
		Choi 2007
		Kang 2008
		Morgan 2009
		Chung 2009
	PEG	Stosich 2007
		Forzdar 2008
		Stacey 2009
		Brandl 2010
	PCL	Wiggenhauser 2012

	PU	Wiggenhauser 2012
	Polyesteramide	Hemmrich 2006
	PGA	Weiser 2008
		Itoi 2009
Blend	pNIPAAM-HA	Tan 2009
Natural	Denatured Collagen	Mauney 2005
	Collagen	Mauney 2007
		Stosich 2007
		Shanti 2008
		Itoi 2009
		Tsuji 2009
	Collagen-Chitosan	Wu 2006
	Collagen-HA	Davidinko 2010
	Alginate	Jing 2007
		Chandler 2011
		Kim 2011
	Gelatin	Kimura 2003
		Hong 2005
		Hong 2006
	Fibronectin	Hemmrich 2004
	Fibrin	Verseijden 2012
	ECM	Flynn 2006
		Flynn 2007
		Flynn 2008
		Marra 2008
		Abberton 2008
		Uriel 2008
		Choi 2009
		Young 2010
	Matrigel	Kelly 2006
		Stillaert 2007
	HA	Flynn 2007
		Flynn 2008
		Itoi 2009
		Borzaciello 2007
		Stacey 2009
	HA-Chitosan	Tan 2010
	Silk	Mauney 2007
		Kang 2009
		Mandal 2009

	Choi 2010
	Choi 2011
	Choi 2011

Table 1.3- Cell types used for adipose tissue engineering.

Cell Type	Source	Reference
3T3 preadipocyte cell line	mouse	Weiser 2008
		Chung 2009
		Brandl 2010
		Davidinko 2010
		Chandler 2011
1° preadipocytes	rat	Patrick 1999
		Fozdar 2008
	mouse	Kelly 2006
		Borzaciello 2007
	human	Kimura 2003
		Hemmrich 2004
		Hemmrich 2006
		Marra 2008
		Stacey 2009
Adipose derived stem cells	mouse	Jing 2007
		Itoi 2009
	human	Choi 2006
		Flynn 2006
		Hong 2006
		Flynn 2007
		Mauney 2007
		Stillaert 2007
		Kang 2008
		Flynn 2008
		Vallee 2008
		Kang 2009
		Tsuji 2009
		Tan 2009
		Choi 2010
		Young 2010
		Tan 2010
		Choi 2011

		Choi 2011
		Keck 2011
		Kim 2011
		Verseijden 2012
		Wiggenhauser 2012
Bone marrow mesenchymal stem cells	rabbit	Choi 2007
	rat	Mandal 2009
	human	Hong 2005
		Choi 2005
		Mauney 2005
		Neubauer 2005
		Mauney 2007
		Stosich 2007
		Shanti 2008
		Morgan 2009
		Choi 2009

CHAPTER 2: DEVELOPMENT OF A LONG-TERM *IN VITRO* VASCULAR ADIPOSE TISSUE CONSTRUCT

2.1 ABSTRACT

The need for physiologically relevant sustainable adipose tissue models is crucial for understanding tissue development and disease progression, *in vitro* drug and product development as well as for *in vivo* soft tissue regeneration. In this study, we demonstrate the ability to co-culture adipocytes, differentiated from human adipose derived stem cells, and endothelial cells on a porous silk matrix for at least 6 month period, while maintaining adipose-like outcomes. Cultures were assessed for leptin, glycerol production, gene expression for GLUT4 and PPARγ, DNA content, Oil Red O content, and CD31 expression. Co-cultures maintained their shape and size over this period in static cultures. Under spinner flask culture conditions the co-cultures increased in diameter by 1mm. Spinner flask cultures yielded improved adipose tissue outcomes overall. This work establishes a model for which can be applied to development of a metabolic dysfunction model of adipose tissue, as well as for soft tissue regeneration.

2.2 INTRODUCTION

Adipose tissue engineering has implications for studying adipose tissue development, dysfunction and soft tissue regeneration in a regulated and controlled manner. Adipose tissue is a complex organ whose many roles are becoming better understood. Once thought of a static organ for energy storage, adipose tissue has now been discovered to have more dynamic roles, namely those in metabolism and endocrine signaling. Our understanding of its biology is crucial on many levels. Excess adipose tissue is linked to obesity, type II diabetes, increased cardiovascular risk and associated co-morbidities. Currently, adipose tissue biology is mainly studied in the context of monolayer *in vitro* cultures, or small animal *in vivo* studies. Both methods offer insight to the system, yet neither approximate the complex nature of human adipose tissue.

The World Health Organization (WHO) broadly defines those individuals who have a body mass index of greater than 30 to be obese (WHO | Obesity, 2012). Obesity is a risk factor for other

noncommunicable diseases, such as diabetes, cancer, and cardiovascular disease. Obesity affects people of all ages, races, and socio-economic statuses. The WHO estimates about 200 million men and 300 million women were obese in 2008, or about $1/10^{th}$ of the world adult population being obese. As of 2010, about 43 million children under the age of 5 were classified as being overweight (BMI: 25-30), where 35 million lived in developing countries and 8 million in developed countries. The epidemic attributes more deaths to being overweight rather than underweight. In the simplest form, one can define the cause of obesity to be in the balance of energy in versus energy out, where the balance is shifted towards taking more energy in. Calorie rich foods and an increasingly sedentary lifestyle are thought to be the biggest contributions to this worldwide epidemic.

Adipose tissue also functions as a protective layer for our organs and maintains body contours. Soft tissue defects, most often are the result of trauma, congenital defects, or tumor removal. These defects have emotional and social consequences associated with the deformity and fear of not being accepted. One treatment for filling these defects is fat grafting. However, fat grafting, as with other fillers, does not retain volume over time, with 20-90% lost over the first few months. Therefore, there is a large unmet clinical need for a soft tissue filler that maintains its volume.

Autografts have been a treatment for soft tissue reconstruction. Autografts adhere to the surgeons idea of replacing "like with like", however, over half of the grafted material is often resorbed within months. In 1951, Peer and Walker reported on the outcome of 28 human fat grafts[58,59]. It was determined that 50% of the transplanted tissue remained after 1 year, whether it was placed near a vascular supply or a like tissue. The adipocytes that did not survive were seen to be replaced with fibrotic tissue. More recently, studies have shown that in the process of liposuction and preparing that lipoaspirate for lipotransfer some of regenerative aspects are lost[60,61].

Regenerative medicine is a growing field where the body's own raw materials are used to replace or regenerate injured or diseased tissues. The optimal tissue replacement would be not immunogenic, with no risk of disease transmission, little or minimal donor site morbidity and,

specifically for adipose tissue regeneration, able to maintain its volume and function over time[62]. Raw materials include cells, extracellular matrix, whole tissues, but in particular interest for our studies, we will focus on adipose derived stem cells (ASCs). Cells, alone, may not be sufficient to re-create the tissue's environment and can require a biomaterial component to act as a scaffold or cell delivery vehicle.

ASCs have been readily studied in the past decade as an alternative adult stem cell source. They carry no ethical concerns as they are taken directly from the patient and are easily obtained through minimally invasive surgeries. ASCs are of mesenchymal lineage and therefore are able to differentiate into a variety of cell types including, osteoblasts, adipocytes, myocytes, chondrocytes and neurons. More recently, they have also been shown to differentiate into endothelial cells[63,64]. Also, ASCs have been shown to release many potent pro-angiogenic factors[65].

The restoration of traumatic soft tissue defects should start with a strategy that will maintain tissue size and shape to near normal dimensions for extended time frames. Current clinical strategies include free fat transfers and artificial fillers. These options fail to retain volume over time, can require a second surgical site, have avascular necrosis and generally do not regenerate the original tissue.

The goal of this research is to create a physiologically relevant adipose tissue construct to be used as an *in vitro* platform for studying tissue and disease development, as well as a platform for testing potential therapeutics. This adipose tissue construct can serve as a template for *in vivo* soft tissue regeneration. For soft tissue regeneration, the construct must be able to be maintained *in vivo* as the body gradually remodels and regenerates the site into near-normal tissue structure and function. A slowly degrading yet mechanically sturdy matrix is needed for soft tissue engineering. To address these issues, we developed a 3D co-culture of human adipose derived stem cells differentiated to adipocytes and endothelial cells on a laminin coated silk scaffold. The hypothesis was that laminin coating would improve initial cellular adhesion while the silk scaffold maintains the structure and volume for at least 6 months *in vitro.*

2.3 METHODS

2.3.1 Materials

Bombyx mori silkworm cocoons were supplied by Tajimia Shoji Co. (Yokohama, Japan).

All cell culture supplies and collagenase type I were purchased from Invitrogen (Carlsbad, CA) unless otherwise noted. Human recombinant insulin, dexamethasone, pantothenate, biotin, 2,3-thiazolidinediones (TZD), 3-isobutyl-1-methylxanthine (IBMX) , bovine serum albumin (BSA), vascular endothelial growth factor (VEGF) and laminin from human placenta were also purchased from Sigma-Alrich (St. Louis, MO). Primary human adult microvascular endothelial cells and complete endothelial cell media (EGM-2MV) were purchased from Lonza (Walkersville, MD).

Spinner flask units were supplied by Bellco Glass Co (Vineland, NJ).

Histological solvents were purchased from Fisher Scientific (Pittsburgh, PA) and histological reagents were purchased from Sigma-Aldrich. Primary antibody for human CD31, and antibody diluent were purchased from Cell Signaling Technologies (Danvers, MA). The secondary antibody, ABC (avidin, biotin complex) kit, DAB substrate, hematoxylin counterstain and, antigen retrieval solution were purchased from Vector Labs (Burlingame, CA).

ELISA kits for human leptin were purchased from R& D Systems (Minneapolis, MN). Glycerol quantification kit was purchased from Sigma-Aldrich.

DNA content was assessed using the PicoGreen Assay Kit (Invitrogen). Trizol for RNA isolation was purchased from Invitrogen, and RNeasy Mini Kit to purify RNA was purchased from Qiagen (Valencia,CA). All other materials for PCR, and qPCR, including primers, were purchased from Applied Biosystems (Foster City, CA).

2.3.2 Coated Silk Scaffold Preparation

Silk solution was prepared as published[66]. Briefly, cocoons were chopped and placed in boiling 0.02M $NaCO_2$ for 30 minutes to remove sericin, and then washed 3 times in ultrapure water. The

resulting silk fibroin fibers were left to dry overnight. The dry silk was solubilized in 9.3 M LiBr in 20% w/v at 60°C for 4 hours. The silk solution was then dialyzed in ultrapure water in 3500 MWCO membrane for 2 days with a total of 6 water changes, to remove the LiBr. The aqueous silk solution was lyophilized until dry and re-solubilized over 2 days in hexafluoro-2-propanol (HFIP) at 17% w/v. Salt crystals were sieved to the desired range of 500-600 microns, poured into teflon coated petri dishes and either aqueous silk or HFIP-silk solution was added. The petri dish was covered and left in a fume hood for 2 days and, uncovered to let the HFIP evaporate for 1 day. The dish was immersed in methanol overnight, left in the fume hood for 1 day for the methanol to evaporate and then placed in water to leach out the salt particles. The water was changed 3 times a day for 2 days. The scaffolds were removed from the petri dish, cut to the desired dimension, 8 mm diameter x 4 mm height, using a biopsy punch. The scaffolds were left to dry before autoclaving, autoclaved, then kept at 4 C until use. The sterile scaffolds were first rehydrated in PBS, and then placed in 10 µg/mL sterile solutions of VEGF, Laminin, or VEGF+ Laminin for 15 minutes. This coating procedure was repeated twice, with the scaffolds left to soak up the remaining protein solution in the last coating and let to dry. The dry, coated scaffolds were placed into EGM-2MV media for 1 hour before seeding with cells.

2.3.3. Adipose Derived Stem Cell Isolation

Subcutaneous adipose tissue was obtained from abdominoplasties and approved under Tufts University IRB (Tufts University IRB Protocol #0906007) from Tufts Medical Center, Department of Plastic Surgery. No identifying information about the patient was obtained, including name, age, BMI, gender, or disease state and therefore only verbal consent was acquired. The specimens were kept at room temperature in saline and used within the same day. The adipose tissue was separated from the skin by blunt dissection and chopped. Chopped adipose tissue was placed into 50 mL conical tubes and minced well with scissors. The tissues were washed in equal volumes warmed PBS, until essentially free of blood. An equal volume of 1mg/mL collagenase I in 1% bovine serum albumin in PBS was added to the tissue and placed under gentle agitation at 37°C for 1 hour. The tissue samples were centrifuged at 300 x G for 10 minutes at room temperature. The supernatant containing the tissue was removed and the pellet resuspended in PBS and centrifuged at the same settings to remove the collagenase solution. The

pellet was resuspended in growth media and plated so that 70 g of initial tissue volume was plated per T225 cm^2 tissue culture flask. The attached cells are adipose derived stem cells.

2.3.4. Cell Culture and 3D Static Culture

Endothelial cells were cultured and expanded according to manufacturers' protocols. Adipose derived stem cells were expanded in growth media comprised of DMEM/F12, 10% FBS, 1% PSF until confluence. At 2 days post-confluence, the cells were switched to adipogenic induction media comprised of DMEM/F12, 3% PSF, 1% PSF, IBMX, TZD, dexamethasone, pantothenate, biotin and insulin until seeded on scaffolds. The endothelial cells were added in 3 x 20µl seedings with a total of 800,000 cells/ scaffold. The seeded scaffolds were placed in an incubator for 2 hours before media was added to the well. The induced ASCs were added in a similar manner after 1 week, but with 400,000 cells/scaffold. Cells and cultures were fed twice per week, and maintained in 37°C, humidified incubator.

The experiment timeline is outlined in figure 2.1.

2.3.5. Dynamic (Spinner Flask) Culture

Three days after seeding the induced ASCs the scaffolds were placed on stainless steel wires (2-3 per wire) and made to hang from the top of a 250 mL spinner flask. A total of 11 seeded scaffolds were contained per spinner flask. The rpm was set to 50 rpm for the duration of the experiment. Media was exchanged twice weekly from the side arms. The scaffolds were transferred to new spinner flasks every 4 weeks.

2.3.6. Media Sampling

Media was sampled once per week at the time the constructs were fed. Media samples were stored at -80 C until assayed.

2.3.7 Construct Harvest

Constructs were harvested at multiple timepoints for histology, DNA content and gene expression. For histological analyses, constructs were cut in half lengthwise, placed in formalin, and set aside for either cryo-sectioning or paraffin embedding. For DNA content and gene expression analyses, each construct was placed in the well of a 24 well plate, and chopped finely using micro-dissection scissors. 1 mL of Trizol or cell lysis buffer per sample was added and the plates were frozen at -80 C until assayed.

2.3.8. Histology

Constructs were processed according standard histology protocols. Formalin fixed samples were put through a series of dehydration solvents and finally paraffin using an automated tissue processor. Samples were embedded in paraffin, cut in 10 micron sections, and let to adhere on glass slides. The sections were rehydrated and stained with hematoxylin and eosin, or underwent antigen retrieval for immunohistochemistry. Non-specific binding was avoided by incubation with normal blocking serum. After the excess serum was removed, the sections were incubated for 30 minutes with anti-human mouse CD31 diluted 1:100 in antibody diluent. Sections were washed in PBS and, then incubated with a secondary anti-mouse antibody for 30 minutes. The sections were washed in PBS and then incubated with VECTASTAIN Elite ABC reagent for 30 minutes, washed in PBS, incubated with ImmPACT DAB enzyme substrate for 5 minutes and washed in water. The sections were then counterstained with hematoxylin and mounted.

To evaluate lipid accumulation, the formalin fixed constructs were embedded in OCT medium and frozen. The frozen blocks were cut in 10 micron sections, and then stained with Oil Red O.

2.3.9 Soluble Factors

Stored frozen media samples were thawed and immediately assayed according to manufacturer's protocols for both leptin quantification using an ELISA kit, and glycerol concentration using an enzymatic detection kit.

2.3.10 DNA content

Stored frozen lysates were thawed, centrifuged and assayed for DNA content using the PicoGreen Assay according to manufacturers' protocols.

2.3.11 Gene Expression

Scaffolds were finely chopped with micro-scissors; RNA was collected from cells using Trizol, and stored at –80°C until needed. After thawing, scaffolds were centrifuged at 15,700 *x G* for 10 min at 4°C. Supernatants were transferred to new tubes and RNA was isolated using the RNeasy kit according to the manufacturers' protocol. Reverse transcription was performed using high-capacity cDNA reverse transcription kit following manufacturers' protocol. Inventoried, commercially available TaqMan® Gene Expression Assays primers and probes from were used for target genes PPARγ, GLUT4, and normalized to the housekeeping gene, GAPDH, using the 2ΔΔCt formula.

2.3.12. Statistical Analysis

Samples for all quantifiable analyses were n= 4 with each biological replicate having technical duplicates. F-tests were used to determine variance equality and ANOVA tests were used to compare differences among groups. Histological analyses were performed at n=3, with 3 consecutive sections being taken per staining group, only representative images are shown.

2.4 RESULTS

Preliminary Experiments to Determine Scaffold Design

Preliminary 6 month 3D co-culture experiments were performed to determine which coating(s) would yield the best vascular adipose tissue like formation for long-term culture. Three coatings were evaluated as compared to uncoated scaffolds: laminin, VEGF, or laminin and VEGF. Laminin is a basement membrane protein that is involved in cell adhesion to matrix proteins.

VEGF is a potent angiogenic factor. Two scaffold processing windows were examined, those formed from aqueous or HFIP silk.

No significant differences were detected among different coatings or silk types when evaluating for gene expression of adipogenic and vasculogenic genes, or soluble factors, leptin and glycerol. However, when cultures were histologically examined for Oil Red O staining, the laminin coating yielded the best adipose like tissue. Laminin coated HFIP scaffolds contained the greatest amount of Oil Red O staining (results not shown). A VEGF coating yielded the poorest outcome, where fewer cells were present overall. From these results, our current study focused only on two coatings, uncoated and laminin coating on HFIP-silk scaffolds.

Constructs maintained size and shape over 6 month culture

For this study, it is crucial that the scaffold does not degrade in a short time frame but also necessary to maintain its size and shape while the cells have time remodel within. Constructs were evaluated for changes in size throughout the 6 month experiment (Figure 2.2). Constructs were also able to regain their original dimensions after applied pressure was released (Figure 2.2). At 1 and 6 months, the constructs were measured three times. At 1 month, both static and dynamic cultures averaged 8mm in diameter. At 6 months, the static constructs had remained at 8mm, while the dynamic cultures increased to 9mm in diameter (Figure 2.3).

DNA content increases at 1 month with dynamic culture

DNA content was evaluated to determine relative cell numbers over time (Figure 2.4). In both static and dynamic cultures, DNA content decreased from 1 to 6 months. When comparing static to dynamic cultures at 1 month, DNA content was 2 fold greater under dynamic conditions. Yet, by 6 months, there were no significant differences detected among any of the groups (static, dynamic, uncoated, and coated).

Constructs had improved tissue formation with dynamic culture

Over the 6 month culture period all groups accumulated lipid droplets, a hallmark of maturing adipocytes (Figures 2.5-2.6). Under static culture conditions cells were found only near the periphery of the construct at both 1 and 6 months. Under dynamic conditions, cells were found consistently throughout the entirety of the construct. Oil Red O positive staining appeared denser at edges of the constructs.

Constructs show continuous lumen formation

Endothelial cells were identified in the co-cultures by immunohistochemical staining for CD31. Endothelial cells develop into lumen- like structures in all groups (Figure 2.7). Initially, twice as many endothelial cells were seeded as hADs, however very few remain even after a couple of weeks in culture. Those that do survive are organized into lumen like structures and are continuous through more than 100 microns of tissue.

Adipogenic gene expression

Gene expression for common adipogenic genes was assessed. PPARγ is the major transcriptional regulator for adipogenesis, while GLUT4 is produced and translocated to the cell surface in maturing adipocytes in the presence of insulin. Both genes were upregulated early in the study when compared to the 1 month uncoated static control, with the greatest expression of both genes in the static laminin coated group at 1 month. After 6 months in culture, the gene expression levels for both genes had decreased in all groups, however, dynamic cultures have greater gene expression levels than their static controls. Under dynamic conditions, PPARγ levels are maintained, while GLUT4 expression increases.

Soluble factors increase under dynamic conditions but not significantly with coating or time

Leptin is an adipokine released by mature adipocytes. Glycerol is a product of lipolysis. Under the culture conditions here, mature adipocytes should be undergoing lipolysis because insulin (a hormonal mediator of lipolysis) is supplied in the co-culture media. Media samples were evaluated for leptin and glycerol production bi-weekly. Under static conditions, leptin levels at 1

and 6 months were not different (Figure 2.9). However, at 3 months the levels of leptin were nearly 2 fold greater than at 1 and 6 months. Under dynamic conditions, leptin levels were also not different from each other or from the static group at 1 and 6 months (Figure 2.10). A similar trend was seen where the leptin levels peaked at about 3 months and were nearly 3.5 fold greater than at 1 and 6 months. Glycerol levels also did not vary significantly over time under static conditions (Figure 2.11). However, there was a peak glycerol release at 3 months. Under dynamic conditions, glycerol levels increased nearly 2 fold from 1 to 6 months, but also peaked at 3 months (Figure 2.12). At 3 months, glycerol levels were more than 4 fold higher than at 1 month, and 2 fold greater than at 6 months ($p<0.001$). No significant differences were found between uncoated and laminin coated groups for either leptin or glycerol, therefore only laminin coated groups were shown.

2.5 DISCUSSION

The goal of this study was to develop a long-term vascular adipose tissue construct that would ultimately serve as the basis for studying adipose tissue dysfunction or soft tissue regeneration. In both cases, sustained structure is important. Our preliminary study determined that protein coating (laminin, VEGF) or silk scaffold (aqueous, HFIP) type did not have an effect on most adipogenic outcomes (soluble factors, gene expression). Histological observations demonstrated improved tissue formation and Oil Red O staining on laminin coated HFIP based scaffolds. HFIP based silk scaffolds have smoother pores when compared to aqueous based silk scaffolds[67]. Cell density and cytoskeletal forces influence stem cell commitment via the RhoA, ROCK pathways[68]. The HFIP scaffold pores are smoother and have less porosity within individual pore walls than the aqueous based and therefore cells are trapped within the pore with little ability to spread out and attach. We hypothesize that the smoothness of the pore walls leads to increased local cell density and therefore the cells do not experience much cytoskeletal tension, biasing them towards a more adipogenic program[68]. Alternatively, aqueous based scaffolds have rougher pore walls so the cells would experience more cytoskeletal tension and would likely better suited for osteogenic constructs. Additionally, laminin improved initial cell adhesion. Given these preliminary outcomes, we chose to continue following studies with laminin coated HFIP based

silk scaffolds.

Dynamic cultures were explored as a way to improve overall tissue outcomes as a result of enhanced mass transport. DNA content was not significantly greater in dynamic cultures over time as expected as a result of enhanced mass transport. An early increase was seen in dynamic cultures at 1 month, but it is not clear if that was the result of less cell survival in the static group, or increased proliferation of the dynamic group. Dynamic cultures contained tissue formation throughout the entire construct when compared to static groups where cells were found mostly at the periphery. In order for both static and dynamic cultures to have the same DNA content, the same number of cells must be present but just concentrated at the periphery in the static condition. This increased concentration of cells could partially explain why the static group had denser Oil Red O staining at the edge of the construct. All groups contained Oil Red O positive cells. In the dynamic groups, few areas were not positive for Oil Red O staining. Initially, the ratio of hADs to endothelial cells was 1:2, yet not many endothelial cells remained. This was evident with CD31 staining. Yet, the remaining CD31 positive cells were appropriately organized into lumen like formations. Several theories exist on why the endothelial cells did not survive well. In order to undergo sprouting and vasculogenesis, the cells need to be able to generate sufficient contractile forces and are better able to do this in softer matrices with fewer binding ligands[69]. It is likely that the silk scaffolds were too stiff to sustain endothelial cells. Another study found similar results to this study, independent of seeding ratio of ASCs:ECs, order of seeding, in co-cultures, endothelial cell numbers decrease quickly[70]. The stiffness of silk can be easily modified by varying processing parameters, however we need to be able to sustain the long-term degradation profile for this research, and often stiffness and degradation are inversely related. Therefore, increasing the laminin coating or coating with a silk gel may provide a softer substrate for the endothelial cells to feel.

Adipogenesis can only occur with *PPARγ* transcription, therefore it is crucial to have *PPARγ* expression in our cultures[17]. Since adipogenesis cannot be initiated without *PPARγ* expression, it is normally thought of as an early marker of adipogenesis, yet *PPARγ* is continuously expressed through various stages of adipogenesis[17]. Our results showed that expression was highest at 1 month under static conditions, and levels did not vary between dynamic groups. No systematic

study has been done, to our knowledge, on the effect of shear forces directly on adipogenesis. Shear forces may decrease or alter the ability of cells to upregulate *PPARγ* or to undergo adipogenesis at the same rate. *GLUT4* expression did increase, though not significantly, from 1 to 6 months under dynamic conditions. GLUT4 expression is a late marker of adipogenesis and is partially regulated by the presence of insulin, under dynamic conditions, the transport of insulin to the cells may be enhanced.

Leptin is an adipokine released by mature adipocytes which acts on receptors in the brain to signal satiation. Leptin is sensitive to glucocorticoid signaling[71]. Our media contains a constant level of dexamethasone, and therefore we except constant production of leptin if the number of adipocytes is constant. Similarly, glycerol release from lipolysis is also a function of mature adipocytes. Lipolysis is hormonally influenced by insulin as well as glucocorticoids. Our media contains constant levels of insulin and dexamethasone; therefore under normal culture conditions we expect the rate of lipolysis to be somewhat constant. Both leptin and glycerol levels increased with dynamic cultures, likely due to increased mass transport. In this study, we found fluctuations in leptin and glycerol levels at 3 months. No other studies to date, to our knowledge, have studied *in vitro* adipogenic outcomes for such long-term cultures, so it is unclear why we would see such a sharp change at that time. Taken into account with the decrease of DNA content, it is possible cells had ruptured if they had accumulated too much lipid, or had become apoptotic for other unknown reasons.

2.6 ACKNOWLEDGEMENTS

I wish to thank Jennifer Choi for all her advice in starting on adipose tissue engineering, Jeff Gimble for conversations on adipose derived stem cells and stem cell biology, Dean Glettig for conversations on adipose derived stem cells, 3D cultures and helping with stem cell isolation. I'd like to thank the undergrads working with me on projects closely related to this work- early in the project: Tina Jumani, Sorabh Kothari, Michael Schecht- all were helpful in getting the studies off the ground. I'd like to especially thank Aleksandar Mijailovic, who worked hard on trying to improve and understand the vascular portion and challenged me by asking all the right questions. We would like to thank the NIH P41 Tissue Engineering Resource Center for support.

2.7 FIGURES

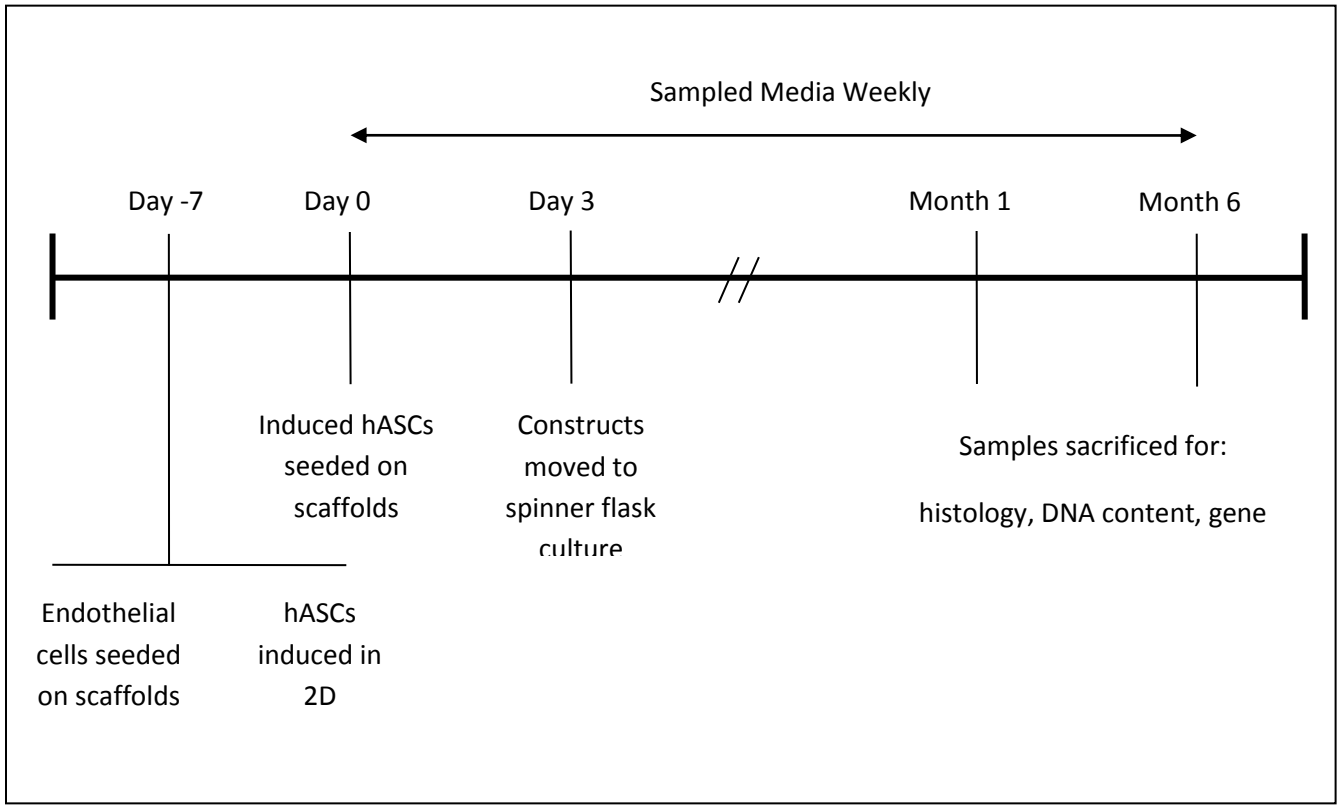

Figure 2.1- Experiment timeline for 6 month cultures**.**

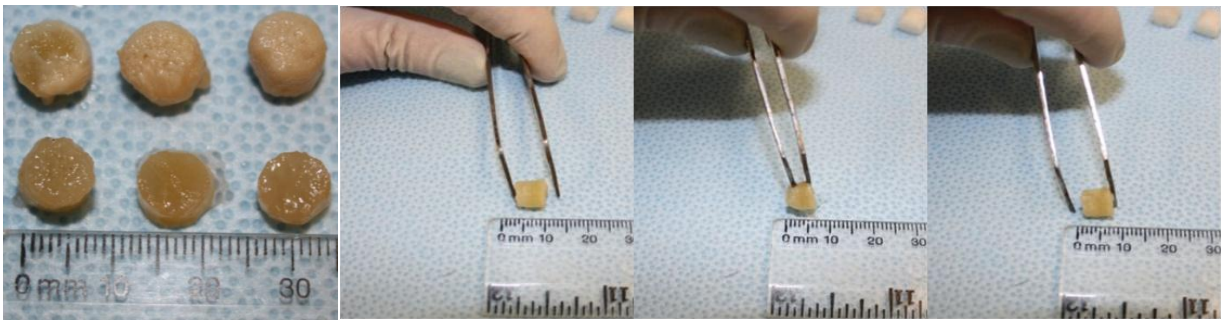

Figure 2.2- *Left panel*- Constructs maintain size and shape over 6 month culture period. Bottom row- static co-cultures. Top row- spinner flask cultures. *Right panel*- Constructs return to original dimensions after applied pressure is released.

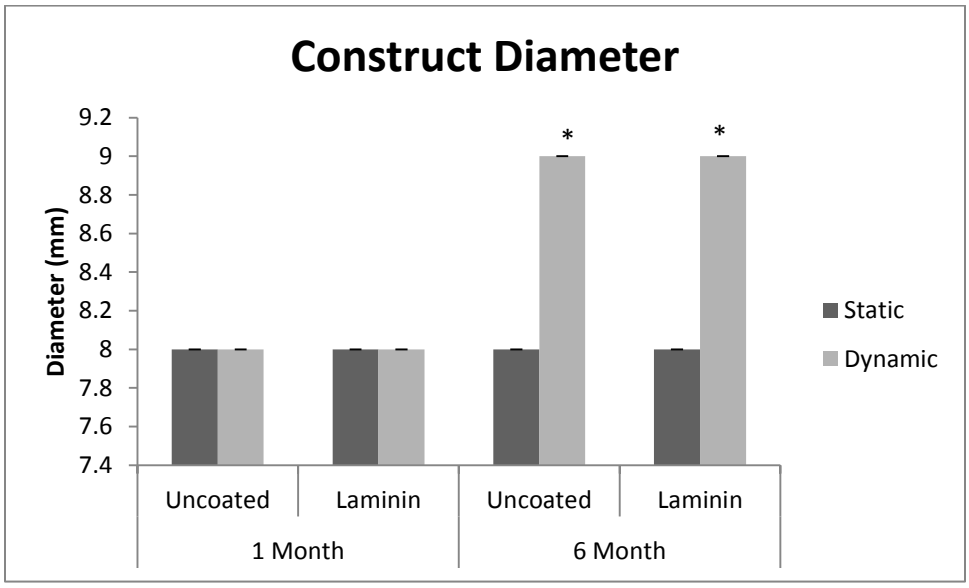

Figure 2.3- Dynamic cultures increased diameter by 1 mm over 6 month culture. Diameter change after 6 months in static or dynamic culture conditions. No differences were seen when scaffolds were coated with laminin, or with static culture over time. Star indicates significance of $p < 0.0001$.

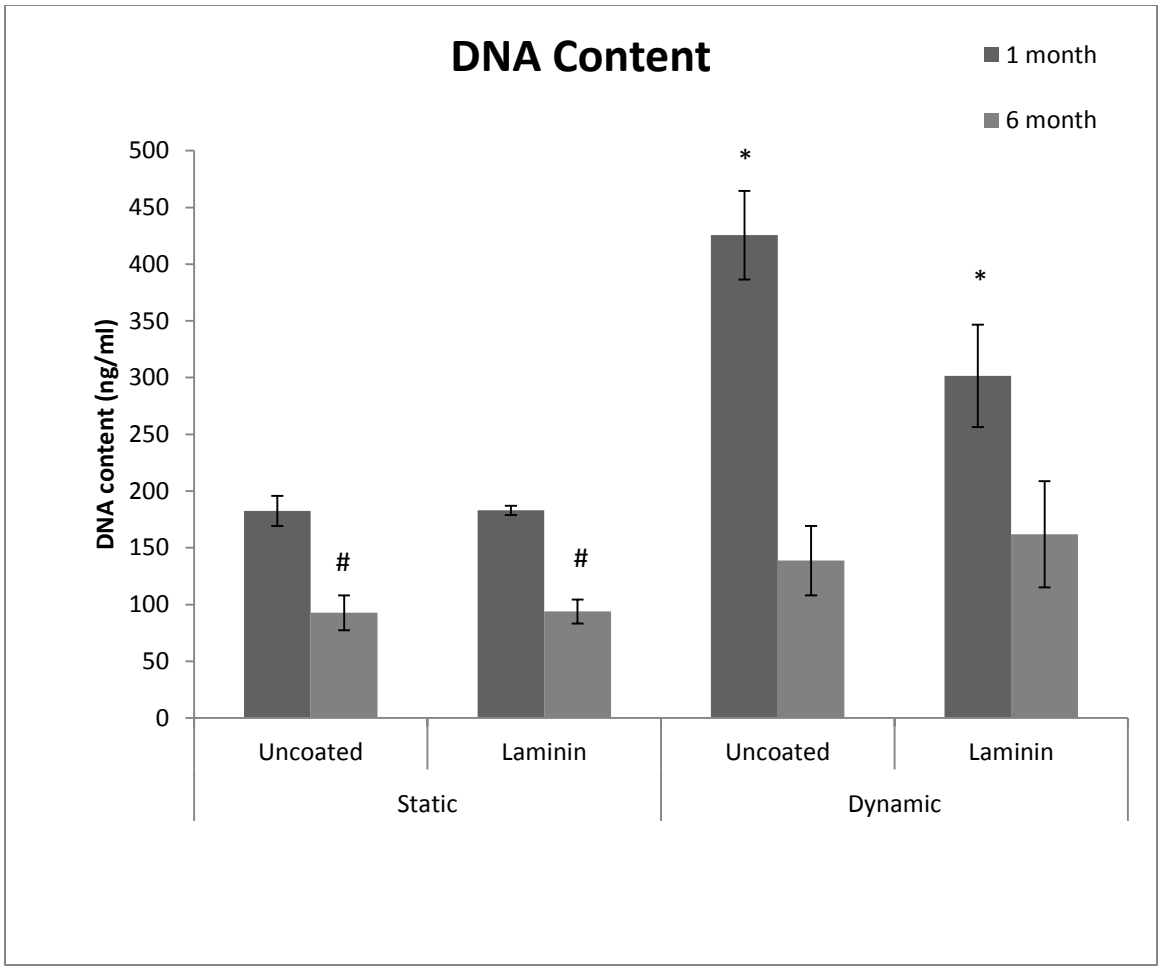

Figure 2.4- DNA content is not increased with long-term culture. At 1 month, dynamic cultures had greater DNA content when compared to the controls (static, uncoated group). By 6 months, static cultures had significantly less DNA content than controls. At 6 months, dynamic cultures did not have significantly different levels of DNA than the control group. * indicates significance of $p < 0.001$. # indicates significance of $p < 0.01$.

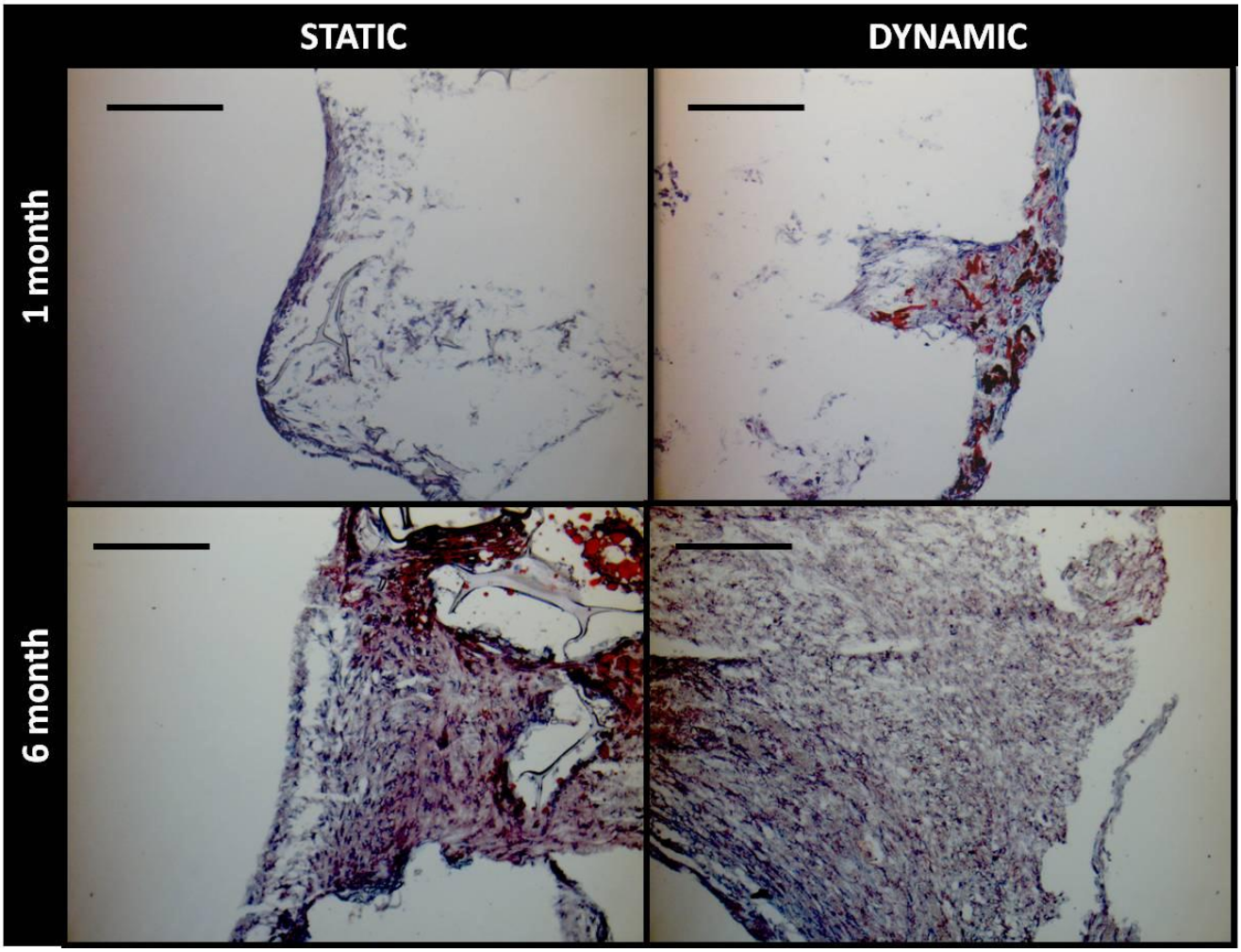

Figure 2.5- Dynamic culture improves overall tissue organization. Representative histological images of Oil Red O staining for mature adipocytes in uncoated scaffold group after 1 (top row) and 6 (bottom row) months in static (left column) and dynamic (right column) culture conditions. Staining for Oil Red O in static cultures was only found at the periphery of the construct, but found throughout construct in dynamic cultures. Scale bar – 200 microns.

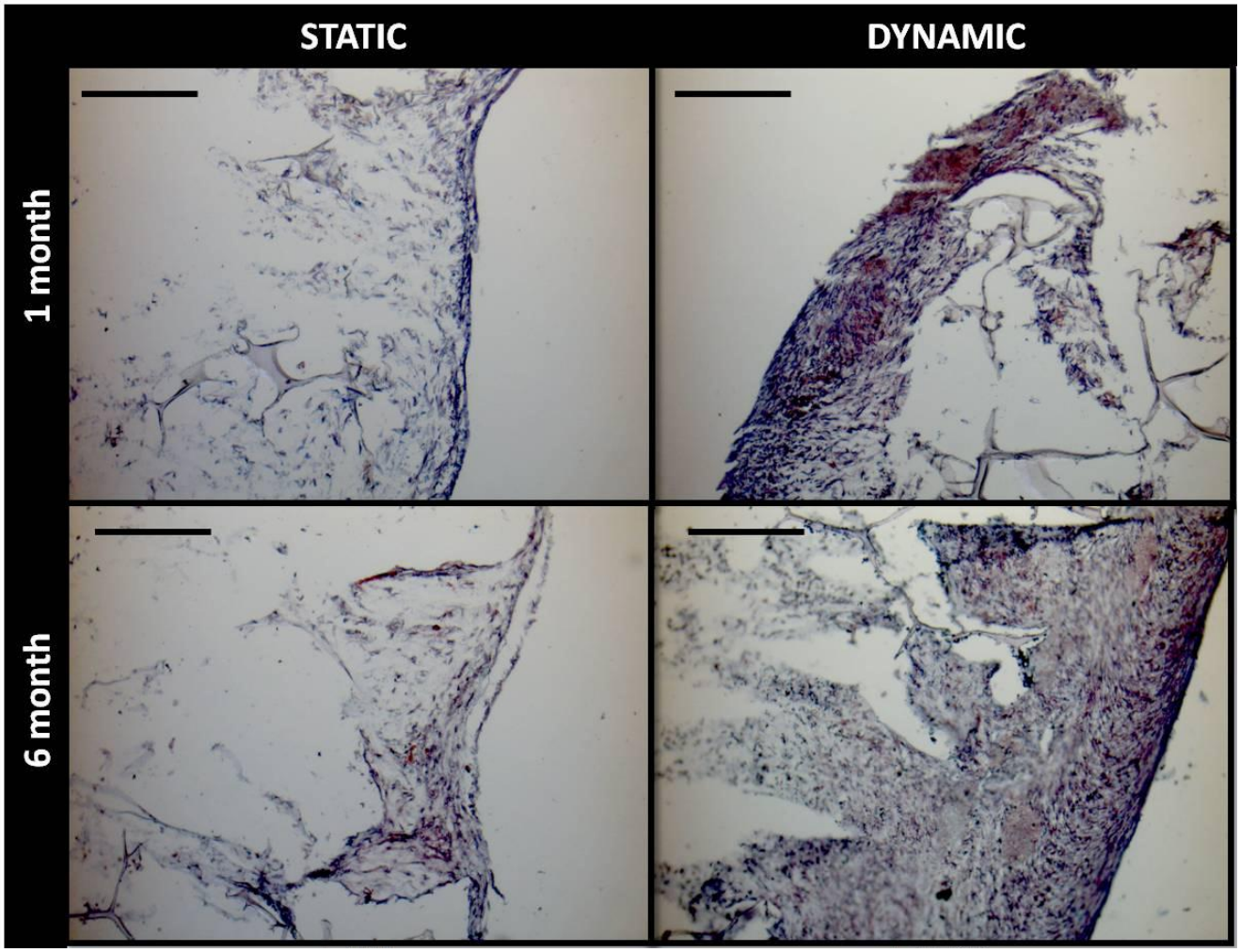

Figure 2.6- Dynamic culture improves overall tissue organization throughout construct over time. Representative histological images of Oil Red O staining for mature adipocytes in laminin coated scaffold group after 1 (top row) and 6 (bottom row) months in static (left column) and dynamic (right column) culture conditions. Similar to uncoated cultures, tissue presence and staining for Oil Red O in static cultures was only found at the periphery of the construct, but found throughout construct in dynamic cultures. Scale bar – 200 microns.

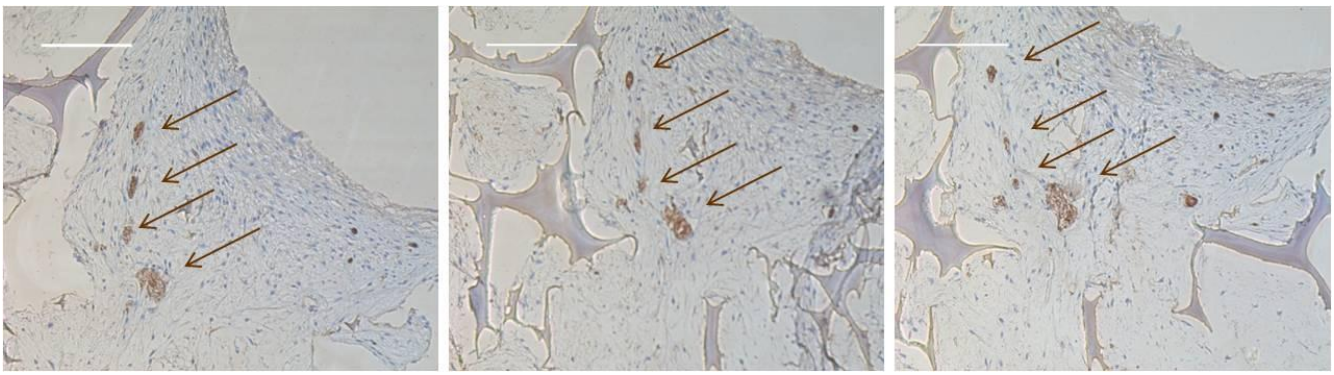

Figure 2.7- Endothelial cells organized into continuous lumen-like structures. Representative immunohistological images of CD31 staining for lumen formation in laminin coated scaffold group after 6 months in dynamic culture conditions. Same 4 lumens are tracked in sections 40 µm apart. Scale bar – 200 microns.

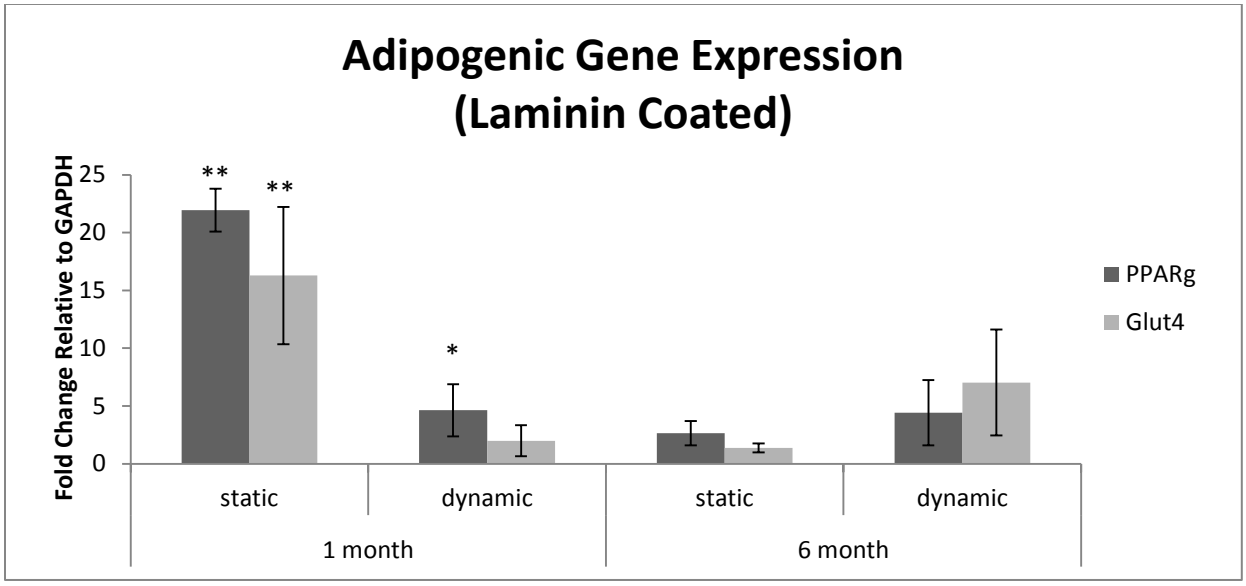

Figure 2.8- Adipogenic gene expression decreases over time. Gene expression levels for PPARγ and GLUT4 in laminin coated groups. Levels are relative to 1 month uncoated static control. At 6 months, dynamic cultures have higher gene expression levels than their static controls. Under dynamic conditions, PPARγ levels are maintained, while GLUT4 expression increases. * indicates significance $p < 0.05$, ** indicates significance $p < 0.01$.

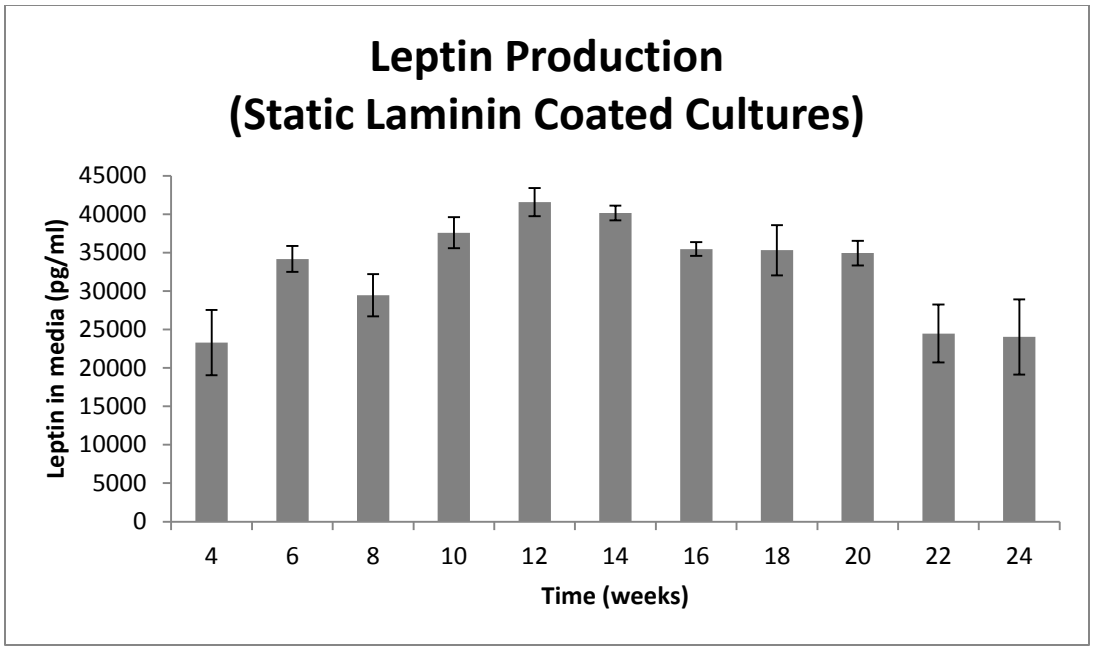

Figure 2.9- Leptin levels are maintained throughout static culture period. Leptin secretion peaks at 3 months, but no difference is present between 1 and 6 month time points.

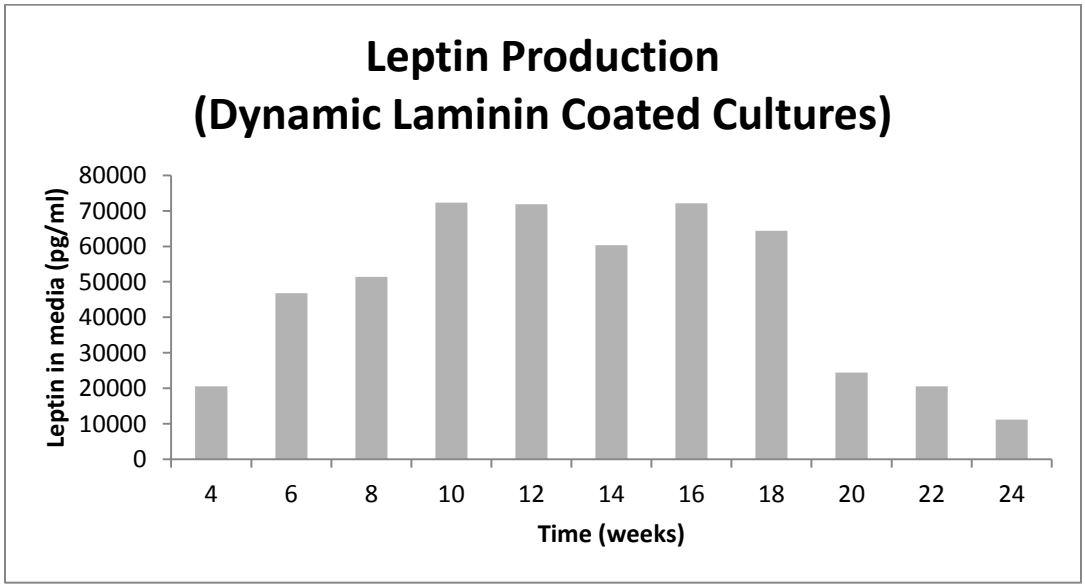

Figure 2.10- Leptin levels increase when cultured under dynamic conditions when compared to static cultures (Figure 2.9). The trends from static cultures are followed under dynamic conditions. No differences are seen when comparing 1 and 6 month cultures; however the peak level is at 3 months. NOTE: Error bars are not included in dynamic cultures as all constructs in one group were maintained in the same spinner flask and therefore we cannot decouple each individual construct contribution from the groups'.

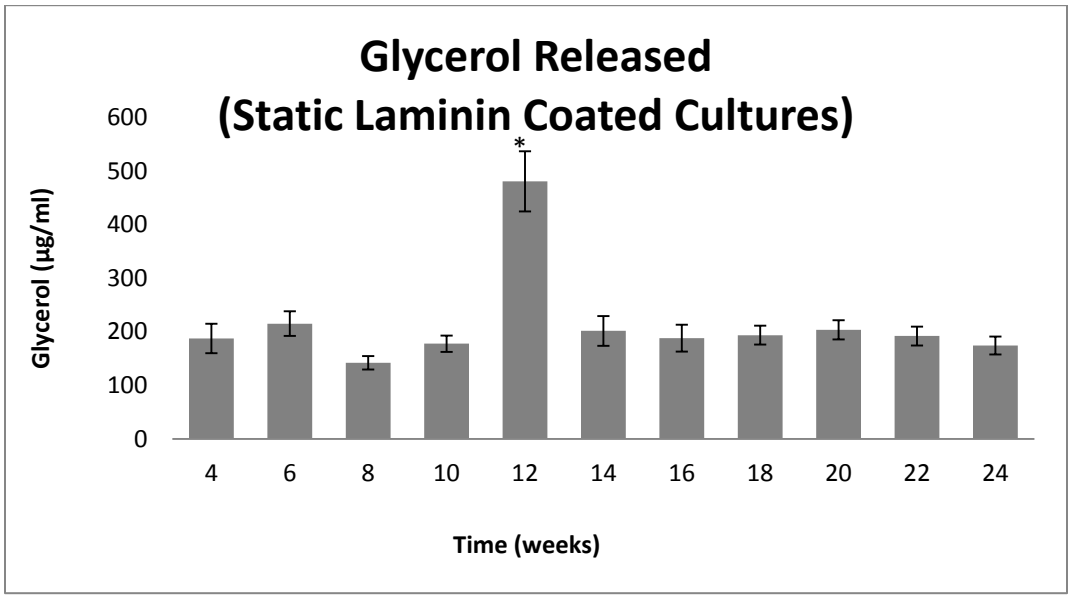

Figure 2.11- Glycerol levels remain stable over time. Glycerol levels were not different at 1 and 6 months, but peaked at 3 months. * indicates significance level of $p < 0.001$ across timepoints.

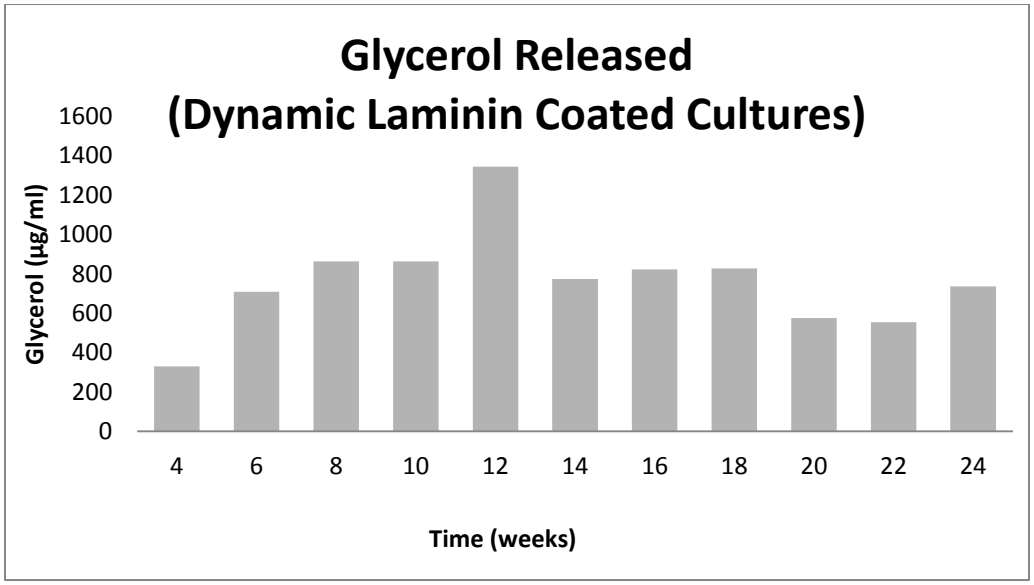

Figure 2.12- Glycerol levels increase with dynamic culture conditions. Levels increased nearly 2 fold from 1 to 6 months with a peak at 3 months. NOTE: Error bars are not included in dynamic cultures as all constructs in one group were maintained in the same spinner flask and therefore we cannot decouple each individual construct contribution from the groups'.

CHAPTER 3. CHRONIC INFLAMMATION OBESITY DISEASE MODEL

3.1 ABSTRACT

Obesity is a growing epidemic worldwide. The WHO estimates about 200 million men and 300 million women were obese in 2008, or about $1/10^{th}$ of the world population being obese. Obesity is a risk factor for other noncommunicable diseases, such as diabetes, cancer, and cardiovascular disease. Calorie rich foods and an increasingly sedentary lifestyle are thought to be the biggest contributions to this worldwide epidemic. Obesity is characterized by a chronic inflammation of the adipose tissue. In this study, we developed a long-term chronic culture of inflamed adipose tissue, using a co-culture of adipocytes/endothelials cells, which are then exposed to dietary free fatty acids and monocytes. Inflammatory marker profiles, MCP-1, TNFα, Il-6, COX-2 and adipose marker profiles, leptin, adiponectin, PPARγ, FABP, were altered by the presense of fatty acids and monocytes. Adiponectin, an adipokine associated with a heathly metabolic profile became undetectable in these chronic cultures. We treated the inflamed cultures with 2 different therapeutics, wogonin, a COX-2 inhibitor, and conjugated linoleic acid, and found that wogonin was generally more effective in reducing inflammatory response in cultures exposed to fatty acids and monocytes. These data suggest that the inflammatory cells should be a target of future anti-obesity therapies.

3.2 INTRODUCTION

The World Health Organization (WHO) broadly defines those individuals who have a body mass index of greater than 30 to be obese (WHO | Obesity, 2012). Obesity is a risk factor for other noncommunicable diseases, such as diabetes, cancer, and cardiovascular disease. Obesity affects people of all ages, races, and socio-economic statuses. The WHO estimates about 200 million men and 300 million women were obese in 2008, or about $1/10^{th}$ of the world population being obese. As of 2010, about 43 million children under the age of 5 were classified as being overweight (BMI: 25-30), where 35 million lived in developing countries and 8 million in developed countries. The epidemic attributes more deaths to being overweight rather than underweight. In the US alone, the medical costs associated with obesity are $147 billion (Obesity and Overweight for Professionals: Data and Statistics: Adult Obesity, 2012).

Behavior, environment and genetic factors all are contributing factors to this epidemic. However, in its simplest form, one can define the cause of obesity to be in the balance of energy in versus energy out, where the balance is shifted towards taking more energy in. Calorie rich foods and an increasingly sedentary lifestyle are thought to be the biggest contributions to this worldwide epidemic.

Obesity is characterized by a chronic inflammation of the adipose tissue. In a healthy state, FAs and glucose are able to be taken up and stored, until needed, as triglycerides within the adipocyte. In the presence of increased dietary stimuli in the form of FAs, the adipocyte attempts to store the FA as TG in the lipid droplet by lipogenesis. However, as the lipid droplet expands the cell experiences cytoskeletal stresses. This causes the release of macrophage chemokines, which cause macrophage infiltration and a local inflammatory response and of MMPs, that breakdown the surrounding matrix to allow for continued growth. It is not well understood what role exactly the ECM breakdown and remodeling plays, whether it is more of a cause or effect for obesity[18,19]. Infiltration of macrophages leads to the release of inflammatory cytokines, such as TNFα and Il-6. TNFα, among other factors, can directly influence lipolysis rates by cAMP phosphorylation of HSL[20–22]. TNFα also acts to impair PPARγ transcription, which can suppress lipogenesis in mature adipocytes and suppress adipogenesis in resident pre-adipocytes. This elevates levels of circulating TG, ultimately leading to ectopic lipid droplets in muscle and liver[20]. TNFα, along with the increase in FAs from enhanced lipolysis and diet, contribute to further aggravation of the inflammatory cycle via the classic innate immune pathway, Toll-Like Receptor 4 (TLR4). Animal models of TLR4 knockdown leads to decreased levels of inflammatory markers and maintenance of insulin sensitivity, while in wild-type animals the downstream activation of FA-TLR4 leads to release of TNFα, Il-6 and insulin resistance[23]. TLR4 is found on both macrophages and adipocytes. The inflammation continues to cycle if left untreated (or without changes in diet) to eventually lead to insulin resistance, type II diabetes, ectopic lipid droplets, and cardiovascular disease.

Various types of therapies exist to reduce obesity. For those considered “morbidly” obese, diet and exercise and/or pharmacological interventions are not often enough, and require surgical intervention as a last option. Bariatric surgery often leads to various nutrient deficiencies due to

modified absorption[72]. There are four main classifications of obesity pharmacological based therapies[10,73]. They are appetite suppressants, gastrointestinal absorption blockers, metabolism stimulators which decrease lipogenesis, and enhancers of energy expenditure which increase lipid oxidation or thermogenesis[10,73]. The first approach, appetite suppression acts on the central nervous system to tell the brain that the body is satiated. This approach has had little pharmacological success due to unsafe side effects leading to FDA recalls (for review of anti-obesity drugs recalled by FDA see Powell et al.[74]). Gastrointestinal absorption blockers, such as Orlistat™, have met some success. Orlistat™ works by inhibiting pancreatic lipases, so that fats are not absorbed but passed. However, this approach could prevent the absorption of fat-soluble vitamins. The third approach relates more specifically to adipose tissue metabolism. 1-acyl-glycerol-3-phosphate acyltransferase (AGPAT) inhibitors and diacylglycerol acyltransferase (DGAT) inhibitors can disrupt the TG synthesis pathway at different steps and are under study as potential therapeutics[10]. Interventions that increase energy expenditure or brown fat activation, such as acetyl-coA carboxylase (ACC) inhibitors, increase the rate of mitochondrial fatty acid β-oxidation and heat production[10]. This approach has become of more interest lately with the discovery of cold-activated brown fat depots in adult humans[75].

In the past decade, two other mechanisms to reduce adipose tissue have become of interest. One potential therapeutic avenue involves replacement of gut microflora, however, it is unclear whether the gut microbiome is the cause or an effect of obesity[76,77]. Another new therapeutic avenue involves treating obesity or excess adipose tissue as a "tumor" that will shrink upon ablation of vasculature[78–80]. Both new approaches offer fresh insight to the existing problem but will need to be researched in more depth before they can be used clinically.

Currently, obesity disease *in vitro* models which focus on adipose tissue primarily look at simple 2D cultures of adipocytes[81,82]. A hallmark of obesity is adipocyte hypertrophy[83–86]. This central feature of obesity renders 2D models unrealistic for two reasons. Firstly, mature adipocytes cannot be cultured *in vitro* because they are too lipid-laden and rupture or float[87,88]. To address this, studies are performed on pre-adipocytes that are differentiated *in vitro*, however, the differentiated cells are multilocular (containing many lipid droplets) cells that do not fully represent a mature, unilocular (a central lipid droplet) adipocyte[89]. Secondly, the cell-matrix interaction cannot be mimicked in a 2D study[89–93]. For example, as an adipocyte expands, as in

obesity, the cell secretes factors to degrade the surrounding ECM, making more room for the adipocyte to expand[94].

Animal models of obesity have been instrumental in our understanding of key roles of adipose tissue in this disease by accounting for much of the complexity of such pathology[95–101]. Obesity can be studied within many contexts, for example, gender, age, or in the context of other pathologies- cardiovascular disease, diabetes, or liver disease. Animal models have led to the discovery of leptin, a key adipocytokine[102,103]. Leptin knockout models caused extreme obesity, hyperphagia (excessive ingestion of food) and many other metabolic diseases[102,103]. When leptin levels were restored, animals returned to normal weights[102,103]. Other knockout models that partially or completely ablate adipose tissue led to the understanding of the adipose tissue mass and insulin resistance. Despite the vast knowledge obtained through rodent models, the need for a viable human model still exists because of disparities between the two species[104]. For example, a mouse study identified the *FTO* gene as a target for obesity and fat mass accumulation[105]. When this gene was further explored in humans, it was discovered that altering that gene causes webbed digits among other deformities[106].

Given the short-comings of 2D *in vitro* cultures and *in vivo* rodent models of obesity, we need a 3D human disease model to fill the gaps left behind. A 3D tissue engineered model allows us to use human cells, even a patient's own cells, in appropriate tissue architecture. Some groups have included macrophages and few have included endothelial cells to study the cross-talk between cells in their 2D studies[82]. To our knowledge, no other group has explored using 3D vascular adipose tissue cultures with macrophages to understand the more complex cell-cell, cell-matrix interactions that can affect tissue outcomes. Another important benefit of the 3D disease model is the option to culture for indefinite periods[107]. This allows us to test the long-term effects of a therapeutic system. Our group has shown that we can successfully develop 3D adipocyte/endothelial co-cultures on silk porous sponges which express adipogenic outcomes[16]. Furthermore, we have shown that we can alter the lipolytic rates of these systems by exposure to different hormonal stimuli[108,109]. This work seeks to build off that work in three ways: 1) by the

inclusion of macrophages, the major inflammatory cells in adipose tissue, 2) by the inclusion of dietary FFAs, to stimulate an overfed condition, and 3) by extending the culture period to better mimic a chronic state.

As described earlier, many anti-obesity therapies are under study currently. Cyclooxgenase-2 (COX-2) mediates inflammation by production of soluble inflammatory messengers, prostaglandins. COX-2 derived prostaglandins are implicated in adiposity, by directly activating to PPARγ, the master transcriptional regulator of adipogenesis[110]. COX-2 deficient mice have a lower body weight, lower % body fat, lower serum glucose, TG, cholesterol levels than wild type mice, while consuming the same amount of food[110]. COX-2 deficient mice also have lower levels of PPARγ, lipoprotein lipase (LPL), and increased levels of preadipocyte factor (Pref-1) and resistin[110]. Inflammatory markers, CD68 and MCP-1, were also dramatically reduced in COX-2 deficient mice[110]. Other groups have reported similar outcomes for COX-2 mediated decreases in adiposity and inflammation[111,112]. COX-2 selective inhibitors, such as Vioxx™, have been used clinically for rheumatoid arthritis, but have been recalled due to cardiovascular complications[113]. However, a class of antioxidant natural products, flavonoids has been found to be selective COX-2 inhibitors, without the side effects seen in non-steroidal anti-inflammatory drugs (NSAIDs) such as Vioxx™[114–116]. Although both NSAIDs and flavonoids inhibit COX-2, the former are thought to cause platelet adhesion, while flavonoids and their metabolites act as anti-aggregating factors for platelets and are actually considered to lower cardiovascular risk[117]. A flavonoid, Wogonin, from *Scutellaria* root, will be explored in this study as an anti-inflammatory therapy.

Another natural therapeutic that will be investigated in this study is conjugated linoleic acid (CLA). CLA is a polyunsaturated fatty acid found in sunflower oil and in meat from ruminant animals, after their gut microbiota covert linoleic acid to CLA by hydrogenation[118]. Several mechanisms are possible for anti-obesity effects seen in rodents and human due to CLA, including increased basal lipolysis rates, fatty acid oxidation and PPARγ inhibition[98,104,118–121]. Two groups report CLA improved anti-obesity outcomes when CLA is supplemented with saturated but not unsaturated fats[120,121].

In this study, we aim to develop a long-term 3D model of inflamed human adipose tissue by first developing a healthy model of adipose tissue as a co-culture of primary adipocytes and

endothelial cells on a silk matrix and then challenging the system with monocytes and dietary free fatty acids. Next, we aim to use the system to test two potential anti-obesity therapies.

3.3 METHODS

3.3.1 Materials

Bombyx mori silkworm cocoons were supplied by Tajimia Shoji Co. (Yokohama, Japan).

All cell culture supplies and collagenase type I were purchased from Invitrogen (Carlsbad, CA) unless otherwise noted. Human recombinant insulin, dexamethasone, pantothenate, biotin, 2,3-thiazolidinediones (TZD), 3-isobutyl-1-methylxanthine (IBMX) , bovine serum albumin (BSA), were purchased from Sigma-Alrich (St. Louis, MO). Primary human adult microvascular endothelial cells and complete endothelial cell media (EGM-2MV) were purchased from Lonza (Walkersville, MD).

Histological solvents were purchased from Fisher Scientific (Pittsburgh, PA) and histological reagents were purchased from Sigma-Aldrich. Primary antibodies were purchased from Abcam (Cambridge, MA), and antibody diluent was purchased from Cell Signaling Technologies (Danvers, MA). The secondary antibody, ABC (avidin, biotin complex) kit, DAB substrate, hematoxylin counterstain and, antigen retrieval solution were purchased from Vector Labs (Burlingame, CA). The multiplex ELISA assay kit was purchased from Millipore (Danvers, MA).

3.3.2 Silk Scaffold Preparation

Silk solution was prepared as published[66,122]. Briefly, cocoons were chopped and placed in boiling 0.02M NaCO2 for 30 minutes to remove sericin, and then washed 3 times in ultrapure water. The resulting silk fibroin fibers were left to dry overnight. The dry silk was solubilized in 9.3 M LiBr in 20% w/v at 60 C for 4 hours. The silk solution was then dialyzed in ultrapure water in 3500 MWCO membrane for 2 days with a total of 6 water changes, to remove the LiBr.

The aqueous silk solution was lyophilized until dry and re-solubilized over 2 days in hexafluoro-2-propanol (HFIP) at 17% w/v. Salt crystals were sieved to the desired range of 500-600 microns, poured into Teflon coated petri dishes and either aqueous silk or HFIP-silk solution was added. The petri dish was covered and left in a fume hood for 2 days and, uncovered to let the HFIP evaporate for 1 day. The dish was immersed in methanol overnight, left in the fume hood for 1 day for the methanol to evaporate and then placed in water to leach out the salt particles. The water was changed 3 times a day for 2 days. The scaffolds were removed from the petri dish, cut to the desired dimension, 4 mm diameter x 2 mm height, using a biopsy punch. The scaffolds were left to dry before autoclaving, autoclaved, then kept at 4°C until use. The dry scaffolds were placed into EGM-2MV media for 1 hour before seeding with cells.

3.3.3 Adipose Derived Stem Cell Isolation

Subcutaneous adipose tissue was obtained from abdominoplasties and approved under Tufts University IRB (Tufts University IRB Protocol #0906007) from Tufts Medical Center, Department of Plastic Surgery. No identifying information about the patient was obtained, including name, age, BMI, gender, or disease state and therefore only verbal consent was acquired. The specimens were kept at room temperature in saline and used within the same day. The adipose tissue was separated from the skin by blunt dissection and chopped. Chopped adipose tissue was placed into 50 mL conical tubes and minced well with scissors. The tissues were washed in equal volumes warmed PBS, until essentially free of blood. An equal volume of 1mg/mL collagenase I in 1% bovine serum albumin in PBS was added to the tissue and placed under gentle agitation at 37°C for 1 hour. The tissue samples were centrifuged at 300 x g for 10 minutes at room temperature. The supernatant containing the tissue was removed and the pellet resuspended in PBS and centrifuged at the same settings to remove the collagenase solution. The pellet was resuspended in growth media and plated so that 70 g of initial tissue volume was plated per T225 cm^2 tissue culture flask.

3.3.4 Monocyte Isolation

Monocytes were isolated freshly from peripheral blood as previously described[123]. Blood was drawn into vacutainers containing sodium citrate. Twenty mL of blood was diluted with 6 mL of PBS with 1mM EDTA and split among 2 50 mL conicals. The diluted blood was slowly underlayered with 10 mL Percoll. The blood was then centrifuged at 400 x *g* for 20 min at room temperature with no brake.

The peripheral blood mononuclear cells (PBMCs) appeared as a white band above the red blood cell and granulocyte layer was collected. DPBS with 1mM EDTA was added to the collected banded PBMCs to dilute it and was then centrifuged at 150 x *g* for 10 min at room temperature with no brake in order to remove the platelets in the supernatant. The pellet containing the PBMCs was then resuspended in 40mL of DPBS w/ 1mM EDTA and centrifuged again at 150 x *g* for 10 min to remove any remaining platelets. The cells were then diluted with monocyte media to yield a concentration of 1 million cells/mL of media. Using an equal volume of 46% Percoll™, the monocyte containing media was underlayered by the 46% Percoll™ at a rate of 25mL/75 seconds. The tube was then centrifuged for 30 min at 550 x *g* at RT with no brakes. The white band formed at the interface between the lower and upper gradients was the monocytes. They were removed, resuspended in 17mL of ice cold DPBS w/ 1mM EDTA and then centrifuged at 400 x *g* for 10 min at RT and the pellets were resuspended in 7 mL of ice cold DPBS (no EDTA) and split accordingly for seeding.

3.3.5 Cell Culture and 3D Culture

Endothelial cells were cultured and expanded according to manufacturers' protocols. Adipose derived stem cells were expanded in growth media comprised of DMEM/F12, 10% FBS, 1% PSF until confluence. At 2 days post-confluence, the cells were switched to adipogenic induction media comprised of DMEM/F12, 3% PSF, 1% PSF, IBMX, TZD, dexamethasone, pantothenate, biotin and insulin until seeded on scaffolds. The endothelial cells were added in 3 x 10ul seedings with a total of 100,000 cells/ scaffold. The seeded scaffolds were placed in an incubator for 2 hours before media was added to the well. The induced ASCs were added in a similar manner after 1 week, but with 50,000 cells/scaffold. Cells and cultures were fed 2 times per

week, and maintained in 37°C, humidified incubator. After 6 weeks of 3D co-culture of endothelial cells and adipocytes, the cultures were subjected to free fatty acids. The monocytes were added the same day as the free fatty acids.

3.3.6 Free Fatty Acid Media

FFA media was prepared by first dissolving palmitic acid, stearic acid in pure ethanol for a final concentration of 0.5 M. Basal media was made by dissolving 11 g FFA-free bovine serum albumin (BSA) into 500 mL DMEM-F12. The 0.5M stock solution of FFA was added dropwise to the BSA containing media, such that the final concentration of FFA in basal media was 0.2mM. The adipogenic supplements were added as described previously and then added to an equal volume of endothelial media, such that the final concentration of FFA in media was 0.1mM.

Oleic acid was purchased pre-mixed with BSA and therefore was added directly to the adipogenic media and mixed with the equal volume of endothelial media.

3.3.7 Drug Treatment

CLA was prepared by dissolving CLA in DMSO for a final concentration of 180mM. The CLA stock solution was added to the adipogenic media containing FFA, mixed with an equal volume of endothelial media, so that the final concentration of CLA was 25µM. Wogonin was prepared by dissolving wogonin in DMSO, and prepared as CLA, so that the final concentration of wogonin was also 25µM.

All media was sterilized by passing through a 0.2 micron filter.

3.3.8 Experiment timeline (Figure 3.1)

The adipocyte/endothelial co-cultures were cultured under normal conditions, in a 1:1 ratio of adipogenic maintenance: endothelial cell media, for 6 weeks to establish a healthy tissue construct. The healthy 6 week constructs were transferred to media containing 0.1 mM FFAs, no FFA (control), palmitic acid, stearic acid, or oleic acid, and cultured for an additional 6 weeks to generate an overfed model. Also at this time, freshly isolated monocytes were added to the cultures. After 6 weeks culture with monocytes and FFAs the cultures were treated with Wogonin, CLA, or left untreated.

3.3.9 Construct Harvest

Constructs were harvested at multiple timepoints for histology. The constructs were cut in half lengthwise, placed in formalin, and set aside for either cryo-sectioning or paraffin embedding.

3.3.10 Histology

Constructs were processed according standard histology protocols. Formalin fixed samples were put through a series of dehydration solvents and finally paraffin using an automated tissue processor. Samples were embedded in paraffin, cut in 10 micron sections, and let to adhere on glass slides. The sections were rehydrated and stained with hematoxylin and eosin, or underwent antigen retrieval for immunohistochemistry. Non-specific binding was avoided by incubation with normal blocking serum. After the excess serum was removed, the sections were incubated for 30 minutes with the primary antibody. Sections were washed in PBS and, then incubated with a secondary anti-mouse antibody for 30 minutes. The sections were washed in PBS and then incubated with VECTASTAIN Elite ABC reagent for 30 minutes, washed in PBS, incubated with ImmPACT DAB enzyme substrate for 5 minutes and washed in water. The sections were then counterstained with hematoxylin and mounted.

To evaluate lipid accumulation, the formalin fixed constructs were embedded in OCT medium and frozen. The frozen blocks were cut in 10 micron sections, and then stained with Oil Red O.

3.3.11 Multiplex Bead Assay

Media samples were collected weekly and stored at -80°C until assayed. Samples were allowed to thaw and incubated with antibody-immobilized microbeads. The beads were conjugated with MCP-1, TNFα, Il-6, Leptin, and Adiponectin. The assay was performed according to manufacturer's (Millipore Human Adipocyte Plate Assay) protocol.

3.3.12 Gene Expression

Scaffolds were finely chopped with micro-scissors; RNA was collected from cells using Trizol, and stored at –80°C until needed. After thawing, scaffolds were centrifuged at 15,700 *x g*for 10 min at 4°C. Supernatants were transferred to new tubes and RNA was isolated using the RNeasy kit according to the manufacturers' protocol. Reverse transcription was performed using high-capacity cDNA reverse transcription kit following manufacturers' protocol. Inventoried, commercially available TaqMan® Gene Expression Assays primers and probes from were used for target genes, and normalized to the housekeeping gene, GAPDH, using the 2ΔΔCt formula.

3.3.13 Statistical Analysis

Samples for all quantifiable analyses were n= 6 with each biological replicate having technical duplicates. F-tests were used to determine variance equality and ANOVA tests were used to compare differences among groups.

3.4 RESULTS

Effect of fatty acids and monocytes on soluble factors

The goal of this work is develop a long-term model of obesity that could serve as a model to study disease mechanisms and as a platform for testing anti-obesity therapies. After developing a healthy model of adipose tissue we exposed the tissue to FFAs and monocytes for 6 weeks. At the end of this period, we assessed the cultures for soluble factors released into the media (Figure

3.2). MCP-1 levels increased in the presence of the saturated fat, palmitic acid, but there was no difference in levels when monocytes were present. Il-6 was also elevated in the presence of palmitic acid, and did increase when monocytes were present. TNFα levels were not detected when cultures did not contain FFAs and monocytes. Levels were elevated but not significantly when monocytes were present. Adiponectin, an adipokine found to be decreased in serum during obesity was found to be decreased in the presence of all FFAs, a further decrease was seen when monocytes were presence[124]. Leptin, an adipokine found to be increased in serum during obesity, was found to be unaffected by FFA or monocytes.

After an additional 6 weeks culture with FFA and monocytes, TNFα and adiponectin levels were not detected. Levels of MCP-1 decreased from 6 to 12 weeks ~ 3 fold in groups without FFAs, and ~ 4 fold when cultured with palmitic acid (Figure 3.3). Levels of Il-6 also decreased significantly over time in the palmitic acid group, ~10 fold without monocytes, and ~ 30 fold with monocytes. Il-6 levels for oleic and stearic acid did not change over time. Leptin levels in the presence of palmitic acid decreased ~2 fold regardless of the presence of monocytes. When no FFAs were present, leptin levels increased almost 2 fold without monocytes present and decreased ~2 fold in the presence of monocytes.

Effect of anti-obesity therapies on soluble factors

One day after being exposed to no treatment control, wogonin or CLA, media samples were analyzed. Similarly to 12 week cultures, TNFα and adiponectin levels were not detectable. Wogonin, a selective COX-2 inhibitor, and CLA , whose mechanisms are still unclear, decreased levels of MCP-1 in the presence of monocytes (Figure 3.4). Il-6 levels did not appear to be affected by either of the therapies. Wogonin treatment decreased leptin levels when cells were cultured with monocytes. CLA did not appear to have a notable effect on leptin levels.

COX-2 levels increase with time with wogonin treatment

COX-2 expression specifically inhibited by wogonin via NF-κB and nitric oxide pathways, yet in our gene expression studies, we found that COX-2 expression increased with increased wogonin

exposure (Figure 3.5).

Adipogenic genes expression with wogonin treatment

PPARγ is the master transcriptional regulator of adipogenesis and is specifically inhibited by TNFα. In this study, PPARγ levels increased over time (Figure 3.6). Gene expression levels for fatty acid binding protein 4 (FABP) were evaluated. In the presence of palmitic acid and monocytes, FABP levels were upregulated nearly 600 fold (Figure 3.6). When monocytes were not present, FABP levels were lower, but increased over the 6 week period.

Histology
Pending

3.5 DISCUSSION

The goal of this work is develop a long-term model of obesity that could serve as a model to study disease mechanisms and as a platform for testing anti-obesity therapies. Three dietary fatty acids were used in this study, palmitic acid, stearic acid, and oleic acid. Palmitic acid was chosen as it is a common dietary saturated fat. Oleic acid is an unsaturated fat, considered to be part of a healthy diet and can be found in olive oil. Stearic acid is another saturated fat, but has the same number of carbons as oleic acid. Saturated fats have been well established as being pro-inflammatory[120,125,126]. They are also less efficiently oxidized and therefore more likely to remain stored as TG in the lipid droplet[95]. Carbon chain length also affects rate of fatty acid oxidation with increased carbons leading to a decrease in fatty acid oxidation[95]. In order to generate an appropriate model of obesity, we cultured the adipocytes for 6 weeks in fatty acid media, to allow for the adipocytes to accumulate more lipids. Adipocyte hypertrophy begins the cascade of events that lead to obesity. MCP-1, the major chemoattractant factor released from adipocytes, was most elevated in the palmitic group. MCP-1 levels have been shown to increase in response to palmitic acid in 2D studies as a result of NF-κB and JNK signaling[81,127–130]. While the exact mechanisms are still not clear, it has been hypothesized that oxidative stress induced by

adipocyte hypertrophy from increased lipid load activates JNK and NF-κB pathways[130]. This hypothesis explains why unsaturated fatty acids do not contribute to MCP-1 secretion, as they are more readily metabolized, and therefore less likely to be stored in the lipid droplet. Interestingly, levels for stearic acid were lower than the control group. We did not investigate dose dependency for these fatty acids. A study found MCP-1 release of 2 doses of various fatty acids- 10 and 100μM of stearic, oleic, palmitic, palmoleic, linoleic acids was dose dependent[131]. In the study, 100 μm stearic acid increased MCP-1 release, while 10μM decreased release. These stearic acid, but not palmitic and oleic acid, results are contradictory to our results, yet were performed in different models (cell line versus primary cells and 2D versus 3D), therefore a more systematic study would need to be performed with varying doses. Another study found a similar contradictory result; monocyte chemotaxis was increased with palmitic acid but decreased with stearic acid and oleic acid[126]. MCP-1 release activates adhesion factors in the vasculature to attract circulating monocytes to extravasate into the adipose tissue. MCP-1 activates TNFα production via NF-κB signaling in the macrophage. TNFα levels in our study did not vary with fatty acids, or with addition of monocytes, with the exception of the control group in which no TNFα was detected. Both adipocytes and macrophages can secrete TNFα, however, visceral and subcutaneous adipocytes are found to differentially produce TNFα[132]. Palmitic acid has been known to interact directly with TLR4 receptors, but more recently a study found that other fatty acid complexes can bind to TLR4 and induce an inflammatory response[131]. Il-6 levels were elevated in the presence of palmitic acid, and further increased with monocytes.

Adiponectin levels are found to be higher in non- obese patients; our data confirm this trend, that in the absence of fatty acids, adiponectin levels were highest. Adiponectin blocks NF-κB signaling and therefore decreases downstream effects of TNFα[124]. Leptin is produced by mature adipocytes under the regulation of the PPARγ and C/EBPα transcription factors, and also upregulated in the presence of glucocorticoids and TNFα[71]. Our results contradict these established data, where TNFα levels are higher, we see lower leptin levels. Our preliminary data (not shown) in a 3D adipose tissue model also showed a decrease in leptin levels over a 2 week period when cultured with palmitic acid. Just as other soluble factors are expressed differentially in visceral versus subcutaneous depots, leptin expression may vary by depot as well. A study comparing visceral and subcutaneous adipocytes should be done.

Extended culture time affects soluble factors. TNFα and adiponectin levels were no longer detectable. MCP-1, Il-6 and leptin levels all decreased, and the effects noted as a result of different fatty acids were muted. It is possible the system had reached a stable state by this time, while at 6 weeks this system was still sensitive to the inflammatory and nutritional cues. To our knowledge, no other study has been conducted over a long culture period to compare trends. Also, in order to sustain long-term culture we need to culture in the presence of fetal bovine serum (FBS) – a mix of many growth factors, cytokines, fatty acids, lipids, etc., in which we do not know the relative concentrations or exact composition. Some studies culture with TZDs throughout their (short-term) culture, although we maintained adipogenic outcomes, a follow-up study should include a PPARγ ligand to ensure the adipogenic program is continuously active.

MCP-1, Il-6 and leptin levels were evaluated after exposure to anti-obesity therapies, CLA and wogonin. Both therapies decreased the levels of MCP-1 when cultured with monocytes. Wogonin selectively blocks COX-2, an inflammatory mediator, and *in vivo* studies demonstrated COX-2 deficiency leads to decreased MCP-1 expression[133]. COX-2 is expressed in all cell types. Wogonin also decreased leptin levels in the presence of monocytes. CLA has been shown to be more effective in reducing obesity outcomes with saturated but not unsaturated fats, however our MCP-1 results did not support this[120,121]. Effects on leptin and Il-6 by CLA were not conclusive.

COX-2 gene expression was evaluated as its expression is directly related to TNFα and inversely related to PPARγ expression[111]. In this study, COX-2 and PPARγ transcription levels increased over time with wogonin treatment. Yet, in the presence of monocytes and palmitic acid, the COX-2 transcription levels were lower than other groups. Fatty acid binding protein 4 (FABP) gene expression was evaluated as well. FABPs intracellularly bind fatty acids and mediate trafficking to different organelles[134]. FABP4 is specifically expressed by macrophages and adipocytes. Knockout models for FABP4 lead to suppression of the NF-κB pathway, MCP-1, Il-6, TNFα, nitric oxide and COX-2[135]. The unbound fatty acids, in FABP4-/- macrophages, were found to block NF-κB while acting as PPARγ agonists[135]. FABP4 -/- mice were also found to have a higher level of circulating fatty acids, yet remain insulin sensitive. In our study, FABP4 was highly upregulated in palmitic acid and monocyte groups in the presence of wogonin. FABP4 transcription expression is upregulated by fatty acids, insulin and PPARγ agonists[134].

These data suggest that FABP4 is upregulated by palmitic acid in adipocytes and/or monocytes, and is regulated independently of inflammatory markers.

This study was the first to explore the chronic effects of monocyte and fatty acid exposure on a 3D culture of human vascular adipose tissue. The soluble factors in this study were chosen not only because they play a major role in disease progression but are also clinical readouts. MCP-1, Il-6, TNFα, leptin are all chronically elevated in blood plasma of obese patients, while adiponectin is decreased[136,137]. Using clinically relevant physiological markers we can relate our disease models to patient data. These data suggest that the inflammatory cells, macrophages, are important for mediating the response to fatty acids and wogonin. Future work on obesity should include therapies that *directly*, not indirectly, decrease the local inflammatory response. These anti-inflammatory therapies could be combined with other anti-obesity therapies to maximize response.

3.6 ACKNOWLEDGEMENTS

I wish to thank Kelly Burke for assistance on adipose stem cell isolation, media formulation and obesity related discussions, and Kristy Townsend for discussions on obesity models.

3.7 FIGURES

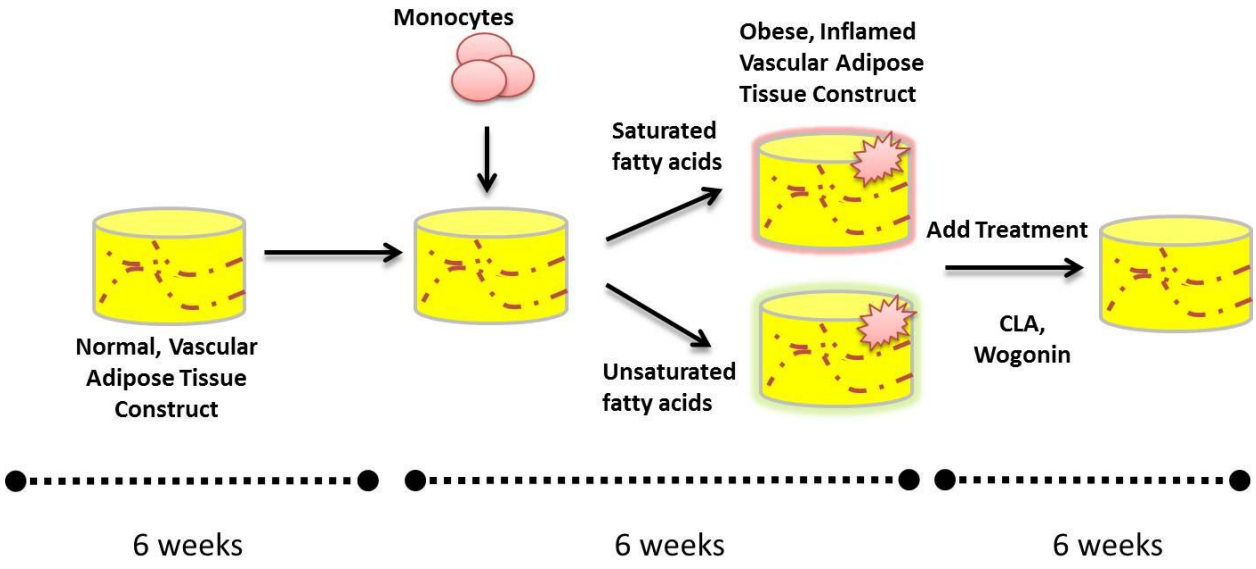

Figure 3.1- Experiment timeline for long-term obesity study.

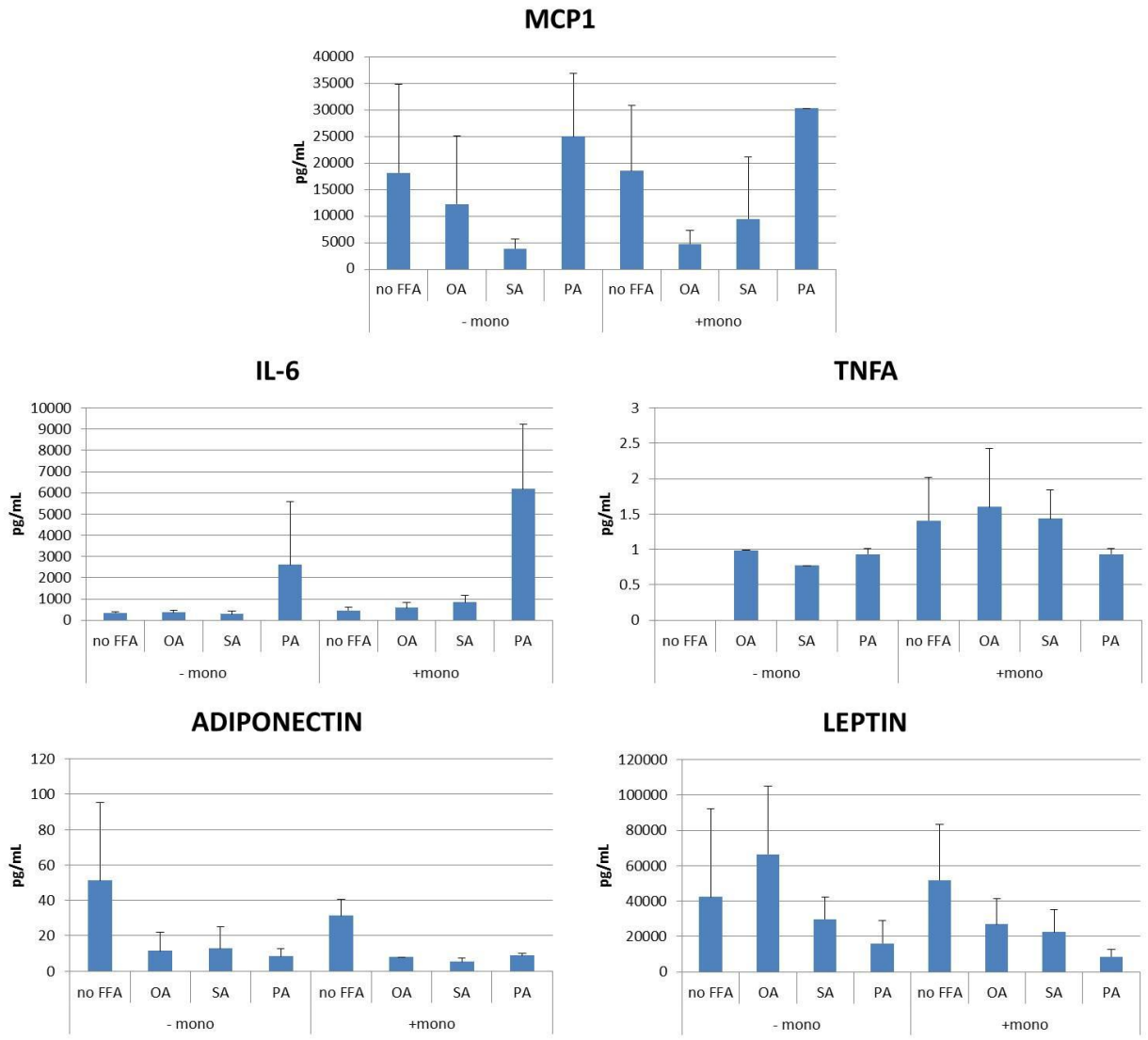

Figure 3.2- Soluble factor release after exposure to FFAs for 6 weeks. Inflammatory factors (MCP-1 and Il-6) were greater in the presence of the saturated fat- palmitic acid (PA). TNFA levels were greater when cultured with monocytes. Adiponectin levels were greatest when FFAs and monocytes were not present. Leptin levels decreased in the presence of saturated fats. Abbreviations- MCP-1- macrophage chemoattractant protein 1, Il-6- interleukin 6, TNFA- tumor necrosis factor alpha, FFA- free fatty acid, OA- oleic acid, SA- stearic acid, PA- palmitic acid, mono- monocyte. All values are expressed in terms of pg/mL.

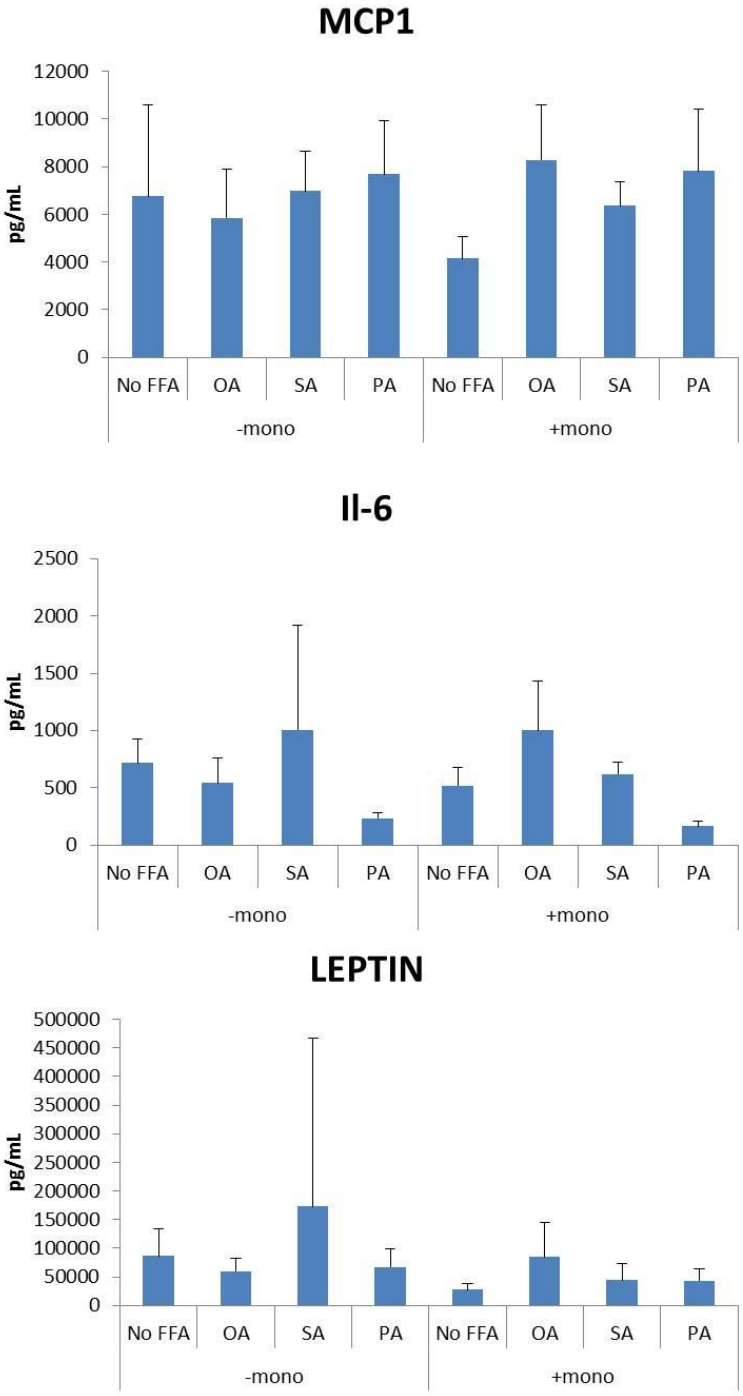

Figure 3.3- Cytokine profile after 12 week exposure to FFAs and monocytes varies from 6 week exposure. Abbreviations- MCP-1- macrophage chemoattractant protein 1, Il-6- interleukin 6, TNFA- tumor necrosis factor alpha, FFA- free fatty acid, OA- oleic acid, SA- stearic acid, PA- palmitic acid, mono- monocyte. All values are expressed in terms of pg/mL.

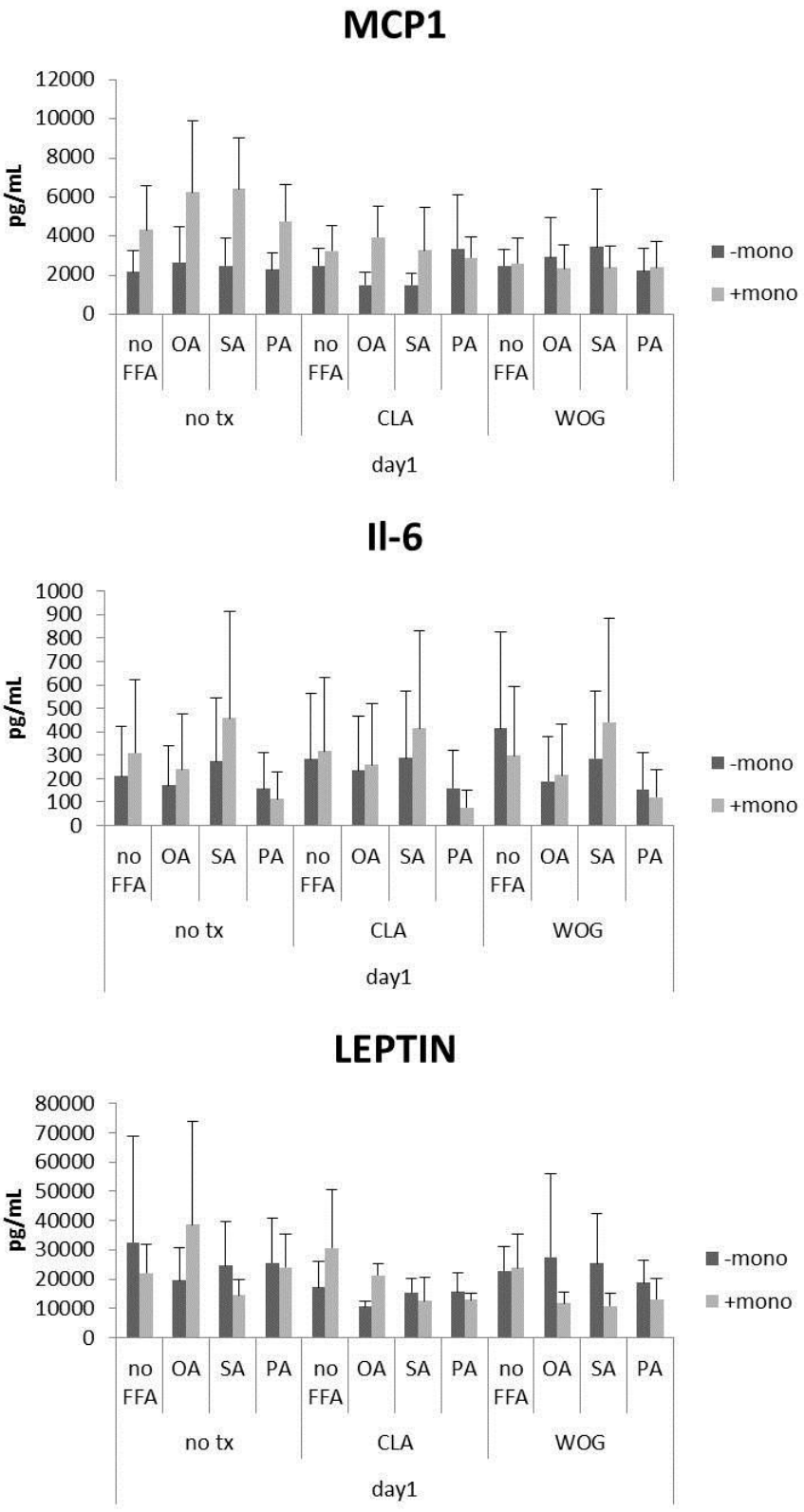

Figure 3.4- Effects of Conjugated linoleic acid and Wogonin on cytokine levels. Abbreviations- MCP-1- macrophage chemoattractant protein 1, Il-6- interleukin 6, FFA- free fatty acid, OA-

oleic acid, SA- stearic acid, PA- palmitic acid, mono- monocyte, CLA- conjugated linoleic acid, WOG- wogonin.

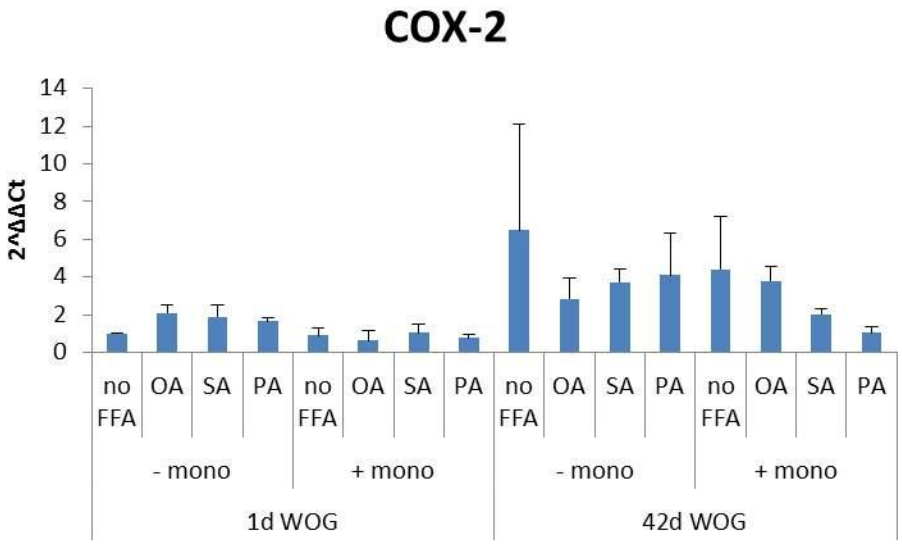

Figure 3.5- COX-2 is upregulated over time. Abbreviations- COX-2- cyclooxygenase 2, FFA- free fatty acid, OA- oleic acid, SA- stearic acid, PA- palmitic acid, mono- monocyte, WOG- wogonin.

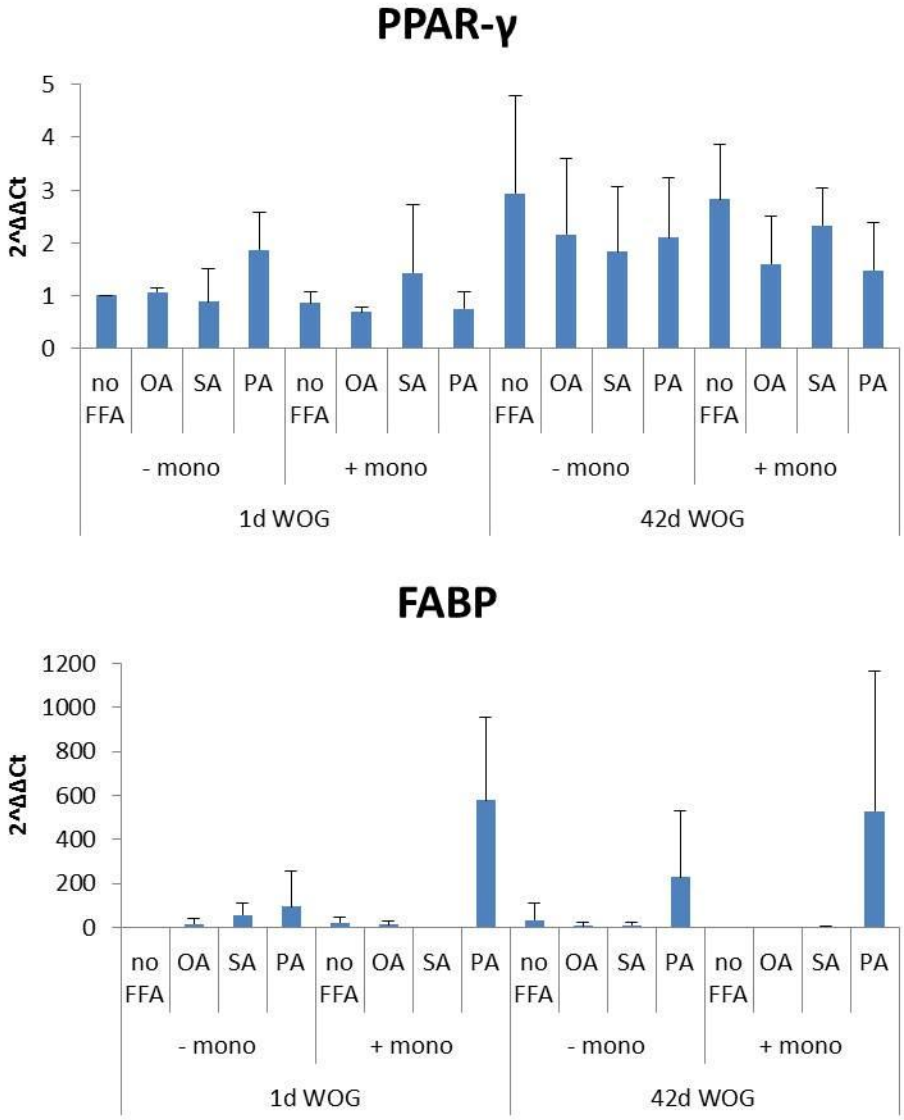

Figure 3.6- PPARγ is upregulated over time with wogonin treatment. FABP is upregulated with palmitic acid and monocytes. Abbreviations- FABP- fatty acid binding protein, FFA- free fatty acid, OA- oleic acid, SA- stearic acid, PA- palmitic acid, mono- monocyte, WOG- wogonin.

CHAPTER 4. SUSTAINABLE SOFT TISSUE REGENERATION WITH SILK BIOMATERIALS

4.1 ABSTRACT

Soft tissue defects result mainly from congenital abnormalities, trauma, or tumor resections and constitute about 4.8 million reconstructive surgery cases per year in the US alone[138,139]. Autografts and lipotransfer have been one treatment for soft tissue reconstruction, however, the success is unpredictable, with 20-90% graft resorption within months[25–27]. In this study, we employed slowly degrading, porous silk sponges alone, or seeded with adipocytes or lipoaspirate in an 18 month subcutaneous nude rat model and assessed for volume retention, sponge degradation, remodeling, and overall tissue regeneration. The silk sponge degraded slowly over 18 months, while regenerating subcutaneous tissue and maintaining volume. The addition of a cellular component yielded an adipose tissue outcome, while no cellular component formed a connective tissue outcome. These data suggest a simple, clinically relevant approach to filling soft tissue defects.

4.2 INTRODUCTION

Soft tissue defects result mainly from congenital abnormalities, trauma, or tumor resections and constitute about 4.8 million reconstructive surgery cases per year in the US alone[138,139]. Autografts and lipotransfer have been one treatment for soft tissue reconstruction, however, the success is unpredictable, with 20-90% graft resorption within months[25–27]. This leaves significant problems for the patient and thus the regeneration of large soft tissue defects remains an unmet clinical need. Silk, a protein biomaterial that has been used for decades for sutures[140,141], and recently FDA approved for use as a surgical mesh, can be processed into a variety of formats with control of degradation rate[67]. We demonstrate sustained tissue regeneration by combining mechanically robust, porous silk sponges that degrade slowly *in vivo*[66] to foster soft tissue regeneration. The sponges can be combined with a biological component, adipose stem cells (ASCs) or lipoaspirate. These systems were for studied for 18 months *in vivo* in a rat model and assessed for volume retention, sponge degradation, remodeling, tissue regeneration and vascularization. The silk sponge degraded slowly over 18 months, while regenerating subcutaneous tissue and maintaining volume. The data suggest a

simple, safe and clinically relevant solution to fill soft tissue defects with sustained volume and function.

4.3 METHODS

4.3.1 Materials

Bombyx mori silkworm cocoons were supplied by Tajimia Shoji Co. (Yokohama, Japan).

All cell culture supplies and collagenase type I were purchased from Invitrogen (Carlsbad, CA) unless otherwise noted. Human recombinant insulin, dexamethasone, pantothenate, biotin, 2,3-thiazolidinediones (TZD), 3-isobutyl-1-methylxanthine (IBMX) , bovine serum albumin (BSA), and laminin from human placenta were also purchased from Sigma-Aldrich (St. Louis, MO).

Histological solvents were purchased from Fisher Scientific (Pittsburgh, PA) and histological reagents and Masson's Trichrome Stains Kit were purchased from Sigma-Aldrich. Primary antibody for rat CD31, and antibody diluent were purchased from Cell Signaling Technologies (Danvers, MA). Primary antibody forhuman anti-nuclei, clone 235-1, was purchased from Millipore (Billerica,MA). The secondary antibody, ABC (avidin, biotin complex) kit, DAB substrate, hematoxylin counterstain and, antigen retrieval solution were purchased from Vector Labs (Burlingame, CA).

4.3.2 Silk Sponge Preparation

Silk solution was prepared as published[122]. Briefly, cocoons were chopped and placed in boiling 0.02M $NaCO_2$ for 30 minutes to remove sericin, and then washed 3 times in ultrapure water. The resulting silk fibroin fibers were left to dry overnight. The dry silk was solubilized in 9.3 M LiBr in 20% w/v at 60 C for 4 hours. The silk solution was then dialyzed in ultrapure water in 3,500 MWCO membrane for 2 days with a total of 6 water changes, to remove the LiBr. The aqueous silk solution was lyophilized until dry and re-solubilized over 2 days in hexafluoro-2-propanol

(HFIP) at 17% w/v. Salt crystals were sieved to the desired range of 500-600 microns, poured into Teflon coated petri dishes and either aqueous silk or HFIP-silk solution was added. The Petri dish was covered and left in a fume hood for 2 days and, uncovered to let the HFIP evaporate for 1 day. The dish was immersed in methanol overnight, left in the fume hood for 1 day for the methanol to evaporate and then placed in water to leach out the salt particles. The water was changed 3 times a day for 2 days. The sponges were removed from the petri dish, cut to the desired dimension, 5 mm diameter x 2 mm height, using a biopsy punch. The sponges were left to dry before autoclaving, autoclaved, then kept at 4^{o}C until use.

4.3.3 Adipose Derived Stem Cell Isolation

Subcutaneous adipose tissue was obtained from abdominoplasties under Tufts University IRB (Tufts University IRB Protocol #0906007) from the Tufts Medical Center, Department of Plastic Surgery. The specimens were kept at room temperature in saline and used within the same day. The adipose tissue was separated from the skin by blunt dissection and chopped. Chopped adipose tissue was placed into 50 mL conical tubes and minced well with scissors. The tissues were washed in equal volumes warmed PBS, until essentially free of blood. An equal volume of 1 mg/mL collagenase I in 1% bovine serum albumin in PBS was added to the tissue and placed under gentle agitation at 37^{o}C for 1 hour. The tissue samples were centrifuged at 300 x g for 10 minutes at room temperature. The supernatant containing the tissue was removed and the pellet resuspended in PBS and centrifuged at the same settings to remove the collagenase solution. The pellet was resuspended in growth media and plated so that 70 g of initial tissue volume was plated per T225 cm^2 tissue culture flask.

4.3.4 Cell Culture and 3D Culture

Adipose derived stem cells were expanded and cultured as previously described[16,142]. Cells were expanded first in growth media comprised of DMEM/F12, 10% FBS, 1% PSF until confluence. At 2 days post-confluence, the cells were switched to adipogenic induction media comprised of DMEM/F12, 3% PSF, 1% PSF, IBMX, TZD, dexamethasone, pantothenate, biotin and insulin until seeded in sponges. The dry, coated sponges were placed into adipogenic maintenance media

for 1 hour before seeding with cells. Maintenance media was identical to induction media but without IMBX and TZD. The induced ASCs were added in 3 x 20 ul seedings with a total of 200,000 cells/sponge. The seeded sponges were placed in an incubator for 2 hours before media was added to the well. Cells and cultures were fed 2 times per week, and maintained in 37^{o}C, humidified incubator.

Lipoaspirate from elective plastic surgery was obtained the same day of sponge implantation. Lipoaspirate was transported aseptically at room temperature just after surgery. Approximately 30 mL of lipoaspirate was added to a 50 mL conical tube and centrifuged at room temperature at 1,000 rpm for 10 minutes. The blood and free lipids were removed. The remaining tissue was placed in sterile petri dishes. The dry, silk sponges were placed into the processed lipoaspirate for 1 hour prior to implantation.

4.3.5 In vivo implantation

Animals were cared for in compliance with Tufts University Institutional Animal Care and Use Committee (IACUC) in accordance with the Office of Laboratory Animal Welfare (OLAW) at the National Institutes of Health (NIH). Congenitally athymic male adult Rowett nude rats (RNU) (9 weeks old) were purchased from Taconic Farms (Cambridge City, Indiana) and were allowed to acclimate for 1 week prior to implantation. The rats were randomly assigned to one of the three implant groups.

The animals were first anesthetized with isoflurane (1-4%) and then administered the following analgesic, anti-inflammatory, antibiotic cocktail: carprofen, 5 mg/kg subcutaneously, buprenorphine, 0.05mg/kg subcutaneously, and procaine penicillin, 200,000 IU/kg intramuscularly. The animals were maintained with 1% (or to effect) isoflurane in oxygen, and kept on a heating pad through the entire procedure. After induction of anesthesia, the surgical site was clipped with electrical clippers. The skin was then aseptically prepared with chlorohexidene scrub followed by an alcohol rinse, repeated three times. A small skin incision (~7 mm) was made between the shoulder blades, and 2 tunnels were formed under the skin by blunt dissection along either side of the spine, 5-8 cm away from the initial skin incision. The

implants were placed above the underlying muscle under the skin at the end of the tunneled area. The skin was stapled at the incision site. The animals were allowed to awaken and had free access to food and water, thereafter.

4.3.6 Histology

Constructs were processed according standard histology protocols. Formalin fixed samples were put through a series of dehydration solvents and finally paraffin using an automated tissue processor. Samples were embedded in paraffin, cut in 10 micron sections, and let to adhere on glass slides. The sections were rehydrated and stained with Hematoxylin and Eosin (H&E) for general morphology and organization, Masson's Trichrome for tissue remodeling, Prussian Blue Test for iron staining. For immunohistochemical staining, the sections underwent antigen retrieval under heated, low pH conditions. Non-specific binding was avoided by incubation with normal blocking serum. After the excess serum was removed, the sections were incubated for 30 minutes with anti-rat mouse CD31 diluted 1:100 in antibody diluent. Sections were washed in PBS and, then incubated with a secondary anti-mouse antibody for 30 minutes. The sections were washed in PBS and then incubated with VECTASTAIN Elite ABC reagent for 30 minutes, washed in PBS, incubated with ImmPACT DAB enzyme substrate for 5 minutes and washed in water. The sections were then counterstained with hematoxylin and mounted. To evaluate lipid accumulation, the formalin fixed constructs were embedded in OCT (Optimal Cutting Temperature) compound medium and frozen. The frozen blocks were cut in 10 micron sections, and then stained with Oil Red O.

4.3.7 Scanning Electron Microscopy Imaging

Explanted implants with surrounding tissue were frozen at -80^{o}C until ready to process for imaging. Explants were washed in 0.1 M phosphate buffer, and then fixed in freshly prepared 2.5% glutaldehyde in 0.1 M phosphate buffer. The explants were washed in phosphate buffer, and then fixed in osmium tetroxide in 0.1 M phosphate buffer. The explants were dehydrated in a graded ethanol series, starting at 50% ethanol until dehydrated at 100% ethanol.

Hexamethyldisilazane (HMDS) was added to the explants, removed, and then the explants were placed in a dessicator overnight to maintain dryness. The dried explants were mounted onto SEM stubs with double sided carbon tape and then sputter coated (208HR Sputter-Coater, Cressington Scientific Instruments, LTD, Walford, England) with platinum for 1 minute. Pt-coated explants were loaded into the 9 stub carousel and placed into the SEM (Supra55VP, Carl Zeiss Nano Technology Systems, Peabody, MA) for imaging.

4.3.8 Tissue Regeneration Measurements

During implant harvest, subcutaneous tissue layers, with the included implant, were carefully dissected away from the underlying muscle. The implants were cut out with the surrounding skin and tissue intact. The implant was then cut along its diameter to expose its cross-section and the cross-sections were photographed. Image analysis was carried out using ImageJ software (U. S. National Institutes of Health, Bethesda, Maryland, USA). Images of implant cross-sections were cropped to the region of interest and converted to 8-bit images. Contrast was enhanced and the image was sharpened (default settings used for both). This allowed for enhanced discrimination between the tissue and the silk sponge, as the tissue would appear light and the silk sponge would appear dark. The height/thickness of the surrounding subcutaneous fat was measured 3 times along the cross-section with the straight line tool, and the 3 measurements were averaged. This same procedure was used to determine the height/thickness of the silk sponge. The average of the silk sponge was subtracted from the subcutaneous fat, to yield an approximated value of regenerated tissue. The average value of subcutaneous fat without any implant was 0.1mm, an order of magnitude less than the regenerated tissue. The average height/thickness values for both regenerated tissue and silk sponge were plotted as a function of time and seeding condition.

4.3.9 Statistical Analysis

Samples for all quantifiable analyses were n= 4-6 with each biological replicate having technical duplicates. Histological analyses were performed at n=3, with 3 consecutive sections being taken per staining group, only representative images are shown. Means ± SEM. ANOVA was used to test for differences among means across groups. F-test was used for determining equality

of variances. All statistical analyses were performed on Excel (Microsoft, Redmond, WA) or MySTAT (SySTAT Software, Chicago, IL).

4.4 RESULTS

Soft tissue restoration or augmentation has been under study for many years. One treatment is fat grafting but the most challenging aspect of this approach has been volume retention over time, due to graft resorption. Volume loss and resorption is caused by many factors: inability of adipocytes to proliferate, adipocyte delipidation or inadequate vascularization[143]. One of the goals of the present work was to determine a biomaterial/tissue construct that would address this problem, while also being amenable to clinical translation. Porous silk sponges are readily formed to desired shape and porosity, and in the dried state these sponges can be autoclaved and stored aseptically at room temperature for years until needed. When these protein sponges were hydrated they were soft and spongy and able to be deformed, returning to their original dimensions immediately after the release of the applied pressure. The silk sponges seeded with ASCs and cultured *ex vivo* in adipogenic conditions formed tissue throughout the entire sponge. The sponges also readily absorbed lipoaspirate (Fig. 4.1a).

Male nude rats were selected for this long term study to minimize hormonal effects on adipogenesis and also to permit the use of human cells or tissue without rejection. The rats weighed 241±39 g at the time of surgery (Figure 4.5) and the constructs were implanted subcutaneously as described in Methods. No acute or chronic adverse reactions were evident after the implants were introduced and all animals returned to their pre-surgery weight within 1 week of surgery (Figure 4.5). All rats continued to gain weight normally over 18 months (Figure 4.5). The spleens were assessed at each time point for changes in size, shape and color, but no differences were noted (Figure 4.5).

Sponge volume retention was stable for at least the 1st 6 months (Fig. 4.2a). All sponges were soft to the touch and retained their ability to return to their shape after deformation. At each time-point small blood vessels were seen surrounding the sponges in the subcutaneous tissue and all groups had integrated with the surrounding tissues (Fig. 4.1c). Integration, as seen by host tissue infiltration had further improved in the groups that were pre-seeded (Fig. 4.1c). Histological images at 3 months show silk sponges were present in all groups (Figure 4.3). The unseeded group showed a poorly organized matrix and less tissue infiltration into pores than the seeded groups, confirming the macroscopic observations. Some macrophages were evident near the sponges demonstrating dynamic remodeling, as silk degrades via proteolytic action[144]. The unseeded group had the greatest number of macrophages present at 3 months while the lipo-seeded group had the least number of macrophages. Oil Red O (ORO) staining for mature adipocytes was performed and positive staining in the vicinity of the sponge was seen in the seeded study groups. In the unseeded group, positive staining for ORO was detected at the interface with the muscle and near the sponges.

By 6 months, the lipo-seeded group was completely encased in a fat pocket, a feature apparent out to 18 months (Fig. 4.2b). The silk sponges were evident in all study groups with fewer macrophages seen than at 3 months. In the unseeded group, the tissue had infiltrated the pores of the sponge, similar to that seen earlier (at 3 months) in the seeded groups. Positive staining for ORO was seen in all study groups, including the unseeded group, albeit less intense in staining than in the seeded groups. Unlike the seeded groups, positive staining was seen more along the periphery of the unseeded group sponge than within. Blood vessels were seen in all study groups and appeared to be functional based on the presence of red blood cells within the lumens.

At 12 and 18 months, integration with the surrounding tissue was even more evident (Fig. 4.1c). The silk sponge structures were still present; however, the pore walls began to fracture as they degraded (Fig 4.4a, 4.4b). The unseeded group had few mature adipocytes present, with more mature adipocytes at the interface between the implant boundaries and the surrounding tissue. The seeded groups contained large, mature adipocytes throughout the constructs. ORO staining

was seen in all study groups, with denser pockets of staining in the lipo-seeded group than the unseeded or ASC-seeded groups. All lipo-seeded groups had prominent blood vessels feeding into the sponges from the underlying *Latissimus dorsi* muscle (Fig. 4.1d).

Degradation of the silk sponges was seen in all study groups, with remaining silk sponge at 18 months (not accounting for tissue regeneration) volumes as follows: unseeded 27±11%, ASC-seeded 21±4%, and lipo-seeded 19± 10% (Fig. 4.2a). We approximated the thickness of the newly formed tissue by measuring the thickness of the subcutaneous fat and subtracting the thickness of the silk sponge. At 12 months, the lipo-seeded group subcutaneous fat tissue thickness measured 2.4 mm and had exceeded the original thickness of the implanted construct (2 mm) even though the silk sponge had degraded to 29% of its original volume. At 18 months, the lipo-seeded group had maintained 1.8 mm of the 2 mm thickness of the implanted construct, even though the silk sponge had degraded to 19% of its original volume. The unseeded groups had a thickness of 1.6 and 1.1 mm while the silk sponge had degraded to 72% and 27% of its original volume for 12 and 18 months, respectively. Pore wall thickness and overall sponge structure were assessed using SEM (Figure 4.6). The unseeded sponge's structure remained intact with open pores and tissue infiltration (Figure 4.6).

4.5 DISCUSSION

The initial sponge volume did not decrease because the silk sponges maintained structure during the tissue remodeling process. Silk biomaterials were chosen based on their ability to be tailored to fit a wide range of mechanical and degradation profile, as well as being unlimited in terms of total sponge size and shape. We have previously demonstrated that silk sponge biomaterials can be processed to last more than 12 months *in vivo* in a rat model[66], or be immediately resorbed[122,145]. We also demonstrated that silk biomaterials can be useful in support of adipose tissue engineering *in vitro* and *in vivo*[16,45]. Other natural biomaterials, such as collagen and hyaluronic acid, degrade quickly unless cross-linked. Even when cross-linked, degradation remains relatively rapid. Silk requires no crosslinking due to the extensive network of physical

crosslinks in the form of beta sheets. Due to these secondary structures, silk as prepared in the present study will not contract or swell significantly, which is a common challenge with other polymeric degradable biomaterials. This maintenance of structure of a very slowly degrading biomaterial allowed tissue regeneration and sustained biological function during the remodeling process, without the loss of implant volume. This represents a major advance over current biomaterial options used for soft tissue regeneration. The remodeling process continued within the sponge structure due to the maintenance of mass transport by keeping the porous structure open. By the time the sponges began to degrade at 12 months, tissue formation in all study groups had been well established, complete with vasculature. In all cases, the sponges began degrading from the outside inward. This was evident in SEM images where the pore wall thickness did not change significantly over time and the aspect ratio of the cylindrical implant remained intact. The surrounding host fibroblasts or macrophages secrete non-specific proteases to slowly break down the silk sponges[66,144].

Animal studies to study soft tissue reconstruction and regeneration are generally run over a relatively short term (~6 weeks). To our knowledge, no prior study has shown greater than 6 months volume maintenance for soft tissue regeneration. Two other studies in rats have demonstrated long-term retention out to 12 months[146,147], however these studies used pedicle flaps which were implanted in another part of the body, allowed to become vascularized and then transplanted to the site of interest. This method is less desirable than our current approach due to the large mass that will need to be harvested from a donor site, as well as the need for multiple surgeries and thereby multiple morbidity sites.

In the present study, silk porous protein sponges, alone, or seeded with *in vitro* differentiated ASCs or freshly isolated lipoaspirate, were implanted into nude rats. We chose the silk sponge alone and lipo-seeded groups as they are clinically translatable, while the ASC-seeded group was a comparison to our *in vitro* work. The harvest of lipoaspirate is already clinically used for fat grafting. The isolation of ASCs from lipoaspirate can be performed in the clinic using rapid and automated procedures, such as the TGI™ System (Tissue Genesis, Inc, Honolulu, HI). We chose

to compare freshly isolated lipoaspirate to *in vitro* differentiated ASCs cultured for 4 weeks on the sponges, as the lipoaspirate contains active vascular growth factors that may enhance tissue regeneration. Fresh ASCs have been postulated to take on a perivascular phenotype. Further, harvesting and processing lipoaspirate can be done the same day as the implantation without scarring, and no *ex vivo* manipulation that would require FDA approval is needed to re-implant the lipoaspirate.

This study, to our knowledge, is the first to successfully demonstrate retention of volume for more than 6 months following implantation of soft tissue regeneration systems in a small animal model. At 12-18 months the sponges began degrading while encased in their own fat pockets, thus tissue regeneration without significant loss of volume. The histological changes over time support the conclusion that the silk porous sponges acted as templates for dynamic tissue regeneration even during this remodeling process. These results point towards a viable clinical strategy to address this major surgical need for soft tissue regeneration.

4.6 ACKNOWLEDGEMENTS

The authors wish to acknowledge Eun Seok Gil, Jelena Rnyak, Rebecca S. Hayden and David Lange for their assistance with SEM preparation and imaging. They also wish to thank Dr. Daniel Driscoll for providing surgical specimens, Marianne Stark and Kimberly Flink for assistance with surgeries and animal care. The SEM work was performed in part at the Center for Nanoscale Systems (CNS), a member of the National Nanotechnology Infrastructure Network (NNIN), which is supported by the National Science Foundation under NSF award no. ECS-0335765. CNS is part of Harvard University. This work was funded by Armed Forces Institute for Regenerative Medicine (AFIRM) W81XWH-08-2-0032 and the NIH - P41 EB002520.

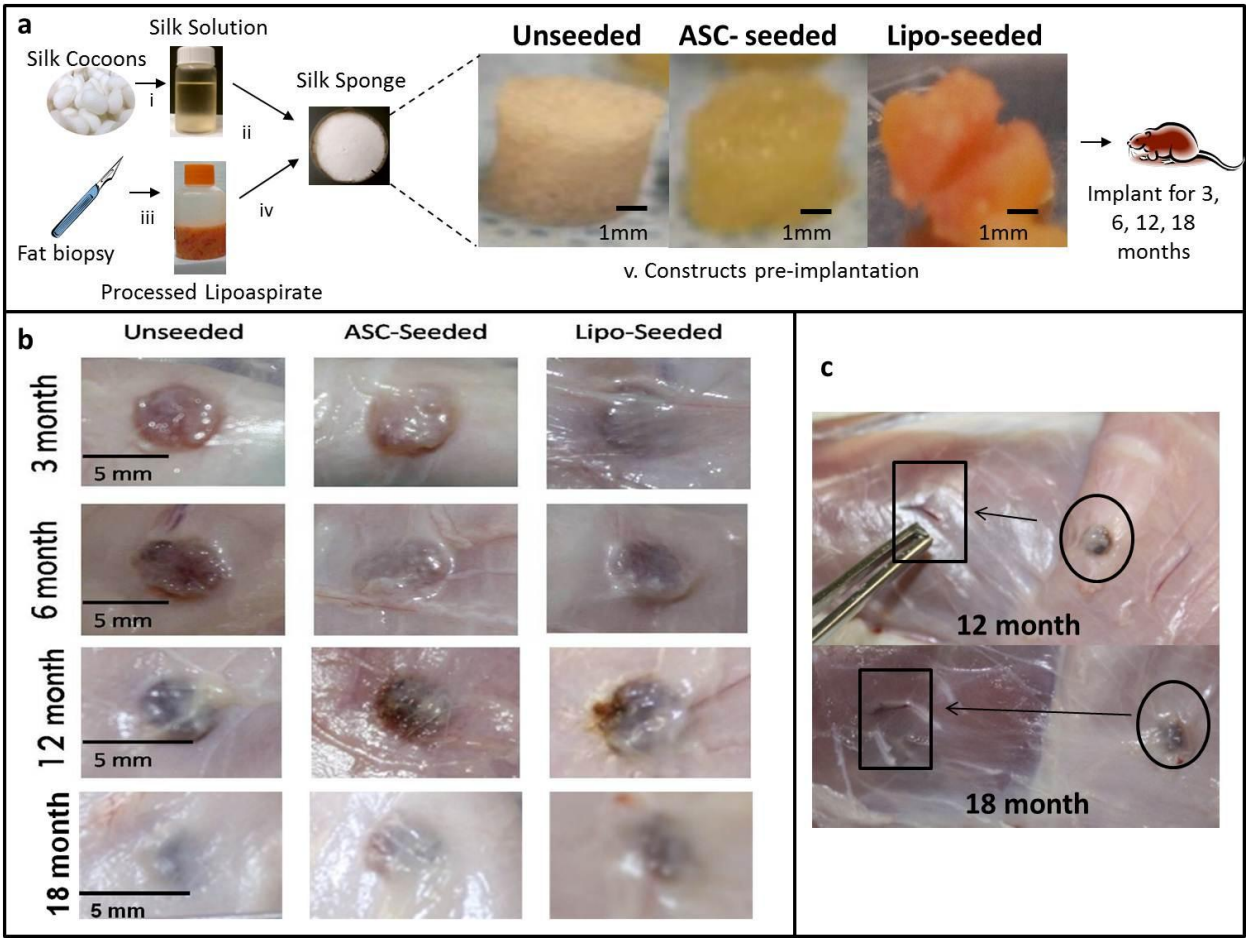

Figure 4.1- Clinically translatable process for soft tissue regeneration. (a) Porous silk sponges were prepared as previously described by boiling silkworm cocoons in sodium carbonate to remove sericin, a gum-like protein, then the fibroin fibers are dissolved in lithium bromide to produce an aqueous protein solution (i). The aqueous solution was lyophilized, re-dissolved in an organic solvent, and cast into a porous sponge format using a salt-leaching method (ii), cut to the desired dimensions and autoclaved. No further processing was required for the unseeded groups. The seeded groups were prepared by first obtaining lipoaspirate, and clearing the fat of free oils and blood (iii). For the ASC-seeded group, the ASCs were isolated by a collagenase digestion followed by an adherence selection process. The ASCs were seeded onto the silk sponges and cultured for 1 month under adipogenic conditions (iv) prior to implantation. For the lipo-seeded group, the silk sponges were soaked in the processed lipoaspirate for 1 hour (iv) prior to

implantation. Macroscopic images of unseeded (left), ASC-seeded (middle) and lipo-seeded (right) constructs prior to implantation (v). The constructs were implanted subcutaneously in the dorsal region of a nude rat for 3, 6, 12 and 18 months. (b) Macroscopic images of constructs after 3 (top row), 6 (second row), 12 (third row) and 18 (bottom row) months *in vivo*, prior to being explanted. Integration with the surrounding host tissue increased when the silk sponges were pre-seeded. By 12 months, all groups were similarly integrated. (c) At 12 and 18 months in the lipo-seeded group, a large vessel was found feeding into the lipo-seeded construct from the underlying muscle. This was not seen at earlier time points or in other groups.

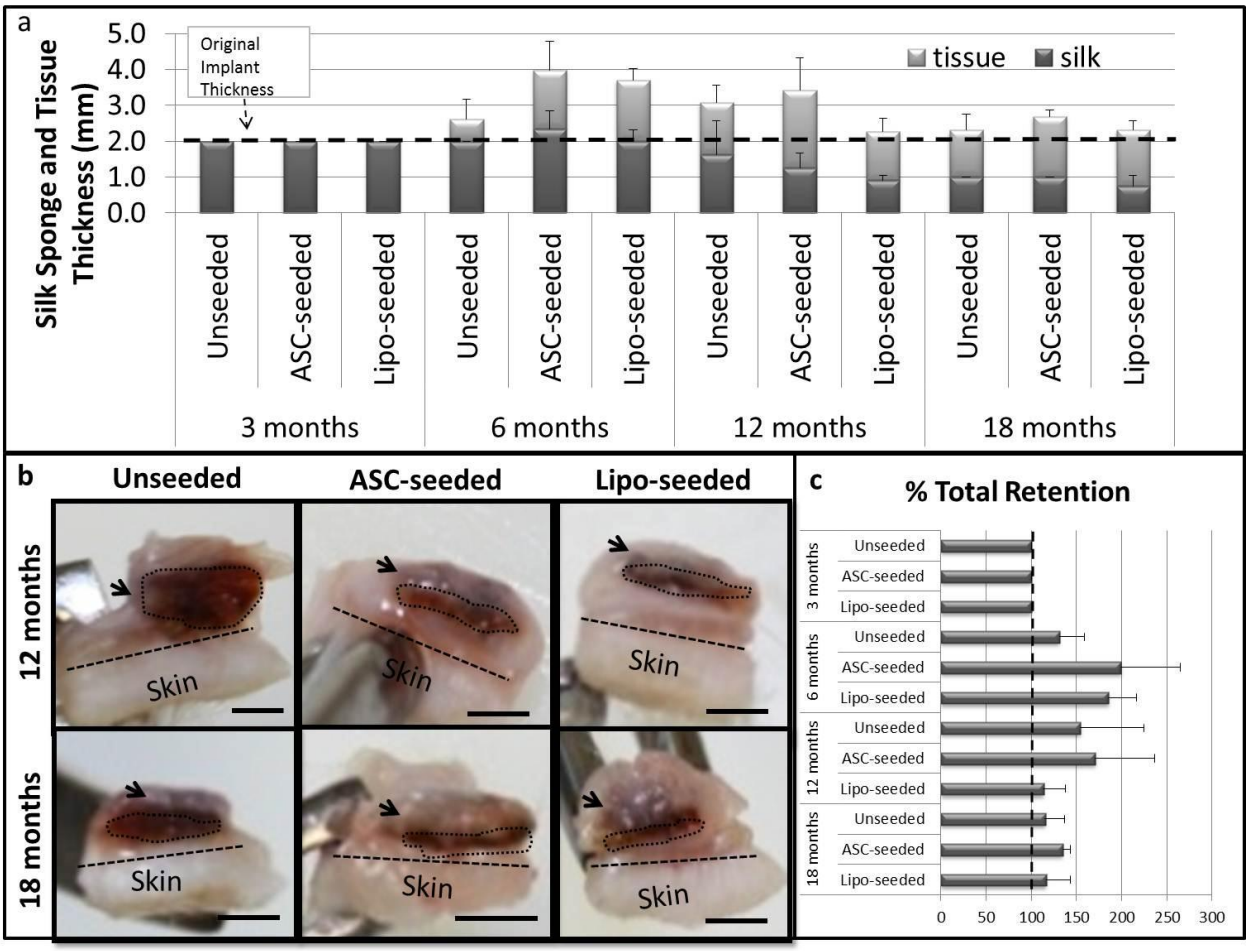

Figure 4.2- Tissue regeneration occurs with silk sponge degradation. (a) The silk sponge volume was calculated by measuring the silk sponge thickness and diameter upon explantation. The volume was maintained, i.e. no biomaterial degradation, through 6 months. At 12 and 18 months, the seeded groups degraded more quickly than the unseeded group. (b) Cross-sections of 12 (top

row) and 18 (bottom row) month explants are shown for unseeded (left), ASC-seeded (middle) and lipo-seeded (right) groups. The square dotted line outlines the silk sponge, while the rectangular dotted line demarcates the skin from the subcutaneous tissue. The arrows point to regions of subcutaneous fat. The subcutaneous fat formation was greatest in the lipo-seeded group (right column) and least in the unseeded group (left column). Scale bar- 2 mm. (c) Approximated thickness of the newly formed tissue was determined by measuring the thickness of the fat and subtracting the thickness of the silk sponge by image analysis in ImageJ. At 12 months, the lipo-seeded group thickness measured 2.4 mm and had exceeded the original thickness of the implanted construct (2 mm) even though the silk sponge had degraded to 29% of its original volume. At 18 months, the lipo-seeded group had maintained 1.8 mm of the 2 mm thickness of the implanted construct, even though the silk sponge had degraded to 19% of its original volume. The unseeded groups had a thickness of 1.6 and 1.1 mm while the silk sponge had degraded to 72% and 27% of its original volume for 12 and 18 months, respectively.

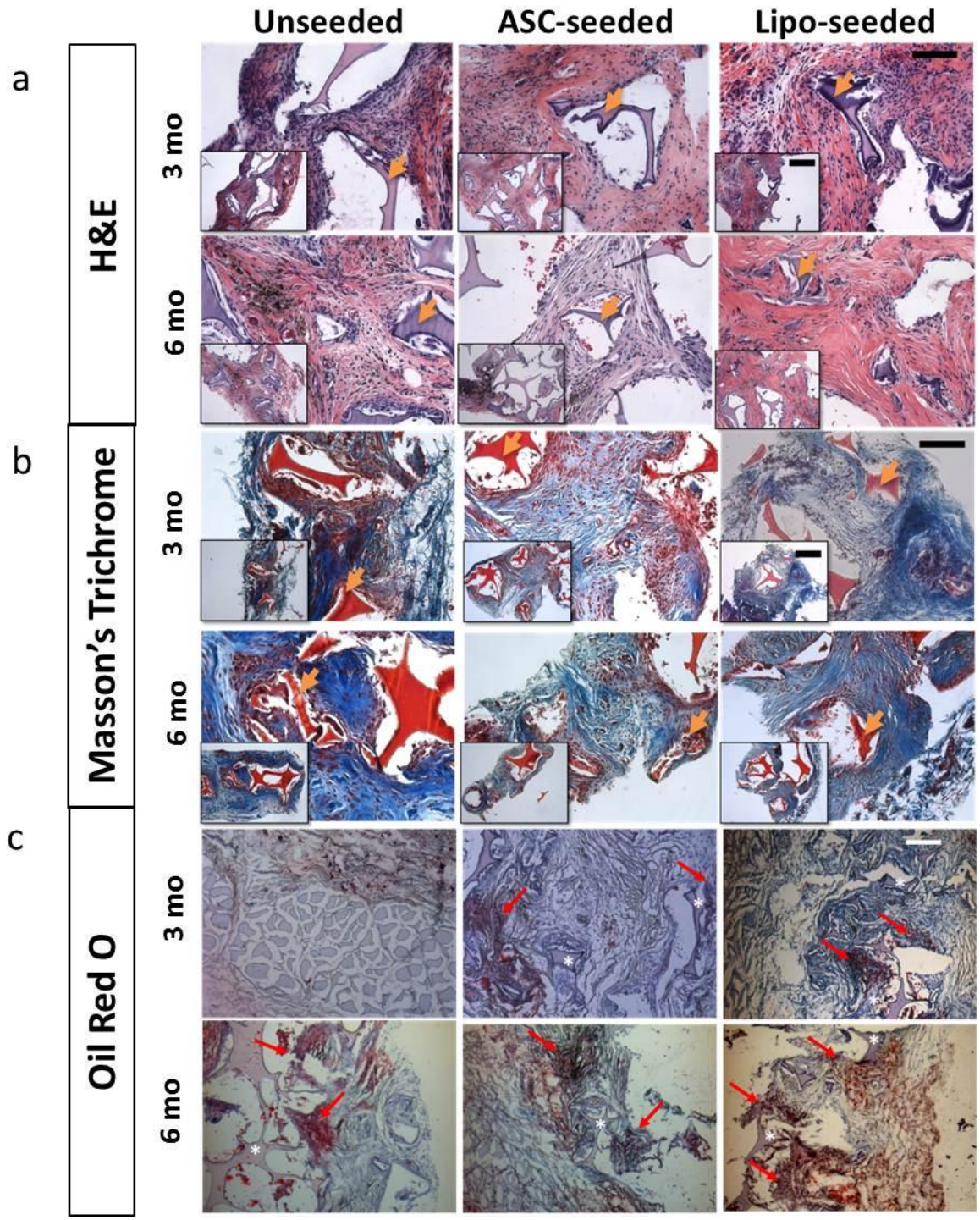

Figure 4.3- Histological tracking of regenerated tissue show an active tissue remodeling process. (a) H&E images at 3 (top row) and 6 months (bottom row) show a decrease in macrophages within the sponge from 3 to 6 months. Macrophages are seen surrounding the silk pore wall in the unseeded group (left) at 3 and 6 months. The intact silk sponge stains a dark purple and is visible in all groups. Hemosiderin deposits (dark or black deposits) were present is some sections

as with the later timepoints (see note in Figure 4). Scale bar- 100 microns, inset- 200 microns. (b) Masson's Trichrome staining for tissue organization at 3 (top row) and 6 months (bottom row). The intact silk sponge stains red and is visible in all groups. At 3 months, the unseeded study group (left) has a collagenous matrix (blue) that is poorly organized in comparison to the seeded groups. By 6 months (bottom row) more matrix (blue) is seen. Scale bar- 100 microns, inset- 200 microns. (c) Oil Red O (ORO) for staining mature adipocytes at 3 (top row) and 6 months (bottom row). The intact silk sponge (asterisk) stains a light purple and is visible in all groups. Areas of ORO positive staining are pointed to with a red arrow. At 3 months (top row), only the seeded groups (middle, right) were positive for ORO, the unseeded group (left) was positive for ORO only near the underlying muscle as shown. The lipo-seeded group (right) stained the most densely for ORO. Scale bar- 200 microns.

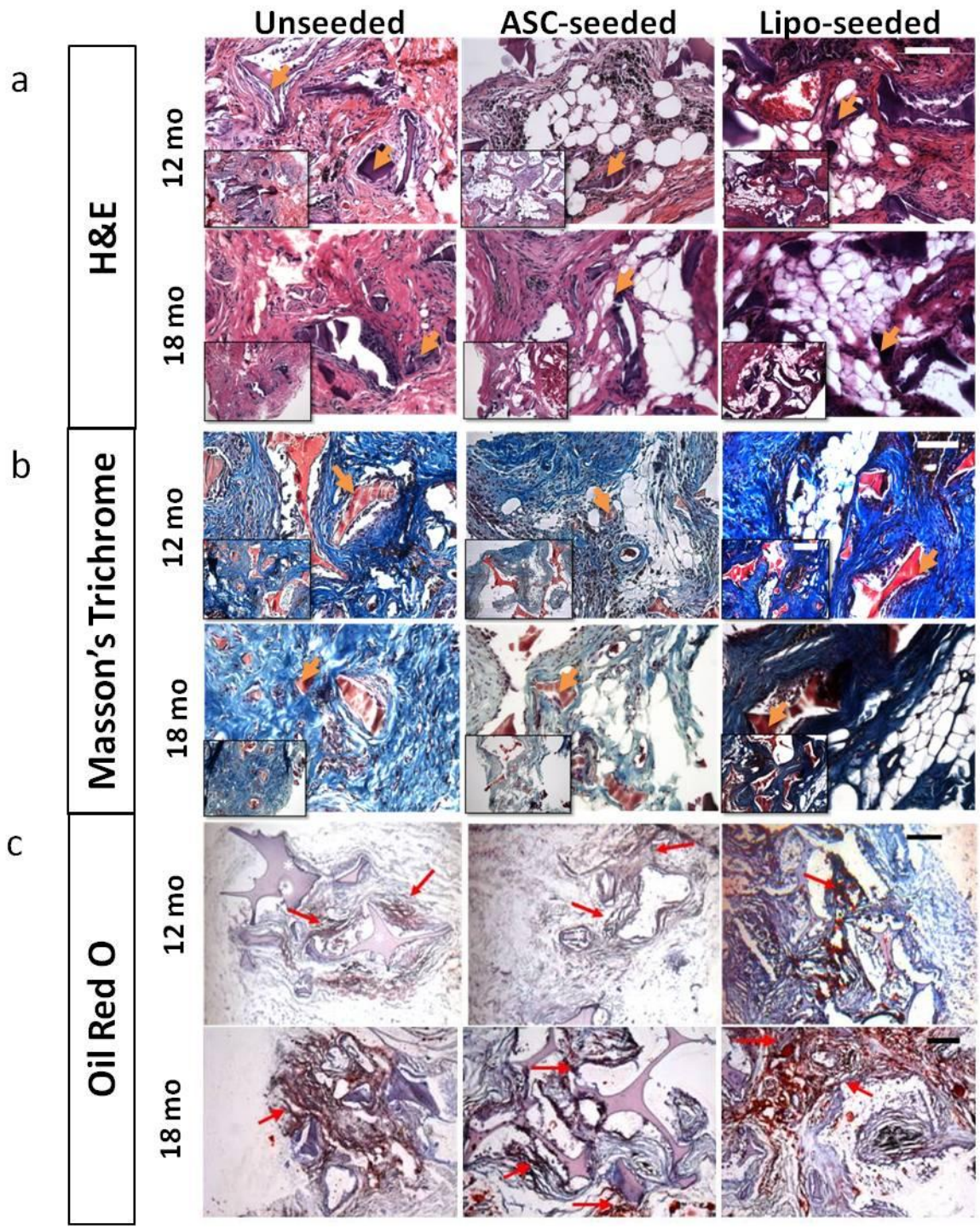

Figure 4.4- Histological tracking of regenerated tissue show mature adipocytes/fat formation in seeded groups at 12 and 18 months. (a) H&E images at 12 (top row) and 18 months (bottom row) show that fat formation was present in seeded groups. The silk sponge stains a dark purple and is visible in all groups. At 12 months, the silk sponge walls began to fracture as the sponge

degraded. In some sections, dark, or black deposits were seen. This was hemosiderin or iron left behind as a result of the healing process when red blood cells are phagocytosed by macrophages (see supplementary figure). Scale bar- 100 microns, inset- 200 microns. (b) Masson's Trichrome staining for tissue organization at 12 (top row) and 18 months (bottom row). The silk sponge stains red and is visible in all groups. The cellularity (nuclei stain dark or black), decreased from 12 to 18 months in all groups, and then is replaced with a well-organized collagenous matrix (blue). Scale bar- 100 microns, inset- 200 microns. (c) Oil Red O (ORO) for staining mature adipocytes at 12 (top row) and 18 months (bottom row). The silk sponge (asterisk) stains a light purple and is visible in all groups. Areas of ORO positive staining are pointed to with a red arrow. The lipo-seeded groups (right) stained the most densely for ORO. Scale bar- 200 microns.

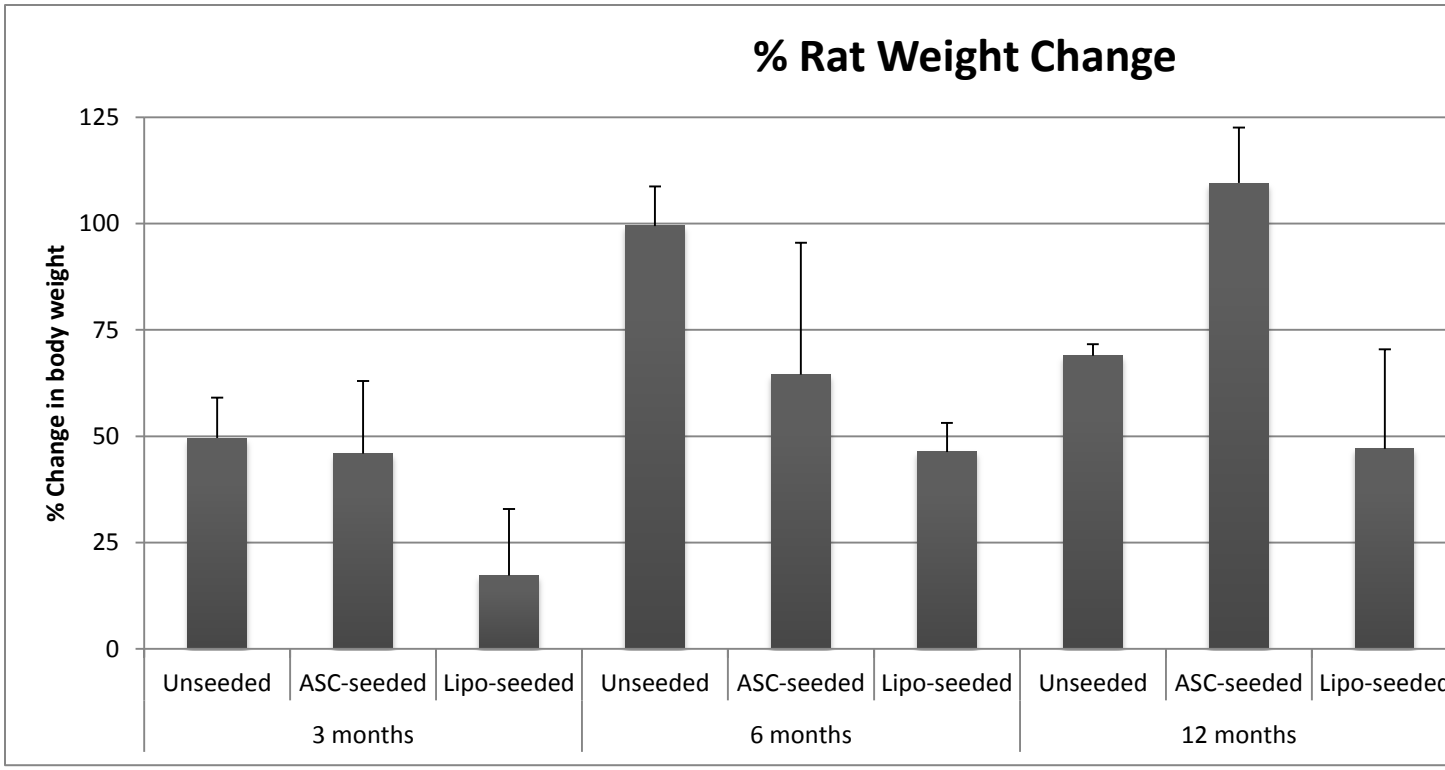

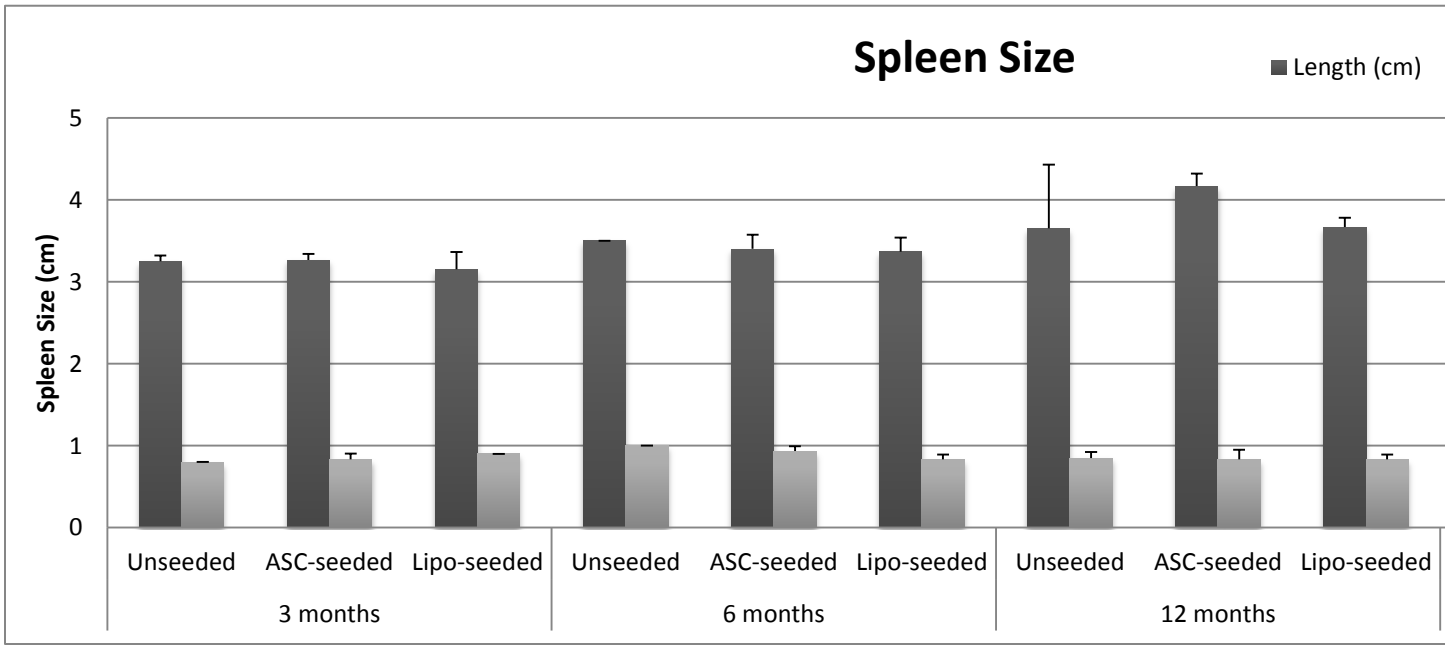

Figure 4.5- Rats maintained normal weights (% weight increase) and spleen size throughout study. (Top) Body weight was used as a marker of general health. Rats returned to their pre-surgery weight within 1 week post-operatively and gained weight normally throughout 18 month study in all groups. (Bottom) The spleen and liver were observed to determine if any toxicity due to degradation products from our biomaterial. No changes in size, shape and color were noted

(not shown). Spleens were normal in size throughout 18 month study in all groups.

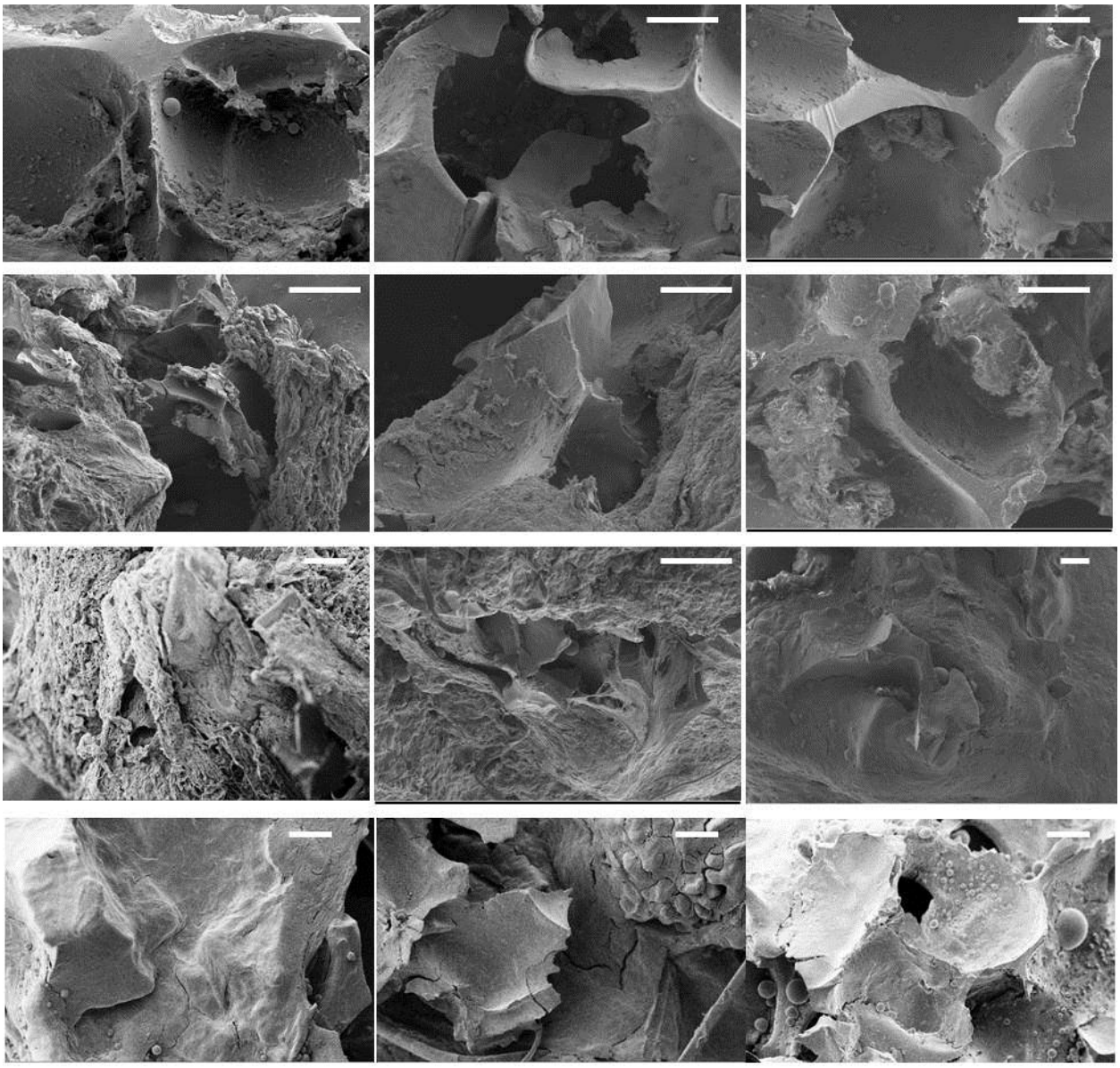

Figure 4.6- Silk sponge pore wall thickness did not change over time. (a) Silk sponge pores were observed by SEM. No differences in thickness were seen over time which confirmed our observation that degradation occurred from outer part of the sponge inwards. (b) The ranges of pore wall thickness were determined by image analysis in SmartTiff (Carl Zeiss Microscopy). Average pore wall thicknesses ranged from ~10-40 microns. The overall sponge structure remained intact with open pores and tissue infiltration. Each pore wall was measured 3 times,

and each sample was measured in 8 different locations per image.

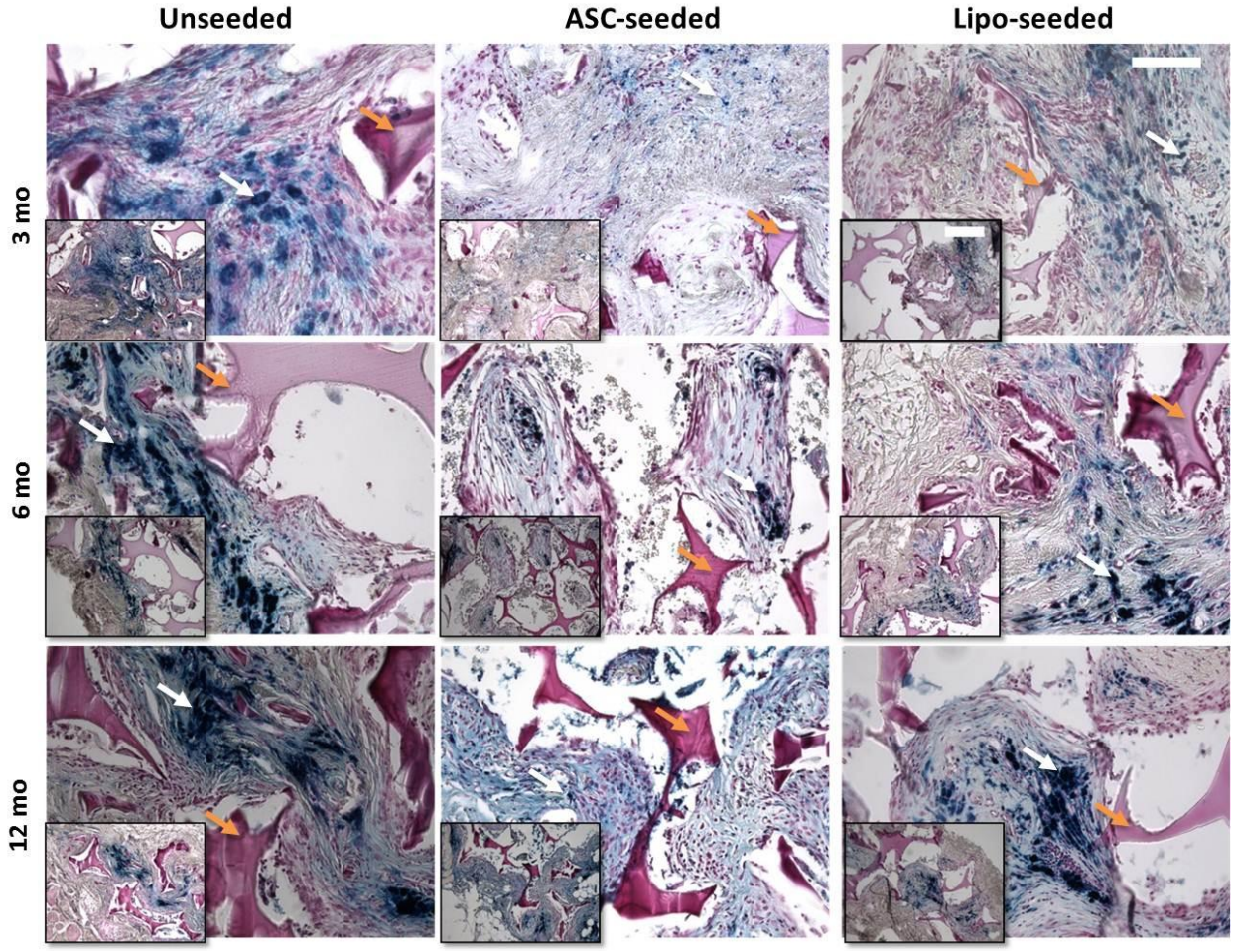

Figure 4.7- Iron deposits present during remodeling process. The Prussian Blue Test for iron deposits first dissociates ferric ions by treating with hydrochloric acid, and then sections are stained with potassium ferrocyanide to yield an insoluble blue compound. Iron deposits stain blue (white arrows, silk-orange arrows). All groups and timepoints contained areas of iron deposition. Iron deposits or hemosiderin deposits are found in areas of a past hemorrhage, in this case, most likely from the time of implantation.

CHAPTER 5. SILK INJECTABLE MATRICES FOR SOFT TISSUE REGENERATION

5.1 ABSTRACT

Soft tissue defects result mainly from congenital abnormalities, trauma, or tumor resections and constitute about 4.8 million reconstructive surgery cases per year in the US alone[138,139]. Autografts and lipotransfer have been one treatment for soft tissue reconstruction, however, the success is unpredictable, with 20-90% graft resorption within months[25–27]. A minimally invasive procedure that maintains volume over time would reduce scarring and recovery time as well as allow for grafted tissue to be placed closer to existing vasculature. Here, we demonstrate the feasibility of an injectable silk foam for soft tissue regeneration. Adipose derived stem cells were able to survive and migrate through the foam over a 10 day period. Injection of the foams into the subcutaneous space in a rat model was successful and foams were well vascularized and integrated with surrounding tissue in a 90 day study.

5.2 INTRODUCTION

Soft tissue defects result mainly from congenital abnormalities, trauma, or tumor resections and constitute about 4.8 million reconstructive surgery cases per year in the US alone[138,139]. Autografts and lipotransfer have been one treatment for soft tissue reconstruction, however, the success is unpredictable, with 20-90% graft resorption within months[25–27]. This leaves significant problems for the patient and thus the regeneration of large soft tissue defects remains an unmet clinical need. Silk, a protein biomaterial that has been used for decades for sutures[140,141], and recently FDA approved for use as a surgical mesh, can be processed into a variety of formats with control of degradation rate[67]. In a previous 18 month study, we demonstrated sustained tissue regeneration by combining mechanically robust, porous silk sponges that degrade slowly *in vivo*[66] to foster soft tissue regeneration. The sponges were combined with a biological component, adipose stem cells (ASCs) or lipoaspirate, degraded slowly over 18 months, while regenerating subcutaneous tissue and maintaining volume. The data suggest a simple, safe and clinically relevant solution to fill soft tissue defects with sustained volume and function. In this study, we explore the use of silk foam as an injectable format for soft tissue regeneration. An injectable format would be ideal to minimize patient discomfort, donor site morbidity, and recovery time. In addition, injecting in several but smaller volume amounts allows more of the grafted tissue to be closer to vasculature, hopefully leading to improved graft survival. Here, we test the injectability and *in vivo* biocompatibility of silk

foams. The 5x2mm (diameter x height) silk foams were easily injected subcutaneously in a rat model, and retained their shape after injection and integrated well with the surrounding tissue over a 90 day study.

5.3 METHODS

5.3.1 Materials

DiI, cell labeling dye and cell culture reagents were purchased from Invitrogen (Carlsbad, CA). Histological solvents were purchased from Fisher Scientific (Pittsburgh, PA) and histological reagents and Masson's Trichrome Stains Kit were purchased from Sigma-Aldrich.

5.3.2 Silk foam development

Silk solution was prepared as published[122]. Briefly, cocoons were chopped and placed in boiling 0.02M $NaCO_2$ for 30 minutes to remove sericin, and then washed 3 times in ultrapure water. The resulting silk fibroin fibers were left to dry overnight. The dry silk was solubilized in 9.3 M LiBr in 20% w/v at 60 C for 4 hours. The silk solution was then dialyzed in ultrapure water in 3,500 MWCO membrane for 2 days with a total of 6 water changes, to remove the LiBr. A silk foam sheet was created by using a freezer processing technique. Silk solution (1, 3, 6% w/v), was poured into a plastic Petri dish. The solution was then stored in an EdgeStar Model FP430 thermoelectric cooler maintained at around 20°F (~-7°C) for 3 days. The material was observed to be gel-like, but not a stiff solid. It was then transferred to a VirTis Genesis (Model 25L Genesis SQ Super XL-70) Lyophilizer for 3 days. After removal, the silk material was seen to have a very consistent interconnected fine-pore structure. The foam was soaked in 70% methanol to induce beta sheet formation. While 10% shrinkage of the foam occurred, the resulting foam exhibited excellent stiffness and toughness. A 5 mm diameter biopsy punch was used to make small foam disks.

5.3.3 Injection gun design

A Hauptner syringe that was custom-modified to implant silk foam subcutaneously during a rat implantation study. The design is based on a commercially available pistol-style (Hauptner) syringe made by Ideal Instruments. This device has a spring-loaded handle that forces an injector drawrod into the syringe body by a pre-set distance (using the injection stroke adjuster). Since this device was to be used for injecting foam and not a solution or gel, a foam ramrod was manufactured to fit through the end of the syringe, where the catheter adaptor is located. In this case, a tapered catheter was seen as a good way to inject foam into a body (the barrel of the catheter is larger than the catheter tip). The taper allows a foam sample to be pre-positioned in the barrel before attaching the catheter to the syringe and allows the foam to be gradually compressed during the process of injection. The rat study protocol involved the initial creation of a small hole in the rat skin using a 14 gauge needle positioned within the catheter. The foam ramrod is inserted into the syringe. The needle/catheter is used to place the catheter in the desired position. The silk foam is positioned in the barrel of the catheter using tweezers. The injection handle is then repeatedly squeezed to slowly inject the foam into the animal.

5.3.4 Adipose Derived Stem Cell Isolation

Subcutaneous adipose tissue was obtained from abdominoplasties under Tufts University IRB (Tufts University IRB Protocol #0906007) from the Tufts Medical Center, Department of Plastic Surgery. The specimens were kept at room temperature in saline and used within the same day. The adipose tissue was separated from the skin by blunt dissection and chopped. Chopped adipose tissue was placed into 50 mL conical tubes and minced well with scissors. The tissues were washed in equal volumes warmed PBS, until essentially free of blood. An equal volume of 1 mg/mL collagenase I in 1% bovine serum albumin in PBS was added to the tissue and placed under gentle agitation at 37^{o}C for 1 hour. The tissue samples were centrifuged at 300 x g for 10 minutes at room temperature. The supernatant containing the tissue was removed and the pellet resuspended in PBS and centrifuged at the same settings to remove the collagenase solution. The pellet was resuspended in growth media and plated so that 70 g of initial tissue volume was plated per T225 cm^2 tissue culture flask.

5.3.5 Cell Culture and 3D Culture

Adipose derived stem cells (ASCs) were expanded and cultured as previously described[16,142]. Cells were expanded first in growth media comprised of DMEM/F12, 10% FBS, 1% PSF. A preliminary *in vitro* study was performed to ensure cells were able to attach, migrate, and survive on the foams. Foams (8mm x 8mm, dxh) were autoclaved to sterilize. The foams were soaked for 1 hour in growth media, then 250,000 ASCs were seeded in 3 20 µl aliquots. The cells were labeled with DiI, prior to seeding. The seeded foams were placed in an incubator for 2 hours before media was added to the well. Cells and cultures were fed 2 times per week, and maintained in 37^{o}C, humidified incubator, for 10 days until imaged.

5.3.6 Lipoaspirate soaking test

Lipoaspirate from elective plastic surgery was obtained the same day of sponge implantation. Lipoaspirate was transported aseptically at room temperature just after surgery. Approximately 30 mL of lipoaspirate was added to a 50 mL conical tube and centrifuged at room temperature at 1,000 rpm for 10 minutes. The blood and free lipids were removed. The remaining tissue was placed in sterile petri dishes. The silk foams were placed into the processed lipoaspirate and allowed to soak.

5.3.7 In vivo implantation

Animals were cared for in compliance with Tufts University Institutional Animal Care and Use Committee (IACUC) in accordance with the Office of Laboratory Animal Welfare (OLAW) at the National Institutes of Health (NIH). Female Sprague-Dawley rats, 9 weeks old were purchased from Charles River Breeding Labs, and were allowed to acclimate for 1 week prior to implantation.

The animals were first anesthetized with isoflurane (1-4%) and were maintained with 1% (or to effect) isoflurane in oxygen, and kept on a heating pad through the entire procedure. After

induction of anesthesia, injection site was wiped down with alcohol. The skin was pinched into a tent, to form a space for the catheter. The catheter and needle was fed into the tented space, and the needle retracted. The foam was placed in the catheter, the injection gun was attached to the catheter and then the handle squeezed until the foam was injected subcutaneously. The catheter was removed and the animals were allowed to awaken and had free access to food and water. Six injections were made per animal, 3 along each side of the spine.

5.3.8 Histology

Constructs were processed according standard histology protocols. Formalin fixed samples were put through a series of dehydration solvents and finally paraffin using an automated tissue processor. Samples were embedded in paraffin, cut in 10 micron sections, and let to adhere on glass slides. The sections were rehydrated and stained with Hematoxylin and Eosin (H&E) for general morphology and organization and, Masson's Trichrome for tissue remodeling.

5.3.9 Scanning Electron Microscopy Imaging

Explanted implants with surrounding tissue were frozen at -80^{o}C until ready to process for imaging. Explants were washed in 0.1 M phosphate buffer, and then fixed in freshly prepared 2.5% glutaldehyde in 0.1 M phosphate buffer. The explants were washed in phosphate buffer, and then fixed in osmium tetroxide in 0.1 M phosphate buffer. The explants were dehydrated in a graded ethanol series, starting at 50% ethanol until dehydrated at 100% ethanol. Hexamethyldisilazane (HMDS) was added to the explants, removed, and then the explants were placed in a dessicator overnight to maintain dryness. The dried explants were mounted onto SEM stubs with double sided carbon tape and then sputter coated (208HR Sputter-Coater, Cressington Scientific Instruments, LTD, Walford, England) with platinum for 1 minute. Pt-coated explants were loaded into the 9 stub carousel and placed into the SEM (Supra55VP, Carl Zeiss Nano Technology Systems, Peabody, MA) for imaging.

5.4 RESULTS

In this study, we demonstrated the injectability of silk foams. The custom- designed injection gun (Figure 5.1) was simple to use, easy to sterilize and handle. The foam was compressed during injection but regained its original dimensions after deployment.

Cells adhere and migrate through foam

ASCs were seeded on the 3% silk foams and maintained for 10 days before imaging. A processing artifact of the foams was layers that had formed (Figure 5.2). After 10 days in culture, the cells were found to migrate through the foam (Figure 5.2). Cells were seen throughout the foam except at the bottom surface (opposite the seeding surface). Cells lined the pores of the foam, but did not fill up the pores at this time point (Figure 5.3).

Foams absorb lipoaspirate

The 3% silk foams were placed into lipoaspirate. Within a few minutes the foams had fully adsorbed the lipoaspirate (Figure 5.4).

In vivo injections

Foams were easily injected as pictured in Figure 5.1. The rats healed well, no adverse effects were seen as a result of the injections. By 14 days, the puncture site was fully healed (Figure 5.5). The foams were visible and palpable through the skin, and soft to the touch, out to 90 days. No differences were obvious between different w/v% silk foams. At 14, 30, 60 and 90 days the rats were sacrificed and foams were explanted. The foams had vascularity leading to them at 14 days, and the foams were clearly visible (Figure 5.6- Left panel). At 90 days, the vascularity leading to the foams had decreased as did their visibility (Figure 5.6- Right panel), as they begun to degrade. At day 14, the foam structure was more visible in the 3 and 6% foams, while tissue

had appeared to infiltrate the 1% foam (Figure 5.7- Top left panel). After 90 days all foams clearly had tissue infiltration (Figure 5.7- Bottom right panel).

The explanted foams were sectioned along the cross-sectional face pictured in Figure 5.7. The sections were stained with H&E and cells and tissue had completely infiltrated the foams (Figure 5.8). The foams had more tissue present with decreased silk %. The silk pore walls were clearly present through 90 days. Macrophages were present within the foam. Masson's Trichrome staining showed a mix of some collagen but mostly cells (Figure 5.9). By 90 days, it was difficult to discern any differences between groups. In SEM images, the foams maintain open pore structure at 14 days (Figure 5.10-Top panel). Less matrix deposition is visible with increased silk %, similar to histological results. By 90 days, the silk foam structure was only visible in the 6% silk foam group (Figure 5.10- Bottom panel). Tissue and cells have completely remodeled the 1 and 3% silk foam groups making it difficult to determine the silk structure.

5.5 DISCUSSION

The goal of this work was to determine the *in vivo* biocompatibility of injected silk foams for soft tissue regeneration. For regenerative medicine applications, the foams must be easy to handle, sterilize, store and seed with a biological component, such as adipose derived stem cells and lipoaspirate. Our previous study with implantable silk sponges yielded fully regenerated tissue over an 18 month period in a rat model (not yet published). The sponges implanted as is without any biological, yielded a well-organized connective tissue like tissue. However, when pre-seeded with lipoaspirate or pre-cultured ASCs, the tissue formed was adipose-tissue like. The silk sponge degraded in rate slow enough to allow for cells to repopulate and regenerate within the silk matrix template. In this current study, we aimed to develop a similar system, but minimally invasive. Development of a minimally invasive system allows smaller volumes to be injected, and for the grafted tissue to be closer to surrounding vasculature. Yoshimura et al, have been using this method in women for cosmetic breast augmentation[60]. In their study, stem cell enriched lipoaspirate was injected, yet of the 270 mL injected only about 100-200 mL remained after 2 months. The inclusion of a slowly degrading injectable matrix, such as these silk matrices, could act as a template for regeneration while the body remodels around the matrix. The study

presented here was a first attempt at injection of the foams *in vivo.* After 90 days, about 50% of the foam volume was left. In order to be effective for soft tissue regeneration, we must improve the degradation rate as with our silk sponges (> 6 months). Conventional methods, methanol treatment and autoclaving, from our group to increase the degradation rate by increase crystallinty were employed here. Future iterations may include increasing silk concentration to increase degradation rate. The pore size may need to be increased to account for the subsequent decrease in injectability after silk % has been increased. While the 6% was not difficult to inject, it was more difficult than the 1 and 3% foams. Pore size may be easily altered by controlling freezing temperature, and/or cycling between freezing and partially thawing states.

The *in vitro* preliminary cell study established that ASCs can survive and migrate through the foam. The cells lined the walls of the pores. In addition, we showed that the silk foam will readily adsorb lipoaspirate. Lipo-injections are commonly done clinically, however, we do not know if the addition of silk will impact lipoaspirate tissue survival. Lipoaspirate is a mix of proteins, growth factors, adipocyte precursors as well as mature adipocytes. It is estimated that about 30% of the adipocytes rupture during lipoaspirate processing[148]. A future study should use those methods to determine cell viability before and after injection with a silk matrix.

The *in vivo* study in a subcutaneous rat model demonstrated the feasibility of using silk foam in a minimally invasive context. Macroscopically, the foams integrated well over time and were vascularized. Mature blood vessels were not detected upon histological examination. Macrophages were present in histological sections in all groups. Macrophages can be pro-inflammatory (M1) or a tissue remodeling phenotype (M2). To better understand the type of tissue remodeling, we should investigate the relative macrophage phenotype using immunohistochemistry staining against M1 and M2 cell surface markers. The addition of a cellular component affects polarization and as such a follow-up study including the effect of lipoaspirate seeding on macrophage polarization, and therefore, remodeling, should be conducted [149,150].

This study is the foundation for using silk foam as an injectable matrix to augment soft tissue regeneration, as fat grafting alone has a history of yielding inconsistent results. Previously, we have shown that a slowly degrading injectable silk sponge can act as a template for tissue regeneration. In this study, we aimed to translate that system into a minimally invasive system, reducing scarring, decreasing recovery time and donor site morbidity. Future studies, include increasing foam degradation rate, characterizing the remodeling profile, and injection with lipoaspirate.

5.6 ACKNOWLEDGEMENTS

I wish to thank Gary Leisk and Tim Lo for material and injection gun development and for providing the silk foams. I wish to also thank Tim Lo for assistance during injections. I thank Eun Seok Gil for SEM imaging. I thank Kacey Marra and J. Peter Rubin for discussions on the clinical needs.

5.7 FIGURES

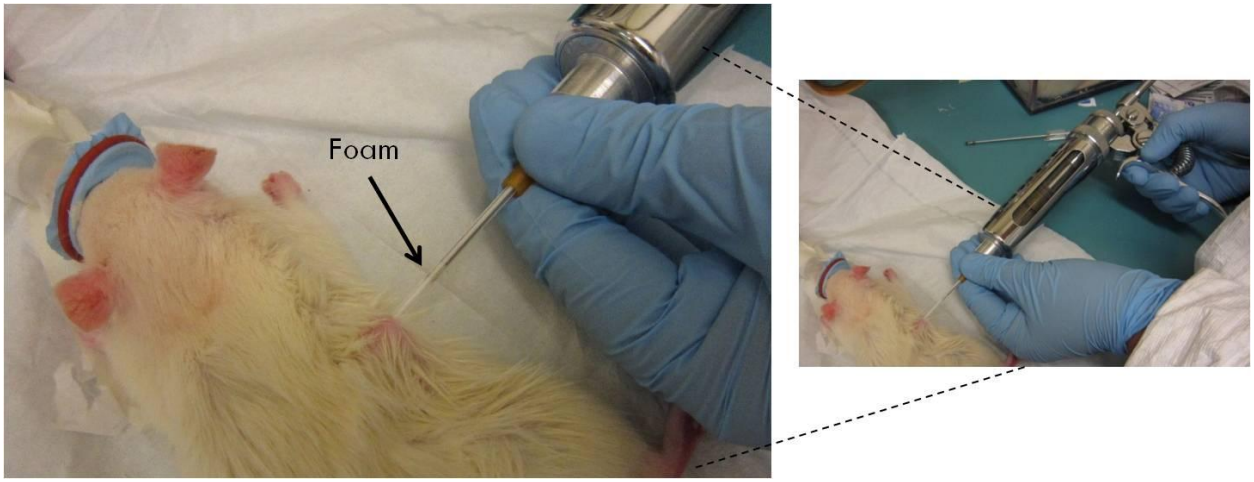

Figure 5.1- *In vivo* foam injection with custom designed injection gun.

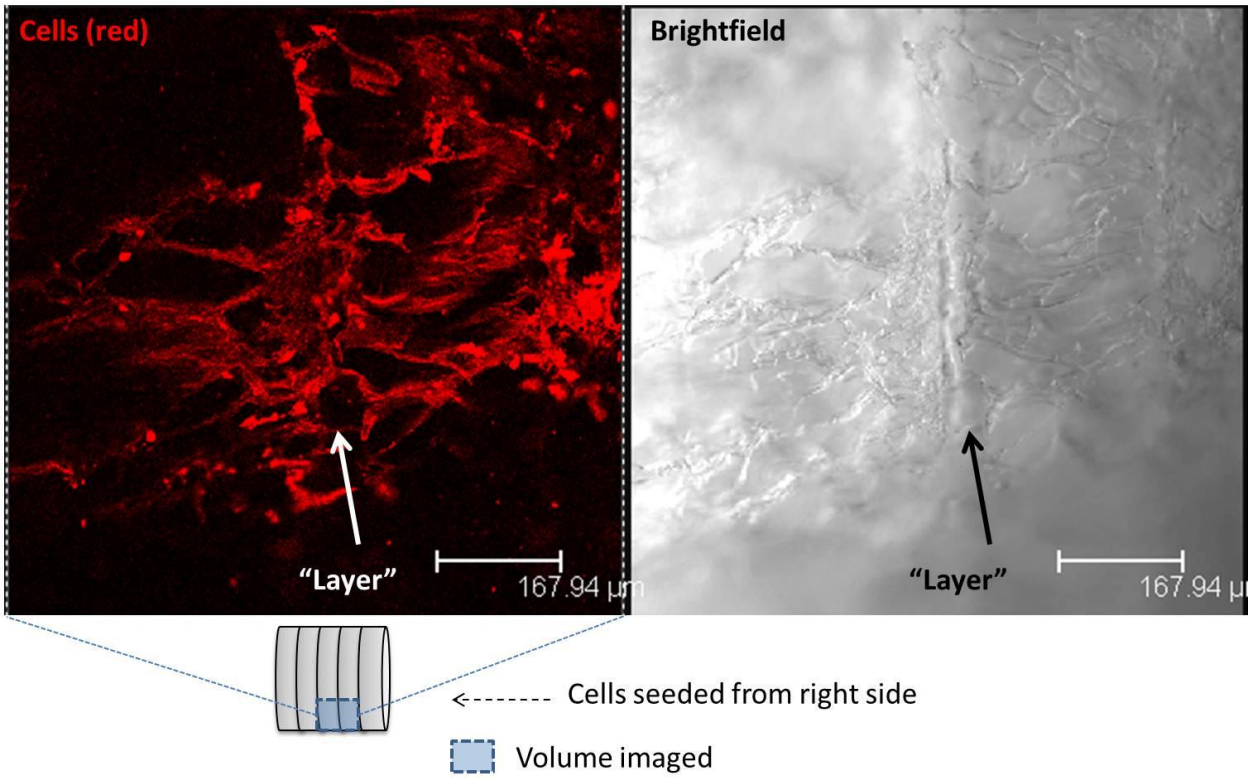

Figure 5.2- Cells migrate through foam layers. Foams contain layers as a result of the processing conditions. Confocal images of fluorescently labeled cells (fluorescent- left; brightfield- right) on silk foam. Side surface perpendicular to seeding surface was imaged.

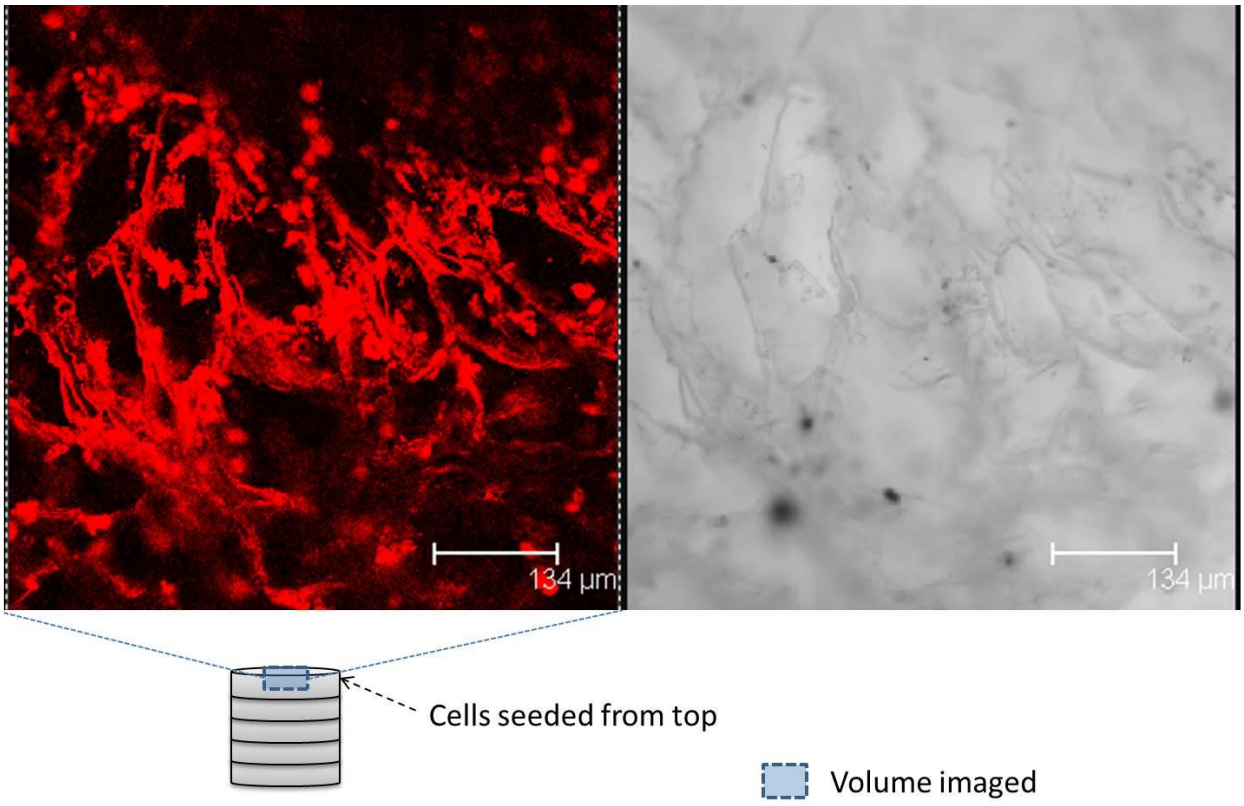

Figure 5.3- Cells populate the foam pores. Confocal images of fluorescently labeled cells (fluorescent- left; brightfield- right) on silk foam. Surface that was seeded was also imaged.

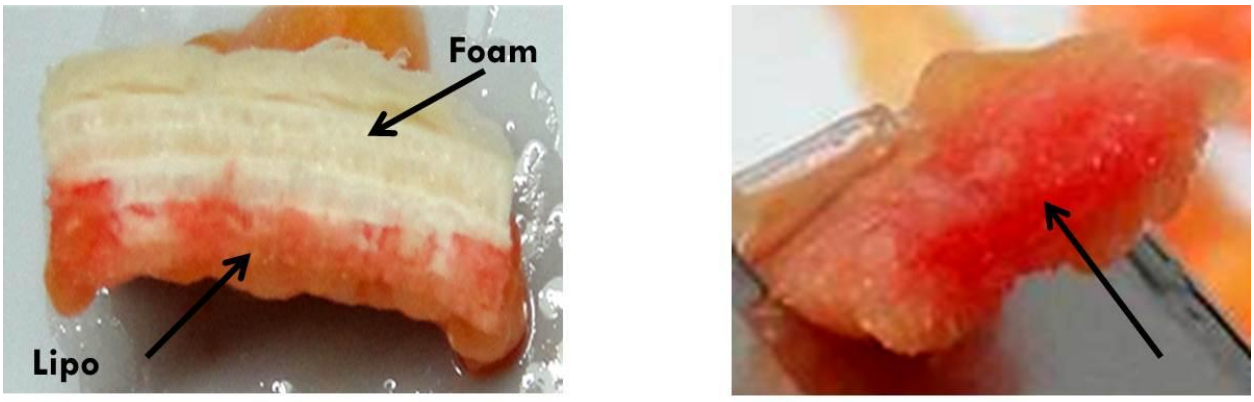

Figure 5.4- Foams adsorb lipoaspirate readily. Left panel- foam in the process of absorbing lipoaspirate. Right panel- within minutes the foam had adsorbed lipoaspirate through its entirety, shown is the cross-section.

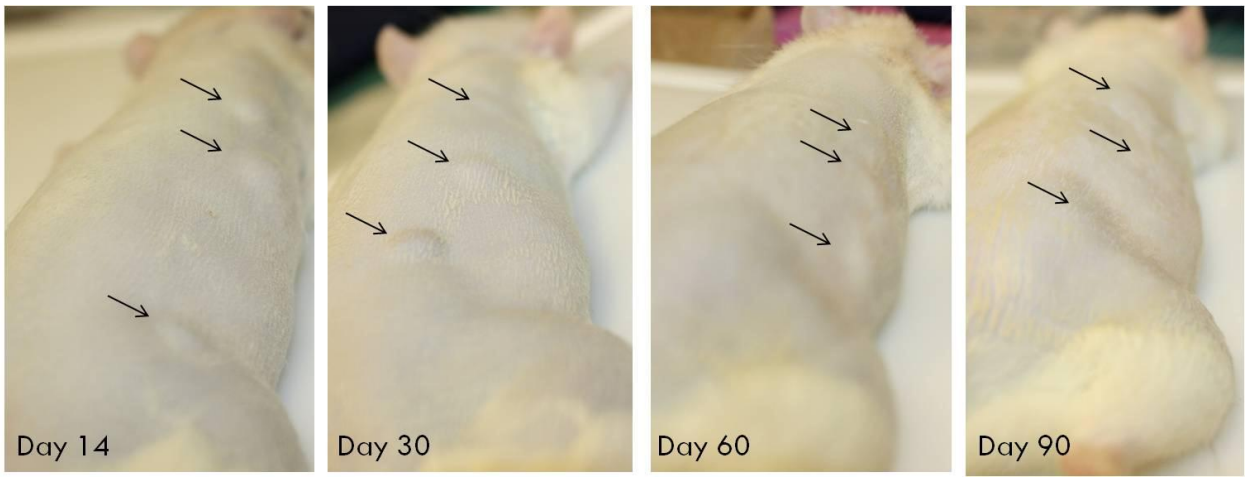

Figure 5.5- Foams visible and palpable through skin. Skin is well healed at injection site.

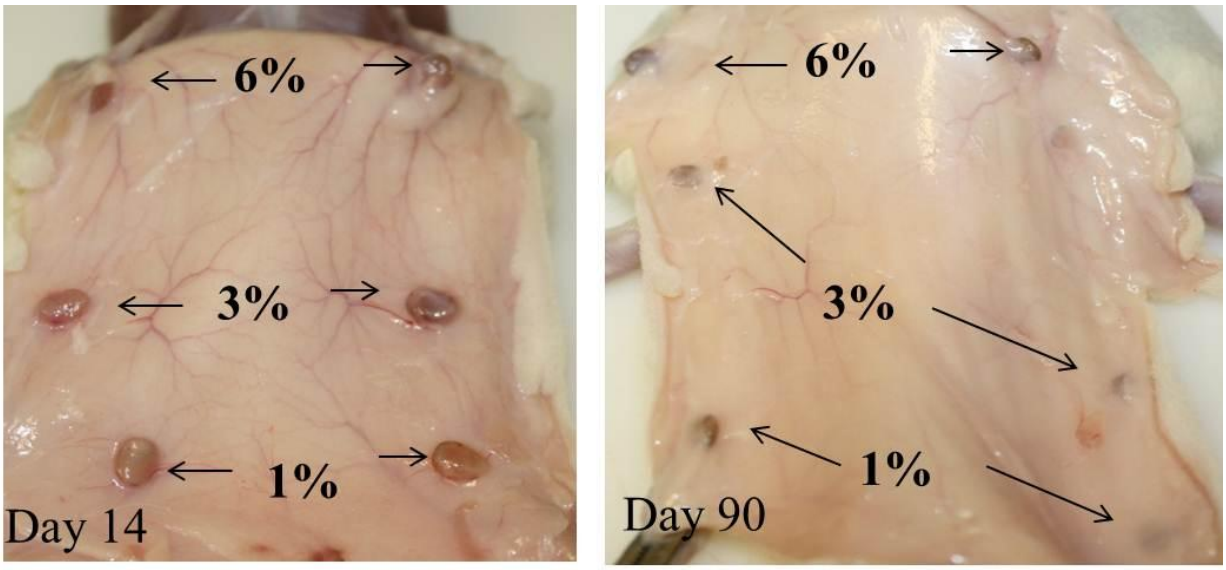

Figure 5.6- Foams after 14 (left) and 90 (right) days *in vivo*. At 14 days, vascularity was clearly leading to foams, but had decreased after 90 days.

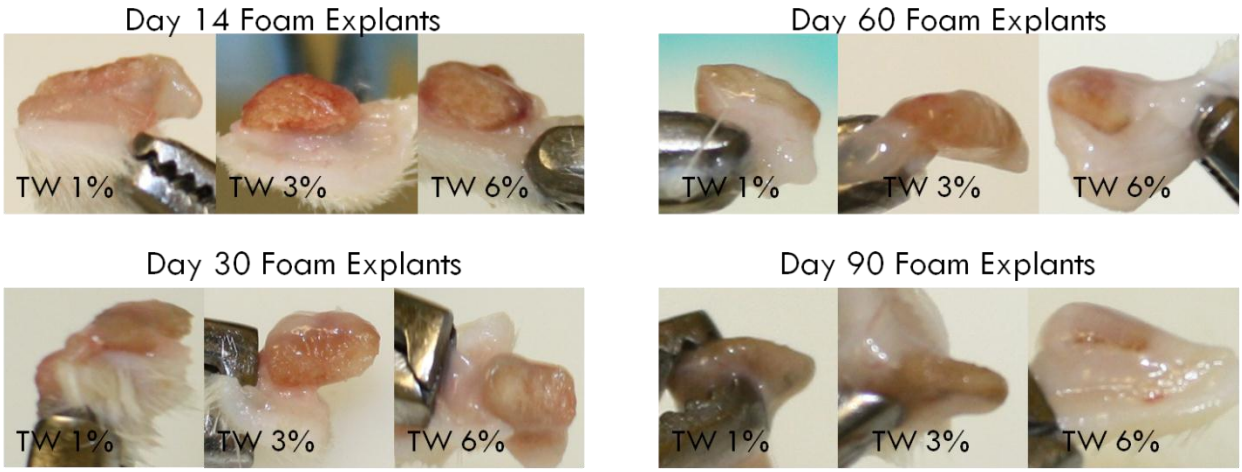

Figure 5.7- Cross-sections of foams after in vivo implantation. Integration with surrounding tissue increased with time.

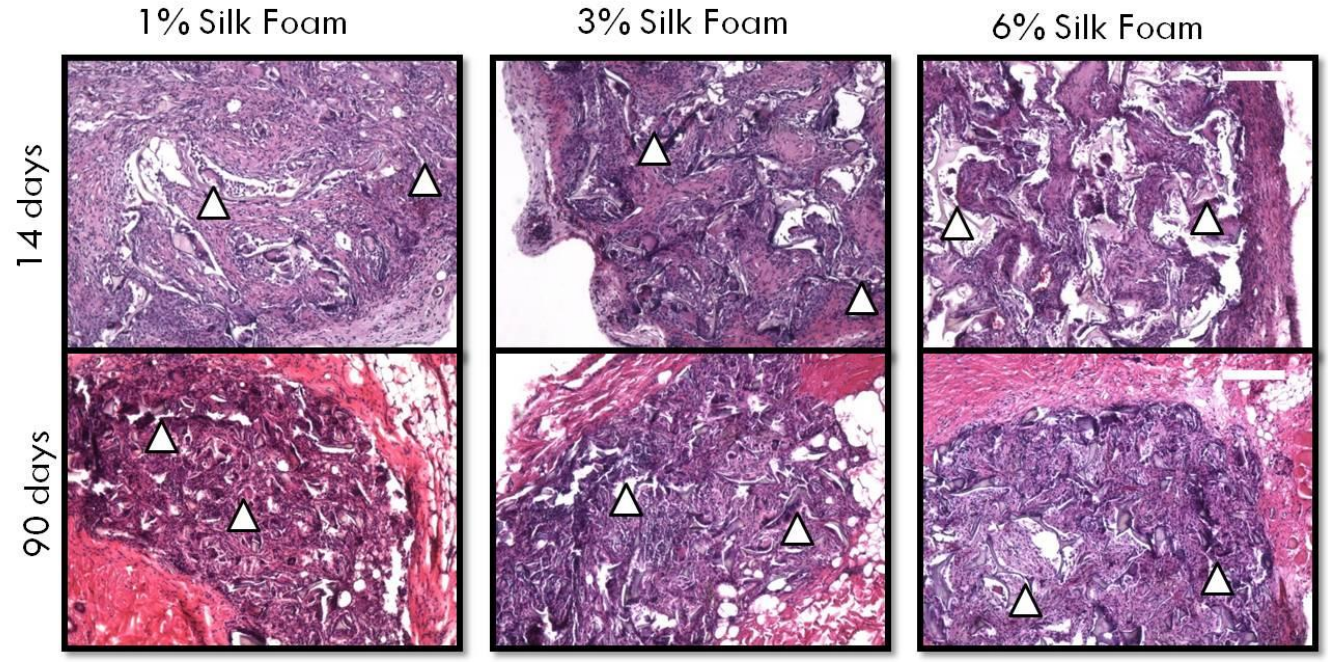

Figure 5.8- Representative H&E images of foams after 14 and 90 days *in vivo*. Arrow heads point to silk foam. Scale bar- 200 microns.

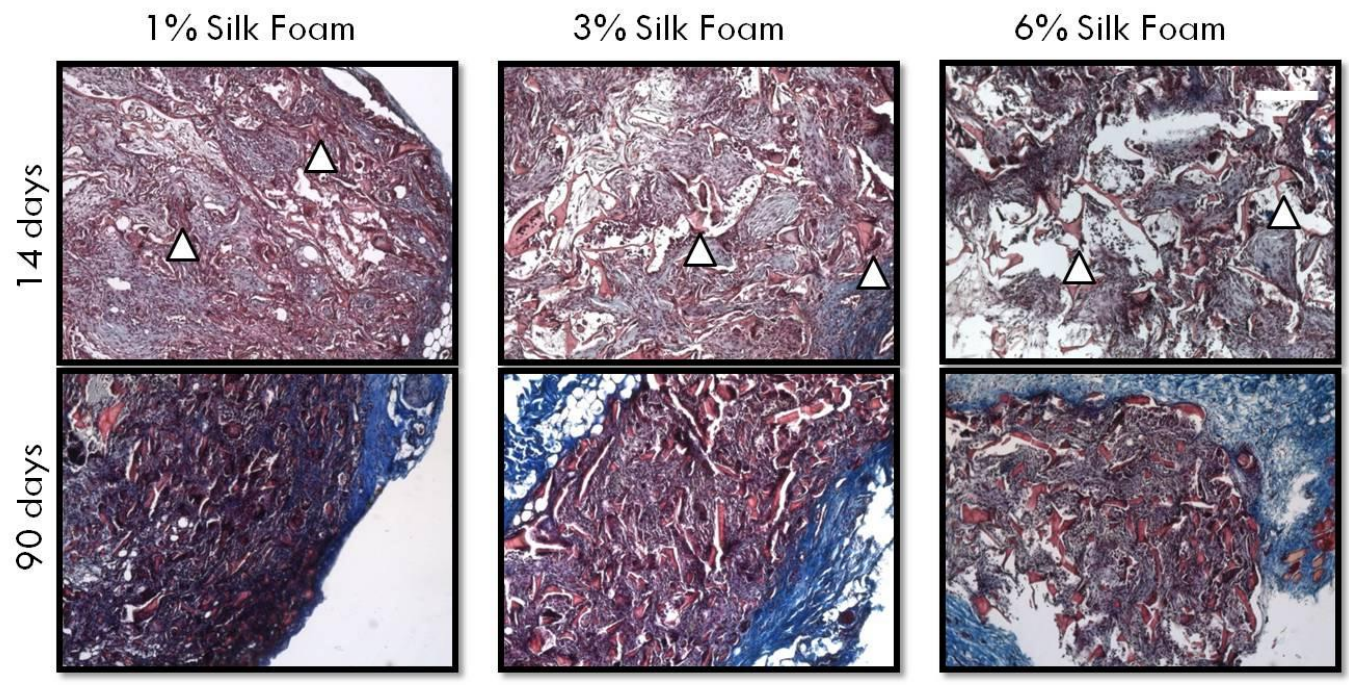

Figure 5.9- Representative Masson's Trichrome images of foams after 14 and 90 days *in vivo*. Arrowheads point to areas of silk. Scale bar- 200 microns.

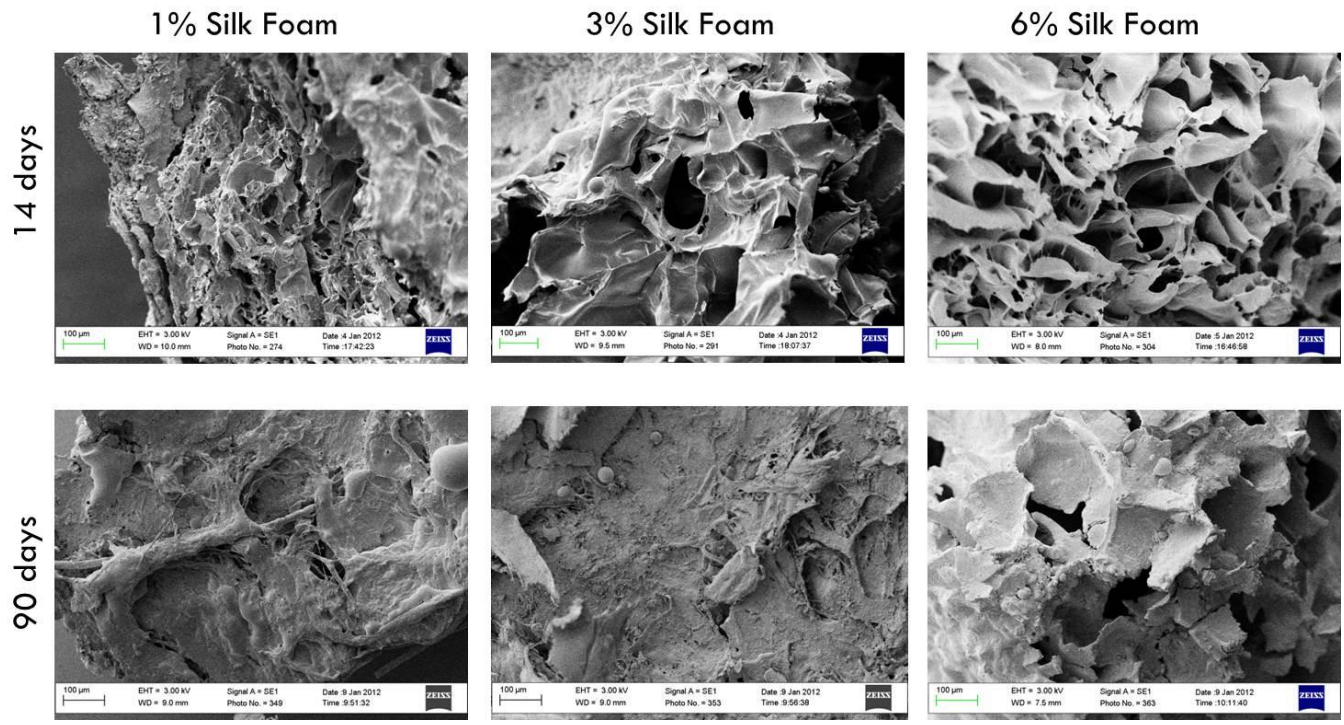

Figure 5.10- SEM of foams after *in vivo* implantation**.**

CHAPTER 6. CONCLUSIONS AND FUTURE DIRECTIONS

6.1 SUMMARY OF RESULTS

6.1.1 Development of a long-term adipose tissue construct

The goal of this thesis was to develop a long-term vascular adipose tissue construct that would ultimately serve as the basis for studying adipose tissue dysfunction or soft tissue regeneration. In both cases, sustained structure is important. Dynamic cultures were explored as a way to improve overall tissue outcomes as a result of enhanced mass transport. Dynamic cultures contained tissue formation throughout the entire construct when compared to static groups where cells were found mostly at the periphery. All groups contained Oil Red O positive cells, with an increase in dynamic cultures. Initially, the ratio of hADs to endothelial cells was 1:2, yet not many endothelial cells remained, albeit appropriately organized into lumen like formations.

Adipogenesis can only occur with *PPARγ* transcription, therefore it is crucial to have *PPARγ* expression in our cultures[17]. Since adipogenesis cannot be initiated without *PPARγ* expression, it is normally thought of as an early marker of adipogenesis, yet *PPARγ* is continuously expressed through various stages of adipogenesis[17]. Our results showed that expression was highest at 1 month under static conditions, and levels did not vary between dynamic groups. No systematic study has been done, to our knowledge, on the effect of shear forces directly on adipogenesis. Shear forces may decrease or alter the ability of cells to upregulate *PPARγ* or to undergo adipogenesis at the same rate. *GLUT4* expression did increase, though not significantly, from 1 to 6 months under dynamic conditions. GLUT4 expression is a late marker of adipogenesis and is partially regulated by the presence of insulin, under dynamic conditions; the transport of insulin to the cells may be enhanced. Both leptin and glycerol levels increased with dynamic cultures, likely due to increased mass transport. In this study, we found fluctuations in leptin and glycerol levels at 3 months. Taken into account with the decrease of DNA content, it is possible cells had ruptured if they had accumulated too much lipid, or had become apoptotic for other unknown reasons. No other studies to date, to our knowledge, have studied *in vitro* adipogenic outcomes for long-term cultures up to 6 months. This study serves as the foundation for the obesity disease model and soft tissue regeneration.

6.1.2 Development of a chronic obesity model

The goal of this work is develop a long-term model of obesity that could serve as a model to study disease mechanisms and as a platform for testing anti-obesity therapies. Three dietary fatty acids were used in this study, palmitic acid, stearic acid, and oleic acid. In order to generate an appropriate model of obesity, we cultured the adipocytes for 6 weeks in fatty acid media, to allow for the adipocytes to accumulate more lipids. Adipocyte hypertrophy begins the cascade of events that lead to obesity. MCP-1, the major chemoattractant factor released from adipocytes, was most elevated in the palmitic group. TNFα levels in our study did not vary with fatty acids, or with addition of monocytes, with the exception of the control group in which no TNFα was detected. Il-6 levels were elevated in the presence of palmitic acid, and further increased with monocytes. Adiponectin levels in the absence of fatty acids were elevated. MCP-1, Il-6 and leptin levels were evaluated after exposure to anti-obesity therapies, CLA and wogonin. Both therapies decreased the levels of MCP-1 when cultured with monocytes. COX-2 is expressed in all cell types. Wogonin also decreased leptin levels in the presence of monocytes. Effects of CLA were not conclusive. In this study, COX-2 and PPARγ transcription levels increased over time with wogonin treatment. Yet, in the presence of monocytes and palmitic acid, the COX-2 transcription levels were lower than other groups. FABP4 was highly upregulated in palmitic acid and monocyte groups in the presence of wogonin. These data suggest that FABP4 is upregulated by palmitic acid in adipocytes and/or monocytes, and is regulated independently of inflammatory markers.

This study was the first to explore the chronic effects of monocyte and fatty acid exposure on a 3D culture of human vascular adipose tissue. The soluble factors in this study were chosen not only because they play a major role in disease progression but are also clinical readouts. MCP-1, Il-6, TNFα, leptin are all chronically elevated in blood plasma of obese patients, while adiponectin is decreased[136,137]. Using clinically relevant physiological markers we can relate our disease models to patient data. These data suggest that the inflammatory cells, macrophages, are important for mediating the response to fatty acids and wogonin. Future work on obesity should include therapies that *directly*, not indirectly, decrease the local inflammatory response. These

anti-inflammatory therapies could be combined with other anti-obesity therapies to maximize response.

6.1.3 Sustainable soft tissue regeneration

Silk biomaterials were chosen based on their ability to be tailored to fit a wide range of mechanical and degradation profile, as well as being unlimited in terms of total sponge size and shape. This maintenance of structure of a very slowly degrading biomaterial allowed tissue regeneration and sustained biological function during the remodeling process, without the loss of implant volume. This represents a major advance over current biomaterial options used for soft tissue regeneration. The remodeling process continued within the sponge structure due to the maintenance of mass transport by keeping the porous structure open. By the time the sponges began to degrade at 12 months, tissue formation in all study groups had been well established, complete with vasculature.

In this study, silk porous protein sponges, alone, or seeded with *in vitro* differentiated ASCs or freshly isolated lipoaspirate, were implanted into nude rats. We chose these study groups as they are clinically translatable. The harvest of lipoaspirate is already clinically used for fat grafting. We chose to compare freshly isolated lipoaspirate to *in vitro* differentiated ASCs cultured for 4 weeks on the sponges, as the lipoaspirate contains active vascular growth factors that may enhance tissue regeneration. Fresh ASCs have been postulated to take on a perivascular phenotype[151]. Further, harvesting and processing lipoaspirate can be done the same day as the implantation without scarring, and no *ex vivo* manipulation that would require FDA approval is needed to re-implant the lipoaspirate.

This study, to our knowledge, is the first to successfully demonstrate retention of volume for more than 6 months following implantation of soft tissue regeneration systems in a small animal model. At 12-18 months the sponges began degrading while encased in their own fat pockets, thus tissue regeneration without significant loss of volume. The histological changes over time support the conclusion that the silk porous sponges acted as templates for dynamic tissue regeneration even during this remodeling process. These results point towards a viable clinical strategy to address this major surgical need for soft tissue regeneration.

6.1.4 Injectable silk foams for soft tissue regeneration

The goal of this work was to determine the *in vivo* biocompatibility of injected silk foams for soft tissue regeneration. For regenerative medicine applications, the foams must be easy to handle, sterilize, store and seed with a biological component, such as adipose derived stem cells and lipoaspirate. Our previous study with implantable silk sponges yielded fully regenerated when pre-seeded with lipoaspirate or pre-cultured ASCs. The silk sponge degraded in rate slow enough to allow for cells to repopulate and regenerate within the silk matrix template. In this current study, we aimed to develop a similar system, but minimally invasive. Development of a minimally invasive system allows smaller volumes to be injected, and for the grafted tissue to be closer to surrounding vasculature. The study presented here was a first attempt at injection of the foams *in vivo.* After 90 days, about 50% of the foam volume remained. The *in vitro* preliminary cell study established that ASCs can survive and migrate through the foam. The cells lined the walls of the pores. In addition, we showed that the silk foam will readily adsorb lipoaspirate. The *in vivo* study in a subcutaneous rat model demonstrated the feasibility of using silk foam in a minimally invasive context. Macroscopically, the foams integrated well over time and were vascularized. Mature blood vessels were not detected upon histological examination. Macrophages were present in histological sections in all groups.

This study is the foundation for using silk foam as an injectable matrix to augment soft tissue regeneration, as fat grafting alone has a history of yielding inconsistent results. Previously, we have shown that a slowly degrading injectable silk sponge can act as a template for tissue regeneration. In this study, we aimed to translate that system into a minimally invasive system, reducing scarring, decreasing recovery time and donor site morbidity. Future studies, include increasing foam degradation rate, characterizing the remodeling profile, and injection with lipoaspirate.

6.2 FUTURE DIRECTIONS

6.2.1 Large Animal Scale Up Pilot Study

Our long-term *in vivo* small animal model demonstrated that we can regenerate adipose tissue on a small scale. However, the average human is about 350 times the weight of the rats used in our study. Therefore, in order to prove clinical relevance, we must scale up our materials in a large animal model. The large animal model must have easily accessible subcutaneous fat. For this reason, we chose a horse model as they have SQ depots above their gluteal muscles (Figure A.1). In a preliminary large animal study, we implanted $1cm^3$ silk sponges alone or with autologous SQ fat (Figure A.2 top panel) along the dorsal plane of the horse for 6 months (Figure A.2-bottom panel). We found the addition of autologous fat yielded a more tissue like appearance upon initial visual inspection (Figure A.3). The sponges maintained their dimensions, whether or not they were seeded with autologous fat (Figure A.3). Histological characterization of silk alone and lipo-seeded silk sponges after 6 months *in vivo* showed that more cells and tissue are present in the lipo-seeded sponge group (Figure A.4). The silk matrix is clearly visible in both groups at 6 months and is beginning to fracture in the lipo-seeded group (Figure A.4). These results confirm our long-term rat study, where we saw more tissue present, and improved tissue quality with pre-seeding, as well no change in volume in the first 6 months. Currently, an ongoing study where we also modified our silk matrices (gels, foams, sponges) to degrade completely in a 3 month time frame is underway.

6.2.2 3-Layer Skin Equivalent

The development of physiologically relevant *in vitro* human tissue models is paramount to advancing medicine and product development. The cost to develop a drug and bring it to market is extraordinarily high when you consider the cost of small animal studies, pre-clinical studies in large animals and clinical studies in humans. In the last 30 years, costs range from $207-884 million[104,152–155]. Many groups have developed therapeutics that worked very well in animal models and failed to yield the same results in human clinical trials. In addition, the E.U. will no longer allow the sale of new consumer products tested on animals (European Union Council

Directive 76/768/EEC). Therefore, for U.S. companies developing consumer products, and wish to sell them abroad, must also not test products on animals.

This long-term *in vitro* vascular adipose tissue construct could be incorporated with other cell/tissue systems to develop other disease models and drug testing platforms. A layer of adipose tissue makes up the hypodermis, or the subcutaneous tissue. Other groups have created the epidermis and dermis *in vitro*, yet not many have created full thickness skin[156–159]. The co-culture of tissue engineered skin (epidermis, dermis) with our adipose tissue (hypodermis) could serve as disease model for cancers, wound healing, scar prevention and as a testing platform for therapies to treat these pathologies (Figure B.1). This full thickness skin may also have implications in skin grafting in burn victims. Current grafting methods replace the dermis, resulting in scarring and need for repeat grafting, because the fat layer is not present to maintain the structure and counteract the contraction caused by the dermal fibroblasts[160,161]. The expression of dermal and adipose layer related genes confirm that the dermal and the adipose layers of the 3-layer skin equivalents are metabolically active (Table B.1, B.2, B3). No other three layer skin construct is available to date with metabolically active dermal and adipose layers.

6.2.3 Brown Fat

Brown adipose tissue (BAT), a thermogenic adipose tissue, has become researched more heavily since it was found that adult humans have small BAT depots[1,2]. BAT adipocytes are multilocular, or have many lipid droplets, and get their brown color from their many mitochondria. The multilocular phenotype allows for "easy access" to the stored triglycerol (TG) that is used by the mitochondria for FFA oxidative phosphorylation to release heat[3]. In humans, BAT is found interscapularly at birth, and cervical, supraclavicular and paravertrebral regions in adults[1]. Anti-obesity interventions that increase energy expenditure or activate brown fat, increase the rate of mitochondrial fatty acid β-oxidation and heat production[10]. This approach has become of more interest lately with the discovery of cold-activated brown fat depots in adult humans[75]. Generation of a 3D human brown fat model will allow 1) understanding of brown adipocyte biology, 2) understanding of brown fat activation, 3) insight to anti-obesity

mechanisms. Similar to our white fat model, we can develop patient specific models and test potential therapies. ASCs have been shown to differentiate into brown-like adipocytes[162].

6.2.4 Muscle

White fat, brown fat and myoblasts are all derived from the same progenitor population[1]. Therefore, brown fat could be viewed as an intermediate between white fat and muscle. White fat is characterized by a single, central lipid droplet, while brown fat is characterized by many mitochondria and lipid droplets for easy energy usage and energy access, respectively. Muscle contains many mitochrondria and can accumulate lipid. They share many of the same pathways related to metabolism and inflammation. Ectopic lipid formation is detected in patients with metabolic dysfunction and impaired glucose usage. ASCs have been shown to differentiate into myoblasts in several studies, however, no study shows full functional outcomes by accessing contractility.

The generation of a 3D skeletal muscle is important for several reasons: 1) studying skeletal muscle development, 2) studying skeletal muscle disease, 3) regeneration of skeletal muscle defects, 4) understanding metabolic disease, and 5) understanding brown fat.

6.3 CONCLUSIONS

The work presented in this dissertation centers around exploiting our knowledge of adipose tissue engineering. Our long-term vascular adipose tissue construct served as a foundation for further long term studies in obesity modeling as well as for soft tissue regeneration. The long-term vascular adipose tissue maintained adipose-like outcomes over a 6 month period, and was improved by dynamic culture. From this, we developed a model of diet-induced obesity by challenging this system with free fatty acids and monocytes to generate inflammation. Finally, our *in vivo* 18 month study was the first to show that we can maintain volume while actually regenerating tissue when silk sponges are soaked with lipoaspirate. This model now is being translated into injectable formats to be minimally invasive. Ongoing pre-clinical studies are underway in a horse model for soft tissue regeneration.

APPENDIX A

Figure A.1- Subcutaneous fat is readily accessible from above the gluteal muscle (left). The minced fat resembles human lipoaspirate (right).

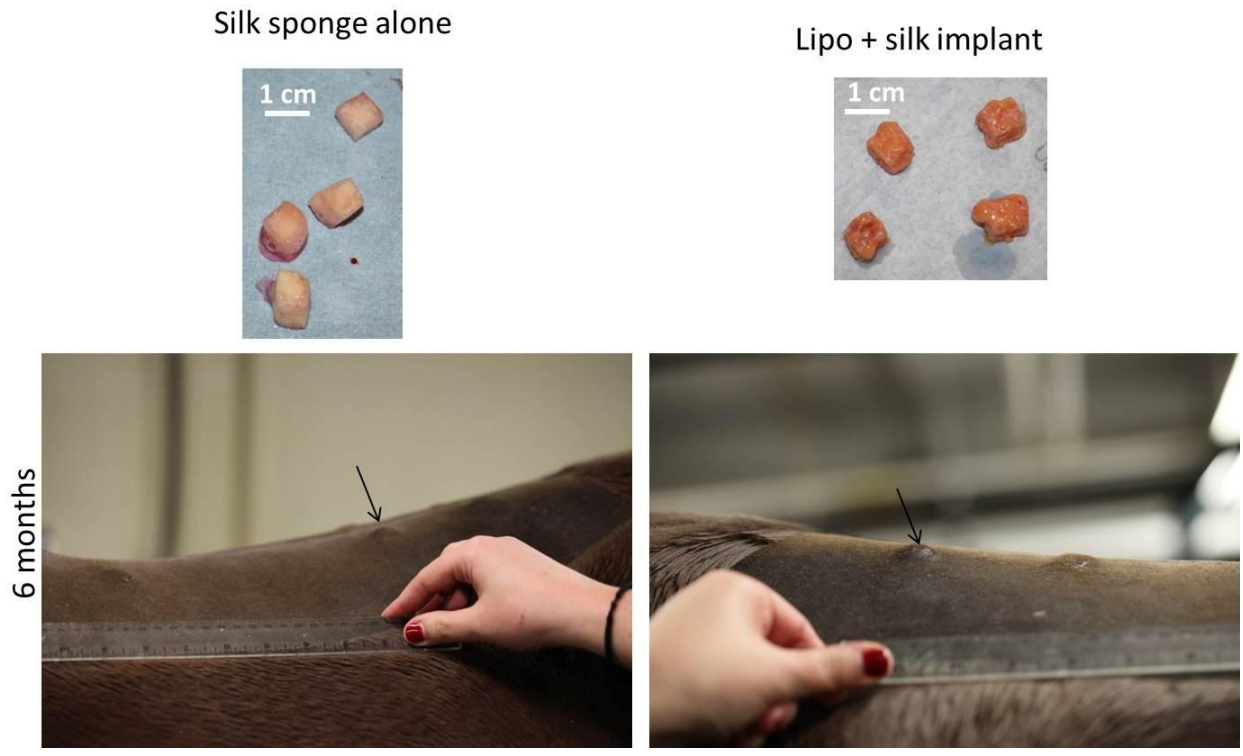

Figure A.2- Silk sponges prior to implantation (top). Implanted silk sponges are visible through skin after 6 months *in vivo* (bottom).

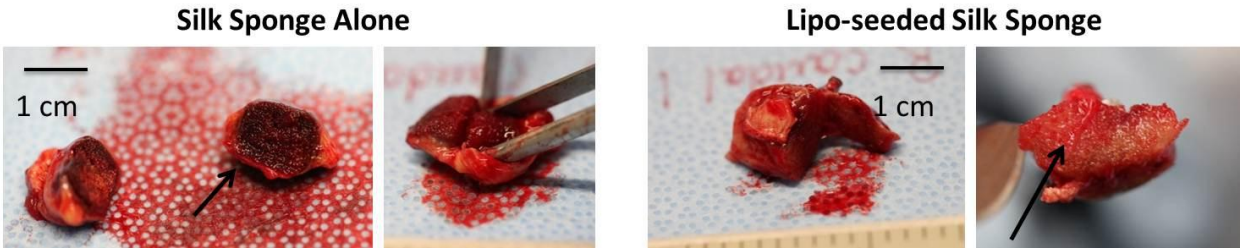

Figure A.3- Silk sponge explants after 6 months *in vivo*. Left panel- silk sponge alone, maintains sponge appearance even after 6 months implantation. RIght panel- lipo-seeded silk sponge appears to have a more natural tissue appearance.

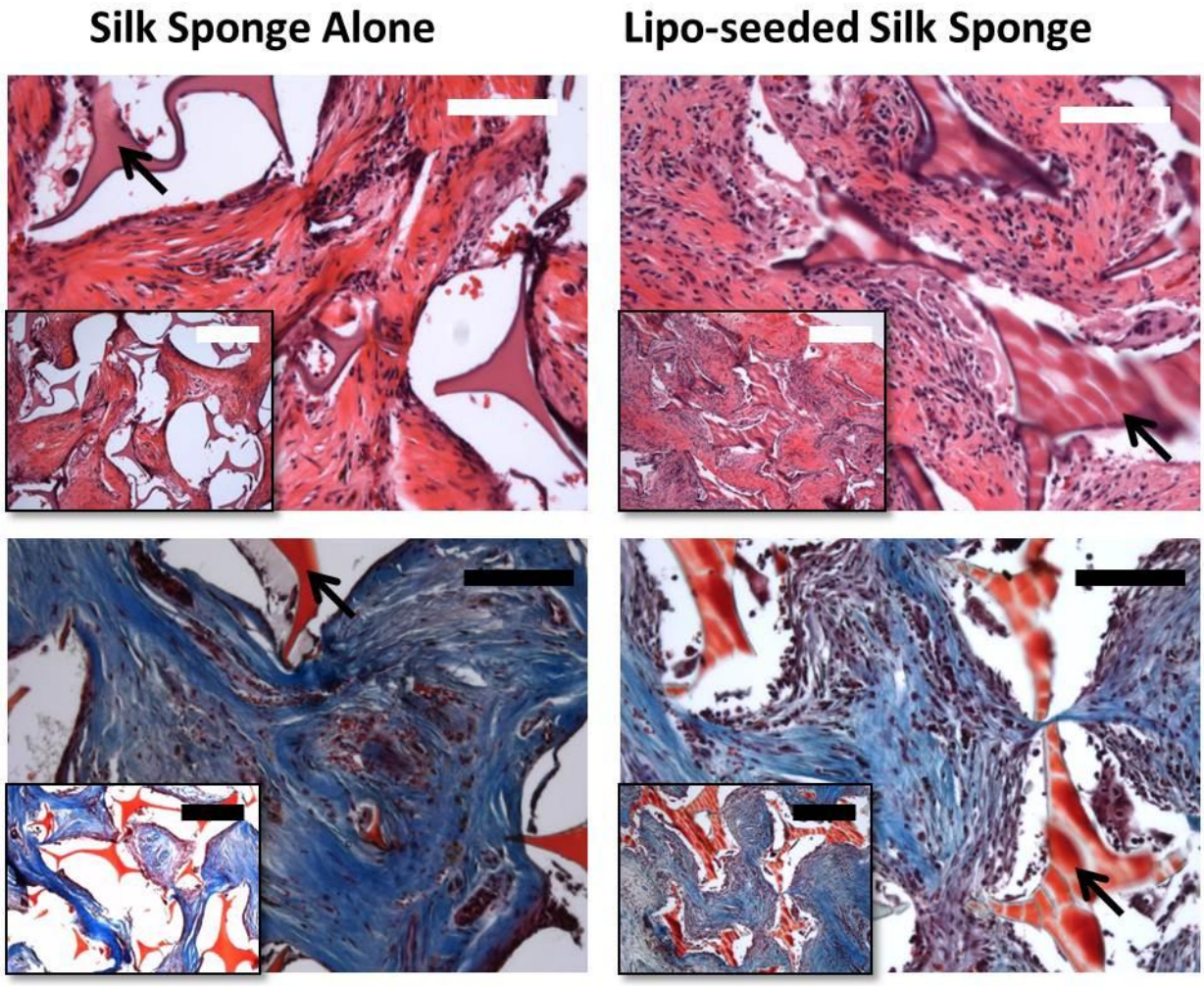

Figure A.4- Top panel- H&E histological images of silk alone (left) and lipo-seeded silk (right) sponge after 6 months *in vivo*. Silk sponge is clearly visible in both groups (black arrow) and is beginning to fracture in the lipo-seeded group. Bottom panel- Masson's Trichrome histological images. More tissue and cells are present with lipo-seeding. Scale bar 100 microns, inset 200 microns.

APPENDIX B

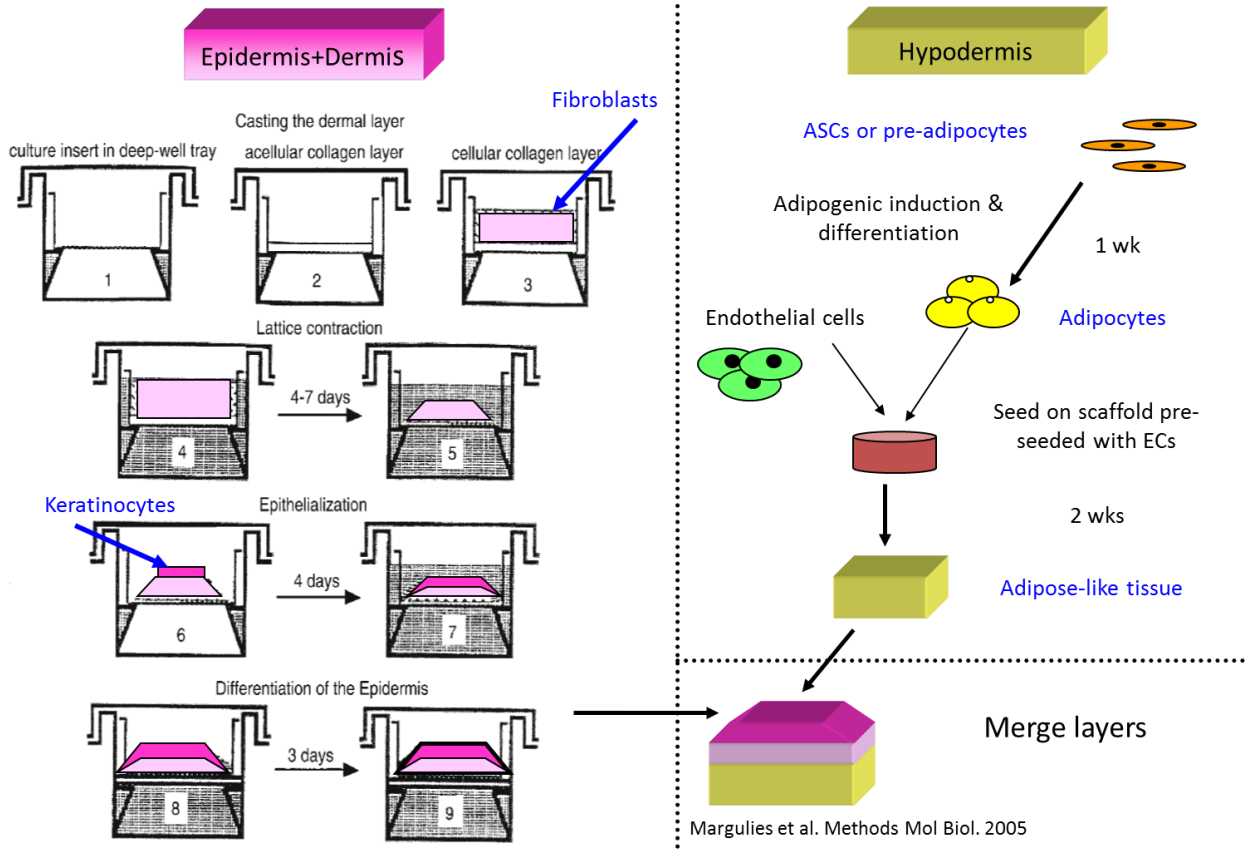

Figure B.1- Full Thickness Skin Tissue Engineering Model Experimental Design. Methods for skin development are taken from Margolies et al, 2005. These two layers will be cultured separately initially, then combined using a collagen glue after ~ 2 weeks.

Table B.1- Gene expression for dermal and fat related genes after 5 and 9 days of culture.

Gene	Compartment	Time	Expression in 3-layer construct
Collagen I	dermal	Day5	+
		Day9	++
Collagen IV	dermal	Day5	++
		Day9	+++
Elastin	dermal	Day5	+/-
		Day9	+/-
Fatty acid synthase	fat	Day5	+
		Day9	+
FABP4	fat	Day5	+/-
		Day9	+/-
Glut4	fat	Day5	++
		Day9	++

Table B.2- Leptin release in media of 3 layer skin equivalents.

Leptin in media (ng/mL)	Tissue			
Day	Media	Epidermal-dermal equivalent	Adipose layer equivalent	3-layer equivalents
0	Epidermal-dermal	-	++	+++
	1:1	-	+++	++
	adipose	-	+++	++
2	Epidermal-dermal	-	++	+++
	1:1	-	+++	+++
	adipose	-	++	++
6	epidermal-dermal	-	++	+++
	1:1	-	++	++
	adipose	-	++	++
8	epidermal-dermal	-	++	++
	1:1	-	++	++
	adipose	-	++	+
controls	media only	epidermal-dermal	-	
		1:1	-	
		adipose	-	

Table B.3- Glycerol release from 3-layer skin equivalents.

Glycerol in media (μM)		Tissue		
Day	Media	epidermal-dermal equivalent	adipose layer equivalent	3-layer equivalent
0	epidermal-dermal	++	+	++
	1:1	+	+	++
	adipose	+	++	++
2	epidermal-dermal	++	+	+
	1:1	+	+	++
	adipose	+	++	++
6	epidermal-dermal	+	+	++
	1:1	+	+	++
	adipose	+	+	++
8	epidermal-dermal	+	+	++
	1:1	+	+	++
	adipose	++	++	++
controls	media only		-	
		epidermal-dermal		
		1:1	-	
		adipose	-	

REFERENCES

1. Gesta, S., Tseng, Y.-H. & Kahn, C.R. Developmental origin of fat: tracking obesity to its source. *Cell* **131**, 242-56 (2007).

2. Schulz, T.J. *et al.* Identification of inducible brown adipocyte progenitors residing in skeletal muscle and white fat. *Proceedings of the National Academy of Sciences of the United States of America* **108**, 143-8 (2011).

3. Sethi, J.K. & Vidal-Puig, A.J. Thematic review series: adipocyte biology. Adipose tissue function and plasticity orchestrate nutritional adaptation. *Journal of lipid research* **48**, 1253-62 (2007).

4. Lafontan, M. Advances in adipose tissue metabolism. *International journal of obesity (2005)* **32 Suppl 7**, S39-51 (2008).

5. Ahmadian, M., Duncan, R.E. & Sul, H.S. The skinny on fat: lipolysis and fatty acid utilization in adipocytes. *Trends in endocrinology and metabolism: TEM* **20**, 424-8 (2009).

6. Wang, S. *et al.* Lipolysis and the integrated physiology of lipid energy metabolism. *Molecular genetics and metabolism* **95**, 117-26 (2008).

7. Voshol, P.J. *et al.* Biochimica et Biophysica Acta Effect of plasma triglyceride metabolism on lipid storage in adipose tissue : Studies using genetically engineered mouse models. *BBA - Molecular and Cell Biology of Lipids* **1791**, 479-485 (2009).

8. Brasaemle, D.L. Thematic review series: adipocyte biology. The perilipin family of structural lipid droplet proteins: stabilization of lipid droplets and control of lipolysis. *Journal of lipid research* **48**, 2547-59 (2007).

9. Shen, W.-J., Patel, S., Miyoshi, H., Greenberg, A.S. & Kraemer, F.B. Functional interaction of hormone-sensitive lipase and perilipin in lipolysis. *Journal of lipid research* **50**, 2306-13 (2009).

10. Shi, Y. & Burn, P. Lipid metabolic enzymes: emerging drug targets for the treatment of obesity. *Nature Reviews Drug Discovery* **3**, 695–710 (2004).

11. Crandall, D. & Hausman, G. A review of the microcirculation of adipose tissue: anatomic, metabolic, and angiogenic perspectives. *Microcirculation* **4**, 211-232 (1997).

12. Cowherd, R.M., Lyle, R.E. & McGehee, R.E. Molecular regulation of adipocyte differentiation. *Seminars in cell & developmental biology* **10**, 3-10 (1999).

13. Tchkonia, T. *et al.* Abundance of two human preadipocyte subtypes with distinct capacities for replication, adipogenesis, and apoptosis varies among fat depots. *American journal of physiology. Endocrinology and metabolism* **288**, E267-77 (2005).

14. Rosen, E.D. & Spiegelman, B.M. Molecular regulation of adipogenesis. *Annual review of cell and developmental biology* **16**, 145–171 (2000).

15. Gregoire, F.M. Adipocyte differentiation: from fibroblast to endocrine cell. *Experimental Biology and Medicine* **226**, 997–1002 (2001).

16. Kang, J.H., Gimble, J.M. & Kaplan, D.L. In vitro 3D model for human vascularized adipose tissue. *Tissue engineering. Part A* **15**, 2227-36 (2009).

17. Tontonoz, P. & Spiegelman, B.M. Fat and beyond: the diverse biology of PPARgamma. *Annual review of biochemistry* **77**, 289-312 (2008).

18. Strissel, K., Stancheva, Z. & Miyoshi, H. Adipocyte death, adipose tissue remodeling, and obesity complications. *Diabetes* **56**, (2007).

19. Divoux, A., Tordjman, J., Lacasa, D. & Veyrie, N. Fibrosis in human adipose tissue: composition, distribution, and link with lipid metabolism and fat mass loss. *Diabetes* **59**, 2817-2825 (2010).

20. Guilherme, A., Virbasius, J.V., Puri, V. & Czech, M.P. Adipocyte dysfunctions linking obesity to insulin resistance and type 2 diabetes. *Nat Rev Mol Cell Biol* **9367**, (2008).

21. Langin, D. Control of fatty acid and glycerol release in adipose tissue lipolysis. *Comptes rendus biologies* **329**, 598-607; discussion 653-5 (2006).

22. Langin, D. & Arner, P. Importance of TNFalpha and neutral lipases in human adipose tissue lipolysis. *Trends in endocrinology and metabolism: TEM* **17**, 314-20 (2006).

23. Shi, H., Kokoeva, M. & Inouye, K. TLR4 links innate immunity and fatty acid-induced insulin resistance. *Journal of Clinical Investigation* **116**, 3015-3025 (2006).

24. Surgery, P. & Statistics, P. American Society of Plastic Surgeons Report of the 2010 Plastic Surgery Statistics. *Surgery* (2010).

25. Stosich, M.S. & Mao, J.J. Adipose tissue engineering from human adult stem cells: clinical implications in plastic and reconstructive surgery. *Plastic and Reconstructive Surgery* **119**, 71-83 (2007).

26. Rohrich, R.J., Sorokin, E.S. & Brown, S.A. In search of improved fat transfer viability: a quantitative analysis of the role of centrifugation and harvest site. *Plastic and reconstructive surgery* **113**, 391-7 (2004).

27. Patrick, C. Tissue engineering strategies for adipose tissue repair. *The Anatomical Record* **366**, 361-366 (2001).

28. Patrick, C., Chauvin, P. & Hobley, J. Preadipocyte seeded PLGA scaffolds for adipose tissue engineering. *Tissue Engineering* **5**, 139-151 (1999).

29. Choi, J.H. *et al.* Adipose Tissue Engineering for Soft Tissue Regeneration. *Tissue Engineering* **16**, (2010).

30. Brayfield, C. a, Marra, K.G. & Rubin, J.P. Adipose tissue regeneration. *Current stem cell research & therapy* **5**, 116-21 (2010).

31. Tanzi, M.C. & Farè, S. Adipose tissue engineering : state of the art , recent advances and innovative approaches. *Tissue Engineering* 533-551 (2009).

32. Choi, Y.S., Park, S.-N. & Suh, H. Adipose tissue engineering using mesenchymal stem cells attached to injectable PLGA spheres. *Biomaterials* **26**, 5855-63 (2005).

33. Kang, S.-W., Seo, S.-W., Choi, C.Y. & Kim, B.-S. Porous poly(lactic-co-glycolic acid) microsphere as cell culture substrate and cell transplantation vehicle for adipose tissue engineering. *Tissue engineering. Part C, Methods* **14**, 25-34 (2008).

34. Chung, H.J. & Park, T.G. Injectable cellular aggregates prepared from biodegradable porous microspheres for adipose tissue engineering. *Tissue engineering. Part A* **15**, 1391-400 (2009).

35. Neubauer, M. *et al.* Adipose tissue engineering based on mesenchymal stem cells and basic fibroblast growth factor in vitro. *Tissue engineering* **11**, 1840-51 (2005).

36. Patrick, C.W., Zheng, B., Johnston, C. & Reece, G.P. Long-term implantation of preadipocyte-seeded PLGA scaffolds. *Tissue engineering* **8**, 283-93 (2002).

37. Anderson, J. & Shive, M. Biodegradation and biocompatibility of PLA and PLGA microspheres. *Advanced drug delivery reviews* **28**, 5-24 (1997).

38. Zhu, J. Bioactive modification of poly(ethylene glycol) hydrogels for tissue engineering. *Biomaterials* **31**, 4639-56 (2010).

39. Vashi, A.V. *et al.* Adipose tissue engineering based on the controlled release of fibroblast growth factor-2 in a collagen matrix. *Tissue engineering* **12**, 3035-43 (2006).

40. Davidenko, N., Campbell, J.J., Thian, E.S., Watson, C.J. & Cameron, R.E. Collagen-hyaluronic acid scaffolds for adipose tissue engineering. *Acta biomaterialia* **6**, 3957-68 (2010).

41. Wu, X., Black, L., Santacana-laffitte, G. & Patrick, C.W. Preparation and assessment of glutaraldehyde-crosslinked collagen – chitosan hydrogels for adipose tissue engineering. *Water* 8-14 (2006).doi:10.1002/jbm.a

42. Flynn, L., Prestwich, G. & Semple, J. Adipose tissue engineering with naturally derived scaffolds and adipose-derived stem cells. *Biomaterials* **283834**, (2007).

43. Flynn, L., Semple, J.L. & Woodhouse, K.A. Decellularized placental matrices for adipose tissue engineering. *Journal of biomedical materials research. Part A* **79**, 359-69 (2006).

44. Choi, J.S. *et al.* Human extracellular matrix (ECM) powders for injectable cell delivery and adipose tissue engineering. *Journal of controlled release : official journal of the Controlled Release Society* **139**, 2-7 (2009).

45. Mauney, J.R. *et al.* Engineering adipose-like tissue in vitro and in vivo utilizing human bone marrow and adipose-derived mesenchymal stem cells with silk fibroin 3D scaffolds. *Biomaterials* **28**, 5280–5290 (2007).

46. Kimura, Y., Ozeki, M. & Inamoto, T. Adipose tissue engineering based on human preadipocytes combined with gelatin microspheres containing basic fibroblast growth factor. *Biomaterials* **24**, 2513-2521 (2003).

47. Borzacchiello, A. *et al.* Structural and rheological characterization of hyaluronic acid-based scaffolds for adipose tissue engineering. *Biomaterials* **28**, 4399-408 (2007).

48. Jing, W. *et al.* Ectopic adipogenesis of preconditioned adipose-derived stromal cells in an alginate system. *Cell and tissue research* **330**, 567-72 (2007).

49. Mandal, B.B. & Kundu, S.C. Osteogenic and adipogenic differentiation of rat bone marrow cells on non-mulberry and mulberry silk gland fibroin 3D scaffolds. *Biomaterials* **30**, 5019-30 (2009).

50. Young, D.A., Ibrahim, D.O., Hu, D. & Christman, K.L. Injectable hydrogel scaffold from decellularized human lipoaspirate. *Acta biomaterialia* **7**, 1040-9 (2011).

51. Tan, H., Rubin, J.P. & Marra, K.G. Injectable in situ forming biodegradable chitosan-hyaluronic acid based hydrogels for adipose tissue regeneration. *Organogenesis* **6**, 173-80 (2010).

52. Chandler, E.M. *et al.* Stiffness of photocrosslinked RGD-alginate gels regulates adipose progenitor cell behavior. *Biotechnology and bioengineering* **108**, 1683-92 (2011).

53. Hong, L., Peptan, I. & Clark, P. Ex vivo adipose tissue engineering by human marrow stromal cell seeded gelatin sponge. *Annals of biomedical engineering* **33**, 511-517 (2005).

54. Itoi, Y., Takatori, M., Hyakusoku, H. & Mizuno, H. Comparison of readily available scaffolds for adipose tissue engineering using adipose-derived stem cells. *Journal of plastic, reconstructive & aesthetic surgery : JPRAS* **63**, 858-64 (2010).

55. Stillaert, F.B. *et al.* Human clinical experience with adipose precursor cells seeded on hyaluronic acid-based spongy scaffolds. *Biomaterials* **29**, 3953-9 (2008).

56. Flynn, L.E., Prestwich, G.D., Semple, J.L. & Woodhouse, K.A. Proliferation and differentiation of adipose-derived stem cells on naturally derived scaffolds. *Ratio* **29**, 1862-1871 (2008).

57. Lidington, E. a, Moyes, D.L., McCormack, a M. & Rose, M.L. A comparison of primary endothelial cells and endothelial cell lines for studies of immune interactions. *Transplant immunology* **7**, 239-46 (1999).

58. Peer, L. & Walker, J. The Behavior of Autogenous Human Tissue Grafts: A Comparative Study. *Plastic and Reconstructive Surgery* (1951).

59. Peer, L. & Walker, J. The Behavior of Autogenous Human Tissue Grafts. II. *Plastic and Reconstructive Surgery* (1951).

60. Yoshimura, K. *et al.* Cell-assisted lipotransfer for cosmetic breast augmentation: supportive use of adipose-derived stem/stromal cells. *Aesthetic plastic surgery* **32**, 48–55 (2008).

61. Matsumoto, D. *et al.* Cell-assisted lipotransfer: supportive use of human adipose-derived cells for soft tissue augmentation with lipoinjection. *Tissue engineering* **12**, 3375–3382 (2006).

62. De Ugarte, D.A., Ashjian, P.H., Elbarbary, A. & Hedrick, M.H. Future of fat as raw material for tissue regeneration. *Annals of plastic surgery* **50**, 215 (2003).

63. Fischer, L.J. *et al.* Endothelial differentiation of adipose-derived stem cells: effects of endothelial cell growth supplement and shear force. *The Journal of surgical research* **152**, 157-66 (2009).

64. Cao, Y. *et al.* Human adipose tissue-derived stem cells differentiate into endothelial cells in vitro and improve postnatal neovascularization in vivo. *Biochem. Biophys. Res. Commun* **332370**, 370 (2005).

65. Kilroy, G.E. *et al.* Cytokine profile of human adipose-derived stem cells: expression of angiogenic, hematopoietic, and pro-inflammatory factors. *Journal of cellular physiology* **212**, 702-709 (2007).

66. Wang, Y. *et al.* In vivo degradation of three-dimensional silk fibroin scaffolds. *Biomaterials* **29**, 3415-28 (2008).

67. Kim, H.J. *et al.* Processing Windows for Forming Silk Fibroin Biomaterials into a 3D Porous Matrix. *Australian Journal of Chemistry* **58**, 716 (2005).

68. McBeath, R., Pirone, D., Nelson, C. & Bhadriraju, K. Cell shape, cytoskeletal tension, and RhoA regulate stem cell lineage commitment. *Developmental cell* **6**, 483-495 (2004).

69. Kniazeva, E. & Putnam, A.J. Endothelial cell traction and ECM density influence both capillary morphogenesis and maintenance in 3-D. *American journal of physiology. Cell physiology* **297**, C179-87 (2009).

70. Merfeld-Clauss, S. & Gollahalli, N. Adipose tissue progenitor cells directly interact with endothelial cells to induce vascular network formation. *Tissue engineering. Part A* **16**, 2953-2966 (2010).

71. Hwang, C.S., Loftus, T.M., Mandrup, S. & Lane, M.D. Adipocyte differentiation and leptin expression. *Annual review of cell and developmental biology* **13**, 231-59 (1997).

72. Koch, T.R. & Finelli, F.C. Postoperative metabolic and nutritional complications of bariatric surgery. *Gastroenterology clinics of North America* **39**, 109-24 (2010).

73. Campfield, L. a. Strategies and Potential Molecular Targets for Obesity Treatment. *Science* **280**, 1383-1387 (1998).

74. Powell, a G., Apovian, C.M. & Aronne, L.J. New drug targets for the treatment of obesity. *Clinical pharmacology and therapeutics* **90**, 40-51 (2011).

75. van Marken Lichtenbelt, W.D. *et al.* Cold-activated brown adipose tissue in healthy men. *The New England journal of medicine* **360**, 1500-8 (2009).

76. Kau, A.L., Ahern, P.P., Griffin, N.W., Goodman, A.L. & Gordon, J.I. Human nutrition, the gut microbiome and the immune system. *Nature* **474**, 327-36 (2011).

77. Tilg, H. & Kaser, A. Gut microbiome, obesity, and metabolic dysfunction. *The Journal of clinical investigation* **121**, 2126-32 (2011).

78. Bråkenhielm, E. *et al.* Angiogenesis inhibitor, TNP-470, prevents diet-induced and genetic obesity in mice. *Circulation research* **94**, 1579-88 (2004).

79. Rupnick, M. a *et al.* Adipose tissue mass can be regulated through the vasculature. *Proceedings of the National Academy of Sciences of the United States of America* **99**, 10730-5 (2002).

80. Kolonin, M.G., Saha, P.K., Chan, L., Pasqualini, R. & Arap, W. Reversal of obesity by targeted ablation of adipose tissue. *Nature medicine* **10**, 625-32 (2004).

81. Takahashi, K. *et al.* JNK- and IkappaB-dependent pathways regulate MCP-1 but not adiponectin release from artificially hypertrophied 3T3-L1 adipocytes preloaded with palmitate in vitro. *American journal of physiology. Endocrinology and metabolism* **294**, E898-909 (2008).

82. Armani, A. *et al.* Cellular models for understanding adipogenesis, adipose dysfunction, and obesity. *Journal of cellular biochemistry* **110**, 564-72 (2010).

83. Jo, J. *et al.* Hypertrophy and/or Hyperplasia: Dynamics of Adipose Tissue Growth. *PLoS computational biology* **5**, e1000324 (2009).

84. Miyoshi, H., Perfield, J.W., Obin, M.S. & Greenberg, A.S. Adipose triglyceride lipase regulates basal lipolysis and lipid droplet size in adipocytes. *Journal of cellular biochemistry* **105**, 1430-6 (2008).

85. Attie, A.D. & Scherer, P.E. Adipocyte metabolism and obesity. *Journal of lipid research* **50 Suppl**, S395-9 (2009).

86. Blüher, M. Adipose tissue dysfunction in obesity. *Experimental and clinical endocrinology & diabetes : official journal, German Society of Endocrinology [and] German Diabetes Association* **117**, 241-50 (2009).

87. Alexander, R.W. Autologous Fat Transfer. 87-112 (2010).doi:10.1007/978-3-642-00473-5

88. Tissue, S., Usingvitro, A., Adipocytes, D. & Study, C.P. Soft Tissue Augmentation Using In Vitro Differentiated Adipocytes: A Clinical Pilot Study. *Methods* 760-767 (2011).doi:10.1111/j.1524-4725.2011.01950.x

89. Fischbach, C. *et al.* Generation of mature fat pads in vitro and in vivo utilizing 3-D long-term culture of 3T3-L1 preadipocytes. *Experimental cell research* **300**, 54 - 64 (2004).

90. Rehfeldt, F., Engler, A.J., Eckhardt, A., Ahmed, F. & Discher, D.E. Cell responses to the mechanochemical microenvironment--implications for regenerative medicine and drug delivery. *Advanced drug delivery reviews* **59**, 1329-39 (2007).

91. Engler, a J., Sweeney, H.L., Discher, D.E. & Schwarzbauer, J.E. Extracellular matrix elasticity directs stem cell differentiation. *Journal of musculoskeletal & neuronal interactions* **7**, 335 (2007).

92. Engler, A.J., Sen, S., Sweeney, H.L. & Discher, D.E. Matrix elasticity directs stem cell lineage specification. *Cell* **126677**, (2006).

93. Ruiz, S.A. & Chen, C.S. Emergence of patterned stem cell differentiation within multicellular structures. *Stem cells (Dayton, Ohio)* **26**, 2921-7 (2008).

94. Chun, T.H. *et al.* pericellular collagenase directs the 3-dimensional development of white adipose tissue. *Cell* **125**, 577-591 (2006).

95. Hariri, N. & Thibault, L. High-fat diet-induced obesity in animal models. *Nutrition research reviews* **23**, 270-99 (2010).

96. Strissel, K.J. *et al.* T-cell recruitment and Th1 polarization in adipose tissue during diet-induced obesity in C57BL/6 mice. *Obesity (Silver Spring, Md.)* **18**, 1918-25 (2010).

97. Horng, T. & Hotamisligil, G.S. Linking the inflammasome to obesity-related disease. *Nature medicine* **17**, 164-5 (2011).

98. Hue, J.-J. *et al.* Anti-obesity activity of diglyceride containing conjugated linoleic acid in C57BL/6J ob/ob mice. *Journal of Veterinary Science* **10**, 189 (2009).

99. Arias, N. *et al.* The combination of resveratrol and conjugated linoleic acid is not useful in preventing obesity. *Journal of physiology and biochemistry* (2011).doi:10.1007/s13105-011-0086-2

100. Kim, S.-J., Choi, Y., Choi, Y.-H. & Park, T. Obesity activates toll-like receptor-mediated proinflammatory signaling cascades in the adipose tissue of mice. *The Journal of nutritional biochemistry* 1-10 (2011).doi:10.1016/j.jnutbio.2010.10.012

101. Fain, J.N., Ballou, L.R. & Bahouth, S.W. Obesity is induced in mice heterozygous for cyclooxygenase-2. *Prostaglandins & other Lipid Mediators* **65**, 199 -209 (2001).

102. Auwerx, J. & Staels, B. Leptin. *The Lancet* **351**, 737-742 (1998).

103. Gautron, L. & Elmquist, J.K. Sixteen years and counting: an update on leptin in energy balance. *Journal of Clinical Investigation* **121**, 2087 (2011).

104. Li, J.-J., Huang, C.J. & Xie, D. Anti-obesity effects of conjugated linoleic acid, docosahexaenoic acid, and eicosapentaenoic acid. *Molecular nutrition & food research* **52**, 631-45 (2008).

105. Ramachandrappa, S. & Farooqi, I.S. Review series Genetic approaches to understanding human obesity. *Regulation* **121**, (2011).

106. Boissel, S. *et al.* Loss-of-function mutation in the dioxygenase-encoding FTO gene causes severe growth retardation and multiple malformations. *American journal of human genetics* **85**, 106-11 (2009).

107. Vandenburgh, H. *et al.* Drug-screening platform based on the contractility of tissue-engineered muscle. *Muscle & nerve* **37**, 438-47 (2008).

108. Choi, J.H., Gimble, J.M., Vunjak-Novakovic, G. & Kaplan, D.L. Effects of Hyperinsulinemia on Lipolytic Function of Three-Dimensional Adipocyte/Endothelial Co-Cultures. *Tissue Engineering Part C: Methods* **16**, 1157-1165 (2010).

109. Choi, J.H., Bellas, E., Gimble, J.M., Vunjak-Novakovic, G. & Kaplan, D.L. Lipolytic Function of Adipocyte/Endothelial Cocultures. *Tissue Engineering Part A* **17**, 1437-1444 (2011).

110. Ghoshal, S., Trivedi, D.B., Graf, G. a & Loftin, C.D. Cyclooxygenase-2 deficiency attenuates adipose tissue differentiation and inflammation in mice. *The Journal of biological chemistry* **286**, 889-98 (2011).

111. Yan, H., Kermouni, A., Abdel-Hafez, M. & Lau, D.C.W. Role of cyclooxygenases COX-1 and COX-2 in modulating adipogenesis in 3T3-L1 cells. *Journal of lipid research* **44**, 424-9 (2003).

112. Fajas, L., Miard, S., Briggs, M.R. & Auwerx, J. Selective cyclo-oxygenase-2 inhibitors impair adipocyte differentiation through inhibition of the clonal expansion phase. *Journal of lipid research* **44**, 1652-9 (2003).

113. Graham, D.J. *et al.* Risk of acute myocardial infarction and sudden cardiac death in patients treated with cyclo-oxygenase 2 selective and non-selective non-steroidal anti-inflammatory drugs: nested case-control study. *Lancet* **365**, 475-81 (2005).

114. Parajuli, P. *et al.* Delayed growth of glioma by Scutellaria flavonoids involve inhibition of Akt, GSK-3 and NF-κB signaling. *Journal of neuro-oncology* **101**, 15-24 (2011).

115. Li-Weber, M. New therapeutic aspects of flavones: the anticancer properties of Scutellaria and its main active constituents Wogonin, Baicalein and Baicalin. *Cancer treatment reviews* **35**, 57-68 (2009).

116. Setty, A.R. & Sigal, L.H. Herbal medications commonly used in the practice of rheumatology: mechanisms of action, efficacy, and side effects. *Seminars in arthritis and rheumatism* **34**, 773-84 (2005).

117. Wright, B. *et al.* A structural basis for the inhibition of collagen-stimulated platelet function by quercetin and structurally related flavonoids. *British journal of pharmacology* **159**, 1312-25 (2010).

118. Kennedy, A. *et al.* Antiobesity mechanisms of action of conjugated linoleic acid. *The Journal of nutritional biochemistry* **21**, 171-9 (2010).

119. Parra, P., Serra, F. & Palou, A. Moderate doses of conjugated linoleic acid isomers mix contribute to lowering body fat content maintaining insulin sensitivity and a noninflammatory pattern in adipose tissue in mice. *The Journal of nutritional biochemistry* **21**, 107-15 (2010).

120. Kloss, R. *et al.* Effects of conjugated linoleic acid supplementation on blood lipids and adiposity of rats fed diets rich in saturated versus unsaturated fat. *Pharmacological research : the official journal of the Italian Pharmacological Society* **51**, 503-7 (2005).

121. Ippagunta, S., Hadenfeldt, T.J., Miner, J.L. & Hargrave-Barnes, K.M. Dietary Conjugated Linoleic Acid Induces Lipolysis in Adipose Tissue of Coconut Oil-Fed Mice but not Soy Oil-Fed Mice. *Lipids* **46**, 821-30 (2011).

122. Rockwood, D.N. *et al.* Materials fabrication from Bombyx mori silk fibroin. *Nature Protocols* **6**, 1612-1631 (2011).

123. Danciger, J.S. *et al.* Method for large scale isolation , culture and cryopreservation of human monocytes suitable for chemotaxis , cellular adhesion assays , macrophage and dendritic cell differentiation. *Journal of Immunological Methods* **288**, 123 - 134 (2004).

124. Tilg, H. & Moschen, A.R. Adipocytokines : mediators linking adipose tissue , inflammation and immunity. *Immunology* **6**, 772-783 (2006).

125. Lee, J.Y., Sohn, K.H., Rhee, S.H. & Hwang, D. Saturated Fatty Acids , but Not Unsaturated Fatty Acids , Induce the Expression of Cyclooxygenase-2 Mediated through Toll-like Receptor 4 *. *Biochemistry* **276**, 16683-16689 (2001).

126. Han, C., Kargi, A., Omer, M. & Chan, C. Differential effect of saturated and unsaturated free fatty acids on the generation of monocyte adhesion and chemotactic factors by adipocytes. *Diabetes* **59**, (2010).

127. Suganami, T., Nishida, J. & Ogawa, Y. A paracrine loop between adipocytes and macrophages aggravates inflammatory changes: role of free fatty acids and tumor necrosis factor alpha. *Arteriosclerosis, thrombosis, and vascular biology* **25**, 2062-8 (2005).

128. Permana, P. a *et al.* Pioglitazone reduces inflammatory responses of human adipocytes to factors secreted by monocytes/macrophages. *American journal of physiology. Endocrinology and metabolism* **296**, E1076-84 (2009).

129. Lacasa, D., Taleb, S., Keophiphath, M., Miranville, A. & Clement, K. Macrophage-secreted factors impair human adipogenesis: involvement of proinflammatory state in preadipocytes. *Endocrinology* **148**, 868-77 (2007).

130. Maury, E. & Brichard, S. Adipokine dysregulation, adipose tissue inflammation and metabolic syndrome. *Molecular and cellular endocrinology* **314**, 1–16 (2010).

131. Schaeffler, A. *et al.* Fatty acid-induced induction of Toll-like receptor-4/nuclear factor-kappaB pathway in adipocytes links nutritional signalling with innate immunity. *Immunology* **126**, 233-45 (2009).

132. Mohamed-Ali, V. *et al.* Subcutaneous adipose tissue releases interleukin-6, but not tumor necrosis factor-alpha, in vivo. *The Journal of clinical endocrinology and metabolism* **82**, 4196-200 (1997).

133. Ghoshal, S., Trivedi, D.B., Graf, G. a & Loftin, C.D. Cyclooxygenase-2 deficiency attenuates adipose tissue differentiation and inflammation in mice. *The Journal of biological chemistry* **286**, 889-98 (2011).

134. Furuhashi, M. & Hotamisligil, G.S. Fatty acid-binding proteins: role in metabolic diseases and potential as drug targets. *Nature reviews. Drug discovery* **7**, 489-503 (2008).

135. Makowski, L., Brittingham, K.C., Reynolds, J.M., Suttles, J. & Hotamisligil, G.S. The fatty acid-binding protein, aP2, coordinates macrophage cholesterol trafficking and inflammatory activity. Macrophage expression of aP2 impacts peroxisome proliferator-activated receptor gamma and IkappaB kinase activities. *The Journal of biological chemistry* **280**, 12888-95 (2005).

136. Keophiphath, M., Rouault, C., Divoux, A., Clément, K. & Lacasa, D. CCL5 promotes macrophage recruitment and survival in human adipose tissue. *Arteriosclerosis, thrombosis, and vascular biology* **30**, 39-45 (2010).

137. Poppitt, S.D. *et al.* Postprandial response of adiponectin, interleukin-6, tumor necrosis factor-alpha, and C-reactive protein to a high-fat dietary load. *Nutrition* **24**, 322-9 (2008).

138. Stosich, M.S. *et al.* Bioengineering strategies to generate vascularized soft tissue grafts with sustained shape. *Methods* **47**, 116-21 (2009).

139. American Society of Plastic Surgeons Report of the 2010 Plastic Surgery Statistics. at <www.plasticsurgery.org>

140. Altman, G., Diaz, F., Jakuba, C., Calabro, T. & Horan, R. Silk-based biomaterials. *Biomaterials* **24**, 401-416 (2003).

141. Vepari, C. & Kaplan, D.L. Silk as a Biomaterial. *Progress in polymer science* **32**, 991-1007 (2007).

142. Choi, J., Bellas, E. & Vunjak-Novakovic, G. Adipogenic Differentiation of Human Adipose-Derived Stem Cells on 3D Silk Scaffolds. *Methods in molecular* **702**, 319-330 (2011).

143. Rubin, J.P., DeFail, A., Rajendran, N. & Marra, K.G. Encapsulation of adipogenic factors to promote differentiation of adipose-derived stem cells. *Journal of drug targeting* **17**, 207-15 (2009).

144. Numata, K., Cebe, P. & Kaplan, D.L. Mechanism of enzymatic degradation of beta-sheet crystals. *Biomaterials* **31**, 2926-33 (2010).

145. Kim, U.J.J. *et al.* Three-dimensional aqueous-derived biomaterial scaffolds from silk fibroin. *Biomaterials* **26**, 2775–2785 (2005).

146. Schoeller, T. *et al.* Histomorphologic and Volumetric Analysis of Implanted Autologous Preadipocyte Cultures Suspended in Fibrin Glue: A Potential New Source for Tissue Augmentation. *Aesthetic Plastic Surgery* **25**, 57-63 (2001).

147. Wechselberger, G. *et al.* Successful Transplantation of Three Tissue-Engineered Cell Types Using Capsule Induction Technique and Fibrin Glue as a Delivery Vehicle. *Plastic and Reconstructive Surgery* **110**, 123-129 (2002).

148. Suga, H. *et al.* Numerical measurement of viable and nonviable adipocytes and other cellular components in aspirated fat tissue. *Plastic and reconstructive surgery* **122**, 103-14 (2008).

149. Badylak, S.F., Valentin, J.E., Ravindra, A.K., McCabe, G.P. & Stewart-Akers, A.M. Macrophage phenotype as a determinant of biologic scaffold remodeling. *Tissue engineering. Part A* **14**, 1835-42 (2008).

150. Brown, B.N., Valentin, J.E., Stewart-Akers, A.M., McCabe, G.P. & Badylak, S.F. Macrophage phenotype and remodeling outcomes in response to biologic scaffolds with and without a cellular component. *Biomaterials* **30**, 1482-91 (2009).

151. Zannettino, A.C.W. *et al.* Multipotential human adipose-derived stromal stem cells exhibit a perivascular phenotype in vitro and in vivo. *Journal of cellular physiology* **214**, 413-21 (2008).

152. Merlo Pich, E. Understanding pharmacology in humans: Phase I and Phase II (Data Generation). *Current opinion in pharmacology* **11**, 557-62 (2011).

153. Morgan, S., Grootendorst, P., Lexchin, J., Cunningham, C. & Greyson, D. The cost of drug development: a systematic review. *Health policy (Amsterdam, Netherlands)* **100**, 4-17 (2011).

154. Kola, I. & Landis, J. Can the pharmaceutical industry reduce attrition rates? *Nature reviews. Drug discovery* **3**, 711-5 (2004).

155. Rothstein, J.D. Of mice and men: reconciling preclinical ALS mouse studies and human clinical trials. *Annals of neurology* **53**, 423-6 (2003).

156. Egles, C., Garlick, J.A. & Shamis, Y. Chapter 24 Three-Dimensional Human Tissue Models of Wounded Skin. *Methods in Molecular Biology* 345-359doi:10.1007/978-1-60761-380-0

157. Carlson, M.W., Alt-holland, A., Egles, C. & Garlick, J.A. Three-Dimensional Tissue Models of Normal and Diseased Skin. 1-17 (2008).doi:10.1002/0471143030.cb1909s41

158. Metcalfe, A.D. & Ferguson, M.W.J. Tissue engineering of replacement skin: the crossroads of biomaterials, wound healing, embryonic development, stem cells and regeneration. *Journal of the Royal Society, Interface / the Royal Society* **4**, 413-37 (2007).

159. Trottier, V., Marceau-Fortier, G., Germain, L., Vincent, C. & Fradette, J. IFATS collection: Using human adipose-derived stem/stromal cells for the production of new skin substitutes. *Stem cells* **26**, 2713-23 (2008).

160. Yannas, I.V., Orgill, D.P. & Burke, J.F. Template for skin regeneration. *Plastic and reconstructive surgery* **127 Suppl** , 60S-70S (2011).

161. Richard, R.L. *et al.* Identification of cutaneous functional units related to burn scar contracture development. *Journal of burn care & research : official publication of the American Burn Association* **30**, 625-31

162. Elabd, C., Chiellini, C., Carmona, M. & Galitzky, J. Human Multipotent Adipose-Derived Stem Cells Differentiate into Functional Brown Adipocytes. *Stem Cells* **27**, 2753-2760 (2009).